1-1-1999

# Lateral Load Behavior and Design of Unbonded Post-Tensioned Precast Concrete Walls with Ductile Vertical Joint Connectors

Felipe J. Perez

Stephen P. Pessiki

Richard Sause

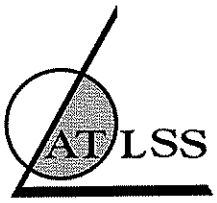


LEHIGH
University

# LATERAL LOAD BEHAVIOR AND DESIGN OF UNBONDED POST-TENSIONED PRECAST CONCRETE WALLS WITH DUCTILE VERTICAL JOINT CONNECTORS

by

**Felipe J. Perez**

**Stephen Pessiki**

**Richard Sause**

**ATLSS Report No. 99-01**

**January 1999**

**ATLSS is a National Center for Engineering Research on Advanced Technology for Large Structural Systems**

117 ATLSS Drive
Bethlehem, PA 18015-4729

Phone: (610)758-3525
Fax: (610)758-5902

www.atlss.lehigh.edu
Email: inatl@lehigh.edu


LEHIGH
University

# LATERAL LOAD BEHAVIOR AND DESIGN OF UNBONDED POST-TENSIONED PRECAST CONCRETE WALLS WITH DUCTILE VERTICAL JOINT CONNECTORS

by

**Felipe J. Perez**
Graduate Research Assistant
Civil and Environmental Engineering

**Stephen Pessiki**
Associate Professor
Civil and Environmental Engineering

**Richard Sause**
Associate Professor
Civil and Environmental Engineering

**ATLSS Report No. 99-01**

**January 1999**

**ATLSS is a National Center for Engineering Research on Advanced Technology for Large Structural Systems**

117 ATLSS Drive
Bethlehem, PA 18015-4729

Phone: (610)758-3525
Fax: (610)758-5902

www.atlss.lehigh.edu
Email: inatl@lehigh.edu

## ACKNOWLEDGMENTS

This research was supported by the Center for Advanced Technology for Large Structural Systems (ATLSS) at Lehigh University. Additional support was provided by the Precast/Prestressed Concrete Institute (PCI). The opinions, findings, and conclusions expressed in this report are those of the authors and do not necessarily reflect the views of the organizations acknowledged above.

## TABLE OF CONTENTS

## ABSTRACT

This research investigates the seismic behavior and design of walls composed of precast concrete panels that are attached to each other along vertical joints with ductile connectors and to the foundation along horizontal joints with post-tensioning steel that is not bonded to the concrete. The research addresses the analytical modeling and behavior of the walls under lateral load. An analytical model for these walls based on fiber elements is presented. Closed-form expressions are derived to estimate the values that define key points on a tri-linear idealized base-shear-roof-displacement behavior of these walls under monotonic lateral loads. A seismic design approach for the walls is proposed. Using the proposed seismic design approach, unbonded post-tensioned precast concrete walls can be designed to have substantial initial lateral stiffnesses and base shear strength exceeding the demands of current model building codes. These walls can be designed to soften and satisfy nonlinear displacement demands corresponding to code specified design level ground motions without yielding in the post-tensioning steel, but with yielding and energy dissipation in the vertical joint connectors. These walls could also be designed to satisfy nonlinear displacement demands under more severe ground motions without fracture of the post-tensioning steel, or compression failure of the concrete in the wall panels but the design approach given in this report does not directly address these ground motions. Using the proposed design approach, a prototype wall was designed. The lateral load behavior of the prototype wall and other similar walls was investigated under monotonic and cyclic static lateral loads. Monotonic lateral load analyses show that, in general, excellent agreement is obtained between the results from the fiber element model and the estimated values that define the key points of the tri-linear idealization of the lateral load behavior of the wall. Cyclic lateral load analyses show that the unbonded post-tensioned horizontal joints combined with the inelastic behavior of the vertical joint connectors results in wide, stable hysteresis loops, which provide self-centering and good inelastic energy dissipation. The vertical joint connectors, which are designed to yield in shear under the action of lateral loads, contribute significantly to the hysteretic behavior of the walls.

# CHAPTER 1

# INTRODUCTION

Past earthquakes have demonstrated the importance of selecting a good seismic structural system and incorporating suitable detailing to provide life safety and property protection. For many years, concrete structural walls have fulfilled both of these requirements at a low cost (Fintel 1995). Today, structural walls are a commonly used earthquake resisting system, particularly in regions of high seismicity.

Precast concrete construction has many benefits such as high quality, fast erection, cost effectiveness, and potential for construction automation. The advantages of precast concrete construction have made it a good candidate for use in seismic and non-seismic regions of the U.S. Thus, the use of precast concrete structural walls in buildings that are located in seismic regions combines the benefits of structural walls and precast concrete construction.

Investigations over the past three decades have shown that buildings with precast walls as the primary lateral load resisting system have performed remarkably well in severe earthquakes around the world. A review of the seismic performance of precast wall building systems in past earthquakes is given by Fintel (1986, 1995), Iverson and Hawkins (1994), and Ghosh (1995). The Romanian earthquake of March 1977 was the first earthquake to subject a large number of precast concrete buildings to earthquake loading. Many of these precast buildings had large-panel shear walls made of precast concrete and cast-in-place slabs. These buildings showed minimum distress. However, the period of the ground motion (approximately 1.5 sec.) did not excite these buildings, which had a period of about 0.6-0.7 sec. (Fintel 1995). The Mexico earthquake of September 1985 caused the collapse of several hundred multistory buildings, killing thousands. Only rarely were shear walls used in these buildings. However, buildings containing shear walls performed well, offering better damage control by limiting drift and reducing the danger of collapse (Fintel 1986). In December 1988 an earthquake struck Armenia in which not a single structure with large precast concrete panels was destroyed (Fintel 1995). Iverson and Hawkins (1994) report that, during the Northridge Earthquake of 1994, structures engineered with precast concrete components generally performed well throughout the region of strong ground motions. The damage in precast concrete buildings was observed in collector elements of the floor system designed to transfer horizontal forces to lateral load resisting vertical elements. Finally, during the Kobe Earthquake of January 1995, the precast concrete structures in the two- to five-story height range with precast concrete wall or panel units did not suffer any functional damage and were ready for continued occupancy immediately after the earthquake (Ghosh 1995).

As noted above, buildings with precast concrete walls as their primary lateral load resisting system performed well when subjected to earthquake loading. However, the use of precast concrete seismic systems in the U.S. is severely constrained by the provisions of model building codes (e.g., the Uniform Building Code (1991) and the NEHRP Recommended Provisions (1994)), which require that precast seismic systems be shown by experiment and analy-

sis to have lateral load resisting characteristics that are equal or superior to those of monolithic cast-in-place reinforced concrete systems. This requirement has led to the development of a design philosophy known as "cast-in-place emulation" (Shultz and Magaña 1996).

The precast concrete systems that can be designed under the current model building codes use "wet" connections, which are made with cast-in-place concrete (El-Sheikh, et al. 1997). The resulting structure is intended to be continuous, thus emulating a cast-in-place structure. However, these systems do not have all of the economic advantages of precast concrete because they require the use of cast-in-place concrete in their connections. An alternative is the use of "dry" connections, which are made by bolting, welding, or by other mechanical means. The behavior of precast concrete systems with "dry" connections differs from that of systems which use cast-in-place concrete because the connections create natural discontinuities in the structure. The connections are often inherently less stiff than the precast members, and so deformations tend to be concentrated in them. This presents an opportunity for the development of innovative structural systems with seismic behavior that is quite different from that of cast-in-place construction (Stanton 1994). However, as stated above, model building codes require precast concrete structures to emulate the lateral load behavior of monolithic cast-in-place reinforced concrete systems. Consequently, the joints between precast members are typically proportioned with sufficient strength to avoid inelastic deformation, causing inelastic behavior to occur away from the connections. These joints are more costly (Schultz and Magaña 1996). Thus, the emulation design philosophy of model building codes not only undermines the cost-effectiveness of precast concrete systems, but also ignores the inherent characteristics of precast concrete construction that can be exploited for seismic resistance.

In response to the recognized need for research on precast concrete systems for seismic regions, the PRESSS (PREcast Seismic Structural Systems) research program was initiated in 1990. The PRESSS research program is a coordinated program of analytical and experimental research aimed at the development of seismic design provisions for precast concrete structures. The PRESSS program is supported by the National Science Foundation (NSF), the Precast/Prestressed Concrete Institute (PCI), and the Precast/Prestressed Concrete Manufacturers Association of California (PCMAC). The main objectives of the PRESSS program are: (1) to develop effective seismic structural systems for precast concrete buildings; and (2) to develop seismic design recommendations for precast concrete buildings (Priestley 1991). The PRESSS research program considers precast concrete buildings that utilize frames and/or walls for the lateral load resisting system. The PRESSS program consists of three phases. Phase I focuses on identifying and evaluating the most promising seismic precast concrete building systems. Phase II focuses on detailed experimental and analytical studies of components and subassemblages of precast systems selected during Phase I. Finally, Phase III involves testing of multi-story full size assemblages and finalizing the seismic design recommendations.

The PRESSS program and other related research have shown that the use of unbonded post-tensioning to connect precast concrete members has beneficial effects on the hysteretic load-deformation behavior of precast concrete subassemblages (Cheok et al. 1993, MacRae and

Priestley 1994, Priestley and Tao 1993). Specifically, this type of construction exhibits a nonlinear elastic load-deformation response. The nonlinearity results from gap-opening that occurs at the connections as the precompression due to prestressing is overcome by the bending moment due to lateral load. Early work, directed primarily at frame structures, has shown that through the use of unbonded post-tensioned construction, it is possible to prevent or delay yielding in the post-tensioning steel, and thus maintain the prestress during seismic response. Similar behavior is not possible in bonded post-tensioned systems.

An analytical study performed by Kurama et al. (1996, 1997) on unbonded post-tensioned precast concrete walls with horizontal joints showed that, as a result of unbonding, large nonlinear lateral displacements can be achieved in a wall without yielding or fracturing the post-tensioning steel. The walls treated by Kurama et al. are comprised of precast panels connected along horizontal joints as shown in Figure 1(a), through the use of unbonded post-tensioning. Kurama et al. showed that a well-designed unbonded post-tensioned precast wall with horizontal joints that is subjected to cyclic lateral loading does not suffer degradation of the initial lateral stiffness and has good self-centering capacity after the lateral loads are removed. The use of unbonded post-tensioning delays yielding in the post-tensioned reinforcement. As a result, the lateral load behavior is very close to being nonlinear-elastic, resulting in little inelastic energy dissipation per cycle of loading. Kurama et al. developed a seismic design approach for buildings with unbonded post-tensioned precast concrete walls as the primary lateral load resisting system. This design approach considered walls composed of precast wall panels with horizontal joints, but without vertical joints.

## 1.1 OBJECTIVES AND APPROACH

### 1.1.1 Objectives

The objective of this research is to investigate the seismic behavior and design of unbonded post-tensioned precast concrete walls with vertical joints and ductile connectors. This type of construction is illustrated in Figure 1(b). The use of unbonded post-tensioning across horizontal joints and ductile connectors along the vertical joints results in a lateral load resisting system with the potential for ductility and energy dissipation without a significant loss in self-centering capability.

### 1.1.2 Approach

In order to achieve the objective stated above, the following research approach is taken:

1. Perform a literature search on previous research related to the behavior of unbonded post-tensioned precast concrete walls, as well as on the seismic behavior of connections for precast concrete walls.

2. Develop closed-form expressions for predicting the lateral load behavior of unbonded post-tensioned precast concrete walls with vertical joints.

3. Develop a design approach for buildings with unbonded post-tensioned precast concrete walls with ductile vertical joint connectors, based on the design approach developed by Kurama et al. (1997).

4. Design a prototype structure with unbonded post-tensioned precast concrete walls with ductile vertical joints.

5. Develop an analytical model for the lateral load response of the prototype wall.

6. Using the analytical model, determine the effect of various structural design parameters on the lateral load behavior of unbonded post-tensioned precast concrete walls with ductile vertical joint connectors.

7. Verify the accuracy of the closed-form expressions in predicting the lateral load behavior of unbonded post-tensioned precast walls with vertical joints when subjected to monotonic lateral loads.

8. Determine the contribution of the ductile vertical joint connectors to the cyclic response of unbonded post-tensioned precast concrete walls.

## 1.2 ORGANIZATION OF REPORT

The remainder of this report is organized into seven chapters (Chapters 2-8) in accordance with the research approach summarized above. A summary of previous research on unbonded post-tensioned precast concrete walls and on vertical joint connectors is given in Chapter 2. Chapter 3 derives a set of closed-form expressions for predicting the lateral load behavior of unbonded post-tensioned precast concrete walls with vertical joint connectors. Chapter 4 presents a proposed design approach for buildings with unbonded post-tensioned precast walls with vertical joint connectors as the primary lateral load resisting system. Chapter 5 describes the design of a prototype structure and a prototype wall. Chapter 6 discusses the analytical model used to study the response of a series of walls under static lateral loads. Chapter 7 presents a study of the effects of several structural parameters on the lateral load behavior of unbonded post-tensioned precast concrete walls with ductile vertical joint connectors. Finally, Chapter 8 presents a summary and the conclusions of the research, and identifies future research topics.

## 1.3 NOTATION

The following notation is used in this report:

$A_j$ = shear area of vertical connectors;
$A_p$ = total cross sectional area of post-tensioning steel in a panel;
$A'_{pl}$ = shear area of each vertical joint connection plate;
$A_w$ = gross cross-sectional area of a wall;
$A'_w$ = effective shear area of wall;
$A_x$ = gross cross-sectional area of a panel;

$A_{x,net}$ = net cross-sectional area of a panel (i.e., gross cross-sectional area minus area of the post-tensioning ducts);
$C_i$ = compression stress resultant in concrete after elastic shortening due to post-tensioning and gravity load;
$C_k$ = compression stress resultant at base of panel k;
$C_{ki}$ = compression stress resultant on panel k after elastic shortening due to post-tensioning and gravity load;
$C_s$ = NEHRP seismic response coefficient;
$c_k$ = depth of compression zone at base of panel k;
$E_c$ = Young's modulus for concrete;
$E_p$ = Young's modulus for post-tensioning steel;
$e_{acc}$ = accidental eccentricity;
$e_{Nk}$ = eccentricity of $N_k$ measured from right edge of panel;
$e_p$ = eccentricity of post-tensioning steel from panel centerline to centroid of post-tensioning steel;
$e_1$ = perpendicular distance between centerline of a wall and center of resistance of structure;
$F_{k,i}$ = lateral force on panel k at level i;
$F_{k,r}$ = lateral force on panel k at roof level;
$F_{vjp}$ = flexibility of a vertical joint steel plate;
$F_{w,i}$ = lateral force on wall at floor i;
$F_{w,r}$ = lateral force on wall at roof level;
$f'_c$ = compressive strength of unconfined concrete;
$f_{ci}$ = stress in concrete after elastic shortening due to post-tensioning and gravity load (also referred to as the initial stress in concrete);
$f_{ci,N}$ = stress in concrete due to N (also referred to as the initial stress in concrete due to gravity load);
$f_{ci,P}$ = stress in concrete due to Pi (also referred to as the initial stress in concrete due to post-tensioning);
$f_{llj}$ = strength corresponding to the linear limit strain on the stress-strain relationship of the vertical connectors;
$f_{pi}$ = stress in post-tensioning steel after elastic shortening due to post-tensioning and gravity load (also referred to as the initial stress in the post-tensioning steel);
$f_{pl}$ = stress corresponding to the linear limit strain on the stress-strain relationship of the post-tensioning steel;
$f_{pr}$ = residual stress in post-tensioning steel after unloading from beyond the linear limit strain on the stress-strain relationship of the post-tensioning steel;
$f_{pu}$ = ultimate stress on the stress-strain relationship of the post-tensioning steel (i.e., ultimate strength of the post-tensioning steel);
$f_{py}$ = yield strength of the truss elements modeling the post-tensioning steel;
$G_c$ = shear modulus of concrete;
$G_{pl}$ = shear modulus of vertical joint connection plate;
$H_i$ = height of floor level i measured from the base of the wall;
$H_r$ = height of roof level measured from the base of the wall (equal to $H_w$);

$H_w$ = total height of wall;
$I_w$ = moment of inertia of the gross cross-section of a wall;
i = floor level;
j = floor level;
k = number of panels in a wall;
$k_{i,sce}$ = initial stiffness in simple connection element;
$k_{wi}$ = initial lateral stiffness of wall;
$L_{pl}$ = length of connection plate across vertical joint;
$l_w$ = length of the wall cross-section;
$l_x$ = length of a panel cross-section;
$M_{dec}$ = base moment when decompression begins at the base of the wall;
$M_{w,i}$ = moment applied at floor i;
m = modular ratio, i.e., $E_p/E_c$;
N = gravity load on each panel;
$N_b$ = number of post-tensioning bars in a wall panel;
$N_k$ = gravity load at the base of a panel k;
n = number of panels in a wall;
$P_i$ = total force in the post-tensioning steel after elastic shortening due to post-tensioning and gravity load on a panel;
$P'_i$ = total force in the post-tensioning steel after elastic shortening due to post-tensioning of a panel;
$P_j$ = total shear force across a vertical joint;
$P_{llj}$ = total linear limit force across a vertical joint;
$P_t$ = total force applied to the truss elements to model $P'_i$;
$Q_d$ = linear-elastic base shear demand for the design level ground motion;
$Q_s$ = linear-elastic base shear demand for the survival level ground motion;
R = NEHRP response modification coefficient;
r = total number of stories in a wall;
$r_{Fi}$ = ratio of the force at the i'th floor level to the wall base shear;
$r_{Fr}$ = ratio of the force at the roof level to the wall base shear;
$r_{Hi}$ = ratio of the i'th floor height to the total height of the wall;
$r_{Hr}$ = ratio of the roof height to the total height of the wall (equal to unity);
T = fundamental period of structure;
$T_a$ = approximate fundamental period of structure;
$T_i$ = total force in a group of post-tensioning steel after elastic shortening due to post-tensioning and gravity load;
$T_{llp}$ = total force in a group of post-tensioning steel at linear limit strain;
$T_1$ = total force in a group of post-tensioning steel to the left of panel centerline;
$T_{1i}$ = total initial force in a group of post-tensioning steel to the left of panel centerline after elastic shortening due to post-tensioning and gravity load;
$T_2$ = total force in a group of post-tensioning steel to the right of panel centerline;
$T_{2i}$ = total initial force in a group of post-tensioning steel to the right of panel centerline after elastic shortening due to post-tensioning and gravity load;
$t_w$ = thickness of wall cross-section;

$t_x$ = thickness of panel cross-section (equal to $t_w$) panels when crushing of the spiral confined concrete occurs;
$V_{csc}$ = base shear when spiral confined concrete crushes;
$V_d$ = wall design base shear demand;
$V^s_d$ = structural design base shear demand;
$V_{d,acc}$ = wall base shear due to story translations from accidental torsion;
$V_{dec}$ = base shear when decompression begins at the base of the wall;
$V_{ell}$ = base shear at effective linear limit of base-shear-roof-displacement relationship;
$V_k$ = panel base shear;
$V_{llj}$ = wall base shear when linear limit strain of vertical joint connectors is reached;
$V_{llp}$ = wall base shear when linear limit strain of post-tensioning steel is reached;
$V_w$ = wall base shear;
W = structure seismic weight;
w = number of walls in building layout resisting lateral load;
$\Delta_{csc}$ = roof displacement when spiral confined concrete crushes;
$\Delta_d$ = maximum roof displacement demand under the design level ground motion;
$\Delta_{dec}$ = roof displacement when decompression begins at the base of the wall;
$\Delta_{ell}$ = roof displacement at effective linear limit of base-shear-roof-displacement relationship;
$\Delta_{Fj}$ = deflection at floor j due to lateral forces;
$\Delta_{F,r}$ = roof displacement of wall in flexure;
$\Delta_{go}$ = roof displacement due to gap opening;
$\Delta_{llj}$ = roof displacement when linear limit strain of vertical joint connectors is reached;
$\Delta_{llp}$ = roof displacement when linear limit strain of post-tensioning steel is reached;
$\Delta_{Nj}$ = wall displacement at floor j in flexure due to eccentrically applied axial forces on a panel;
$\Delta_{N,r}$ = roof displacement due to eccentric axial force;
$\Delta_{Pj}$ = wall displacement at floor j due to different initial prestress forces, $T_{1i}$ and $T_{2i}$;
$\Delta_{P,r}$ = roof displacement due to different initial prestress forces, $T_{1i}$ and $T_{2i}$;
$\Delta_s$ = maximum roof displacement demand for the survival level ground motion;
$\Delta_{Sj}$ = displacement of floor i due to elastic shear deformations;
$\Delta_v$ = gap opening displacement along base of a panel at location of post-tensioning steel centroid on tension side;
$\Delta_r$ = roof displacement;
$\delta_{all}$ = allowable story drift;
$\delta_d$ = maximum story drift demand for the design level ground motion;
$\delta_{xe}$ = story drift;
$\varepsilon_{cu}$ = ultimate compressive strain of spiral confined concrete;
$\varepsilon_{pi}$ = initial strain in the post-tensioning steel;
$\varepsilon_{pl}$ = linear limit strain on the stress-strain relationship of the post-tensioning steel;
$\varepsilon_{pu}$ = strain corresponding to the ultimate stress on the stress-strain relationship of the post-tensioning steel;
$\rho_{sp}$ = volumetric ratio of spiral reinforcement;

$\Phi_f$ = ACI 318 capacity reduction factor;
$\Phi_{gc}$ = initial prestress reduction factor.

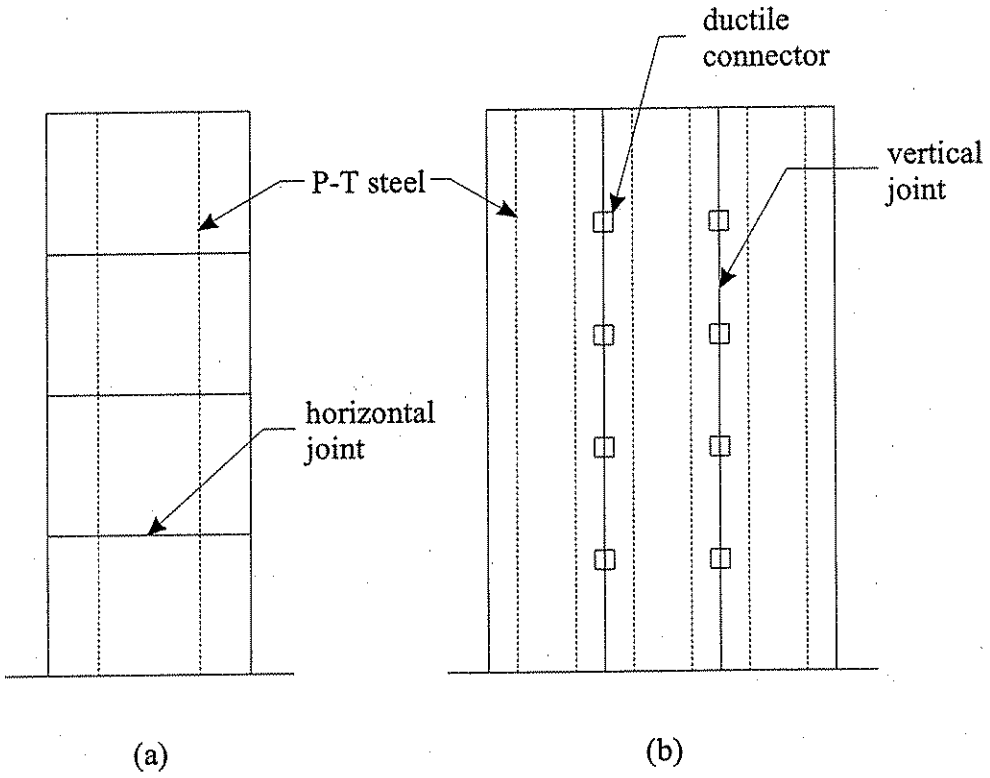


Figure 1 Unbonded post-tensioned walls: (a) with horizontal joints; (b) with vertical joints and ductile connectors.

# CHAPTER 2

# BACKGROUND

This chapter presents background information relevant to the current study. Section 2.1 gives a brief description of unbonded post-tensioned construction. Section 2.2 reviews previous research on unbonded post-tensioned precast concrete walls. Section 2.3 describes a wall composed of precast panels attached to each other along vertical joints with ductile connectors and attached to the foundation along horizontal joints with unbonded post-tensioning steel. Previous work on vertical joint connectors is presented in Section 2.4. Section 2.5 defines the wall parameters and the forces considered in the derivations presented in Chapter 3.

## 2.1 UNBONDED POST-TENSIONED CONSTRUCTION

In unbonded post-tensioned construction, post-tensioning steel is placed in ducts which remain ungrouted after the steel is prestressed. This lack of grout eliminates the opportunity for the post-tensioning steel to bond and thus achieves strain compatibility with the surrounding concrete. As a result, the behavior of unbonded post-tensioned members differs from that of bonded post-tensioned members. For a bonded post-tensioned member, an assumption of strain compatibility between the post-tensioning steel and the adjacent concrete is often made. Thus, the change in strain in the post-tensioning steel is assumed to be the same as the change in strain in the concrete adjacent to the steel. However, for an unbonded post-tensioned member, strain compatibility between the post-tensioning steel and the adjacent concrete does not exist. Instead, the change in strain in the post-tensioning steel is assumed uniform over the unbonded length of the steel and equal to the average change in strain in the concrete adjacent to the post-tensioning steel over the unbonded length. As a result, in unbonded post-tensioned construction, the steel reaches the yield point at larger overall member deformations as compared to that in bonded post-tensioned construction (Kurama et al. 1996).

## 2.2 PREVIOUS RESEARCH ON UNBONDED POST-TENSIONED PRECAST CONCRETE WALLS

Precast concrete walls can have the following configurations: (1) *simple walls* consisting of vertical stacks of (generally) one-story high wall panels with horizontal connections only; (2) *composite* or *coupled walls* consisting of simple walls in the same plane joined together by vertical joint connectors or coupling beams; and (3) *flanged walls* consisting of simple walls at right angles joined together by vertical connections. Kurama et al. (1996, 1997) performed an analytical study on the seismic behavior and design of simple walls made of precast concrete panels joined together along horizontal joints with unbonded post-tensioning. A drawing of this type of construction was shown earlier in Figure 1(a). The behavior of a properly designed wall of this type is gap opening along the horizontal joints and axial-flexural compression deformation in the wall panels, with no shear slip along the connections and little shear deformation in the panels. Gap opening along the horizontal connections in unbonded post-tensioned precast walls and axial-flexural deformations in the wall panels can be accurately modeled using the fiber beam-column element in the DRAIN-2DX program (Prakash

and Powell 1993). The analytical model requires only the wall geometry and uniaxial stress-strain relationships for concrete and post-tensioning steel. A parametric study performed by Kurama et al. (1996) using this model indicates that the base shear and lateral displacement capacity, and the lateral stiffness of unbonded post-tensioned precast walls can be controlled by design and detailing. For example, the base shear capacity of an unbonded post-tensioned precast wall depends on the total area of the post-tensioning steel, cross-sectional dimensions of the wall, and axial load due to gravity. Kurama et al. (1996) found that the lateral displacement capacity of an unbonded post-tensioned precast wall corresponding to the beginning of nonlinear behavior in the post-tensioning bars can be controlled by the unbonded length, and the location of and the initial stress in the post-tensioning steel. The lateral displacement capacity corresponding to failure of the wall as a result of crushing of the concrete confined by spiral reinforcement depends on the initial stress in the concrete and the amount of spiral reinforcement.

Kurama et al. (1997) provide a seismic design approach for unbonded post-tensioned walls that was developed using the seismic load demands recommended by current model building codes. With this design approach, stiff walls can be designed to soften and satisfy estimated nonlinear displacement demands under code specified "design" level ground motions without yielding in the post-tensioning steel or significant damage in the wall panels. Furthermore, under "survival" level ground motions, these walls can be designed to satisfy the displacement demands without shear slip along the horizontal connections, fracture of the post-tensioning steel, or axial-flexural compression failure in the wall panels.

Kurama et al. (1997) also investigated the seismic response of various unbonded post-tensioned precast concrete walls. A series of natural and artificial ground motions were considered. Results of nonlinear dynamic time-history analyses show that under "design" level ground motions, the response of walls designed using this design approach is essentially nonlinear elastic with little energy dissipation and little damage in the walls. Furthermore, walls designed using this approach survived the "survival" level ground motions with damage, but with only small residual lateral displacements.

## 2.3 PRECAST WALLS WITH DUCTILE VERTICAL JOINT CONNECTORS

Figure 2.1 shows a precast concrete wall composed of full-height precast concrete panels that are attached to each other along vertical joints with ductile connectors (referred to as vertical joint connectors). The vertical joint connectors may consist of steel components which are intended to provide a force transfer between panels that comprise the wall, and also to provide ductility and energy dissipation under seismic loading. The vertical joint connector considered in this study is identified in Section 2.4. The wall shown in Figure 2.1 has a horizontal joint located between the base of each panel and the foundation. The panel-to-foundation connection is achieved by using post-tensioning steel that is anchored at the foundation and at the top of each panel. The post-tensioning steel is unbonded over the entire height of the panels because, as discussed in Section 2.1, unbonded construction improves the behavior of precast walls when subjected to lateral loads as compared to bonded construction.

## 2.4 PREVIOUS RESEARCH ON VERTICAL JOINT CONNECTORS

Schultz and Magaña (1996) studied a number of connection details for precast concrete shear walls. The connection details included seven vertical joint connections and four horizontal joint connections. The vertical joint connections, shown in Figure 2.2, consisted of a slotted flexure plate (SFP), inclined flat bar (IFB), X-shaped axial plate (XAP), pinned tension strut (PTS), vertical joint friction (VJF), U-shaped flexure plate (UFP), and a notched shear plate (NSP) connection. The SFP, IFB, XAP, and NSP connection details were modifications of the commonly-used welded loose plate connections, while the PTS, VJF, and UFP connections relied on bolting or a combination of bolting and field welding. These connection details incorporated either flexural yield, tension/compression yield, shear yield, or friction sliding/coulomb friction concepts. The NSP detail, classified as a shear yielding connection, demonstrates stable force-displacement hysteresis with good energy dissipation, as shown in Figure 2.3. Thus, the ductile vertical joint connectors considered in this analytical study consist of four notched shear plates distributed along the height of each of the vertical joints between panels in the wall.

## 2.5 WALL PARAMETERS

As shown in Figure 2.4 a typical wall is comprised of numerous panels and floor levels. The letter k represents the panel number, which ranges from 1 to n, where n is the total number of panels in a wall. The letter i represents the floor level, which ranges from 1 to r. Thus, r defines the total number of floor levels supported by a wall. The length along the base of each panel is denoted by $l_x$. It is assumed that all panels have equal lengths. Therefore, the length along the base of the wall, $l_w$, is the product of n and $l_x$. $H_w$ and $t_w$ are the height and thickness of the wall, respectively, which are the same for all panels.

As shown in Figure 2.5, the height of each floor level, $H_i$ can be expressed as a fraction of the total wall height, $H_w$ by

$$H_i = r_{H_i} \cdot H_w \tag{2.1}$$

where $r_{Hi}$ is the ratio of the height of floor level i to the wall height. The height of the roof level, $H_r$ is calculated using Equation 2.1 with i = r. Since the height of the roof level is the height of the wall, $r_{Hr} = 1$ and $H_r = H_w$ as shown in Figure 2.5.

Figure 2.4 also shows the various forces that act on each panel. These forces are: (1) external lateral loads applied at each floor level and at the roof ($F_{k,i}$ and $F_{k,r}$); (2) a base shear force acting along the base, resisting the lateral loads ($V_k$); (3) an axial gravity force ($N_k$); (4) post-tensioning forces ($T_1$ and $T_2$); (5) a concrete compression stress resultant at the base ($C_k$); and (6) the total shear force that is transferred into the panel across the vertical joint connectors ($P_j$). Each of these forces are described more fully below.

In Figure 2.4, the lateral force acting at an arbitrary level of a given panel is defined as $F_{k,i}$ where k is the panel number ranging from 1 to n, and i is the floor level ranging from 1 to r. This notation is used because the floor and roof lateral loads may be different for each panel.

Figure 2.5 shows that the lateral force acting on the wall at the roof level, $F_{w,r}$ is expressed as the sum of the panel forces at that level, $\Sigma F_{k,r}$ where k=1 to n. As shown in Figure 2.6, $F_{w,r}$ is expressed as a fraction of the total base shear of the wall, $V_w$ by

$$F_{w,r} = r_{Fr} \cdot V_w \tag{2.2}$$

where $r_{Fr}$ is the percent of the total base shear applied at the roof level. The base shear of the wall, $V_w$ is equal to the sum of the panel base shears, $\Sigma V_k$ where k=1 to n (Figure 2.5). Similarly, the lateral force on the wall at floor level i can be expressed as

$$F_{w,i} = r_{Fi} \cdot V_w \tag{2.3}$$

where $r_{Fi}$ is the percent of the total base shear applied at floor level i (Figure 2.6).

As shown in Figure 2.4, the axial gravity force on a panel is $N_k$. This force acts at an eccentricity $e_{Nk}$ measured from the right edge of the panel. The axial gravity force and the eccentricity may vary for each panel.

$T_1$ and $T_2$ in Figure 2.4 are the post-tensioning forces acting on groups of post-tensioning steel toward the left edge and toward the right edge of each panel, respectively. When a panel is post-tensioned, a tension force is applied to the post-tensioning steel. After the anchorages are engaged, the initial prestress force in the steel is transferred to the concrete panel as compression. This compression causes elastic shortening of the concrete and a loss of prestress force in the post-tensioning steel. After the axial (gravity) load is applied to the panel, additional shortening occurs, resulting in a further reduction of the initial prestress force. Thus, the initial prestress force after elastic shortening of the concrete due to post-tensioning and gravity load occurs is denoted by $T_{1i}$ and $T_{2i}$ for the group of post-tensioning steel toward the left edge and toward the right edge of each panel, respectively. Note that in Figure 2.4 the prestress forces are different for groups of post-tensioning steel in a panel, but are the same for a given group in all panels. The two groups of post-tensioning steel in a panel are a distance of $2e_p$ apart, where $e_p$ is the eccentricity of the post-tensioning steel measured from the centerline of the panel to the centroid of the group of steel. The eccentricity of post-tensioning steel is assumed to be constant for all panels.

The concrete compression stress resultant acting at the base of each panel is defined by $C_k$ as shown in Figure 2.4. The concrete compression stress resultant after elastic shortening due to post-tensioning and gravity load, but prior to the application of lateral loads on a panel, is defined as $C_{ki}$. The depth of the compression block at the base of the panel is $c_k$.

Lastly, Figure 2.4 shows the total shear force that is transferred into the panel across the vertical joint connectors is denoted by $P_j$.

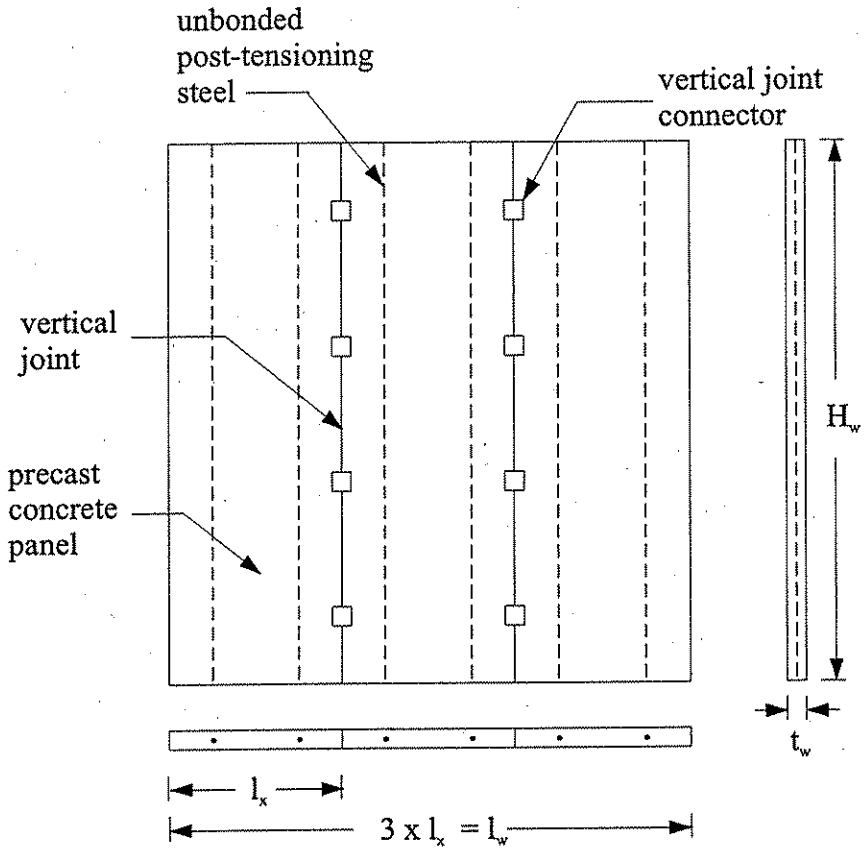


Figure 2.1 Precast wall with vertical joints between panels and vertical joint connectors.

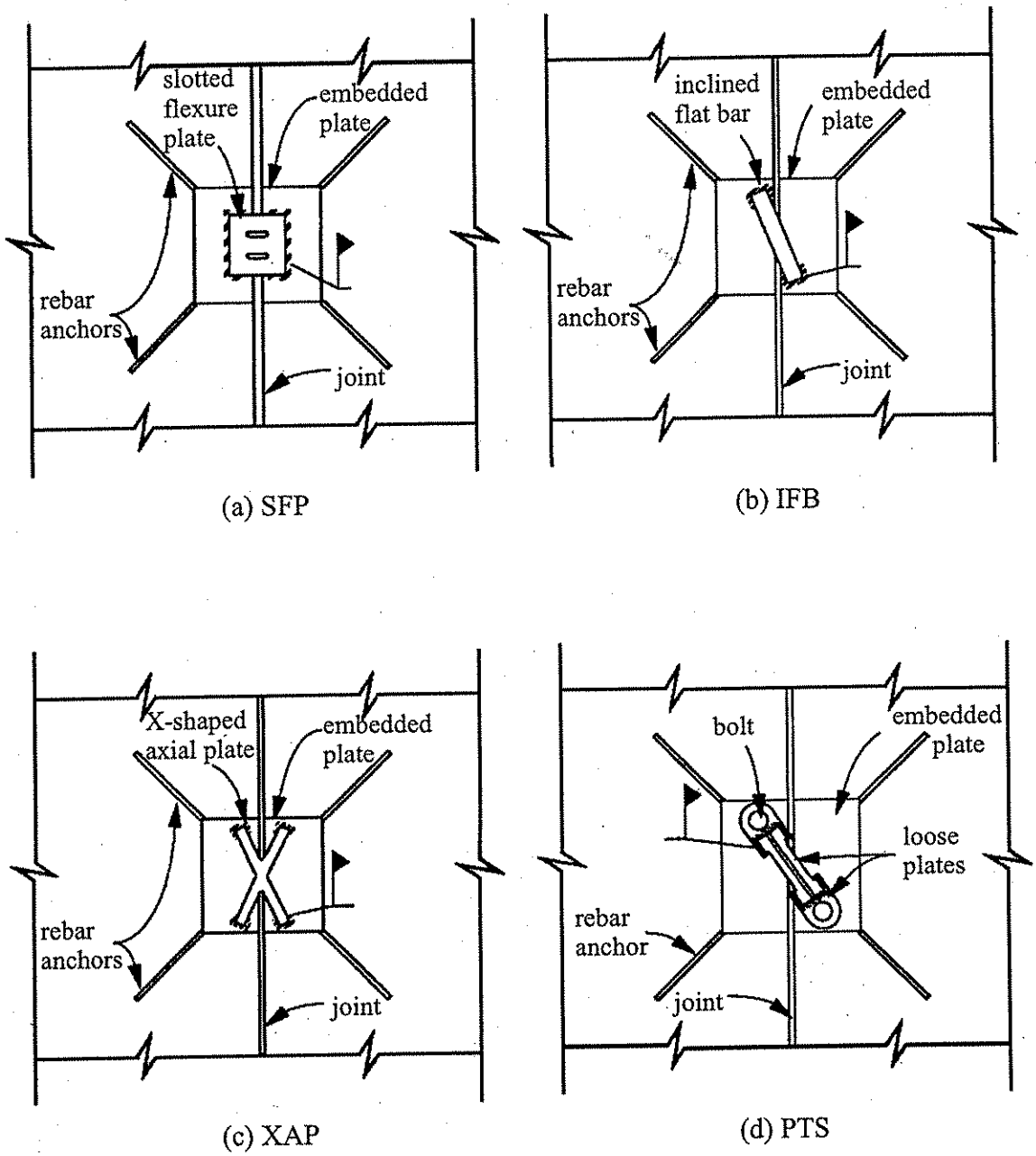


Figure 2.2 Vertical joint connectors studied by Schultz and Magaña (adapted from Shultz and Magaña, 1996).

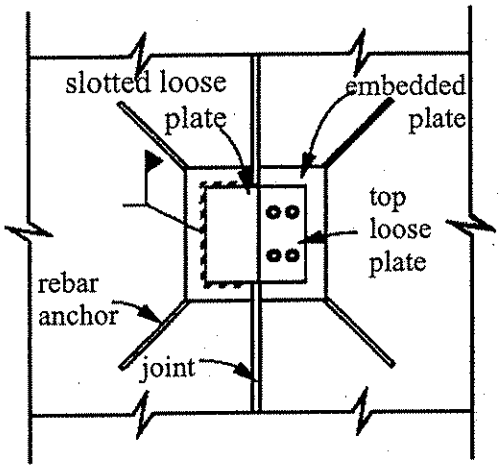


(e) VJF

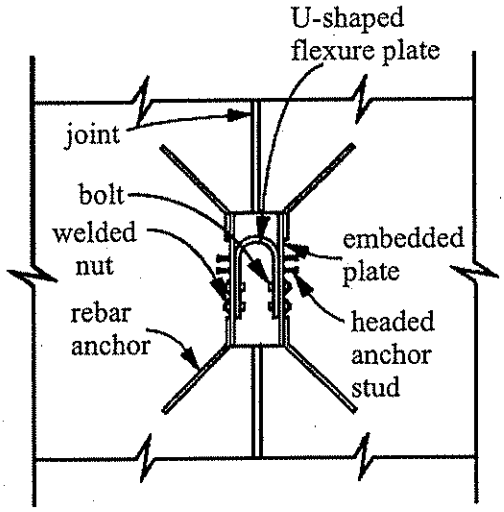


(f) UFP

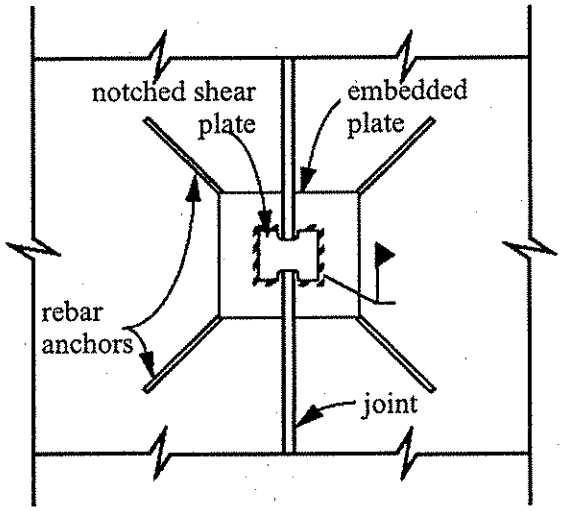


(g) NSP

Figure 2.2 (continued) Vertical joint connectors studied by Schultz and Magaña (adapted from Shultz and Magaña, 1996).

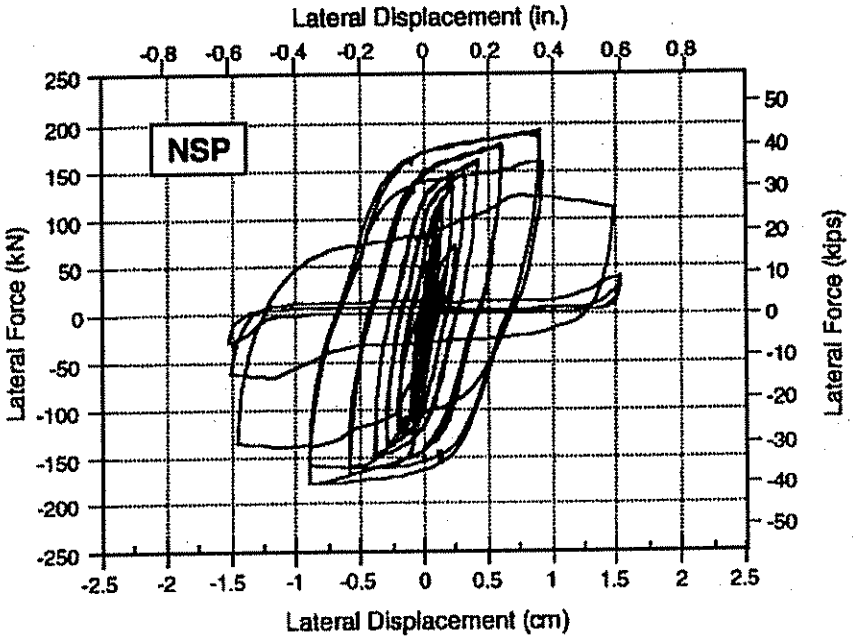


Figure 2.3 Force-displacement hysteresis of detail NSP (adapted from Shultz and Magaña, 1996).

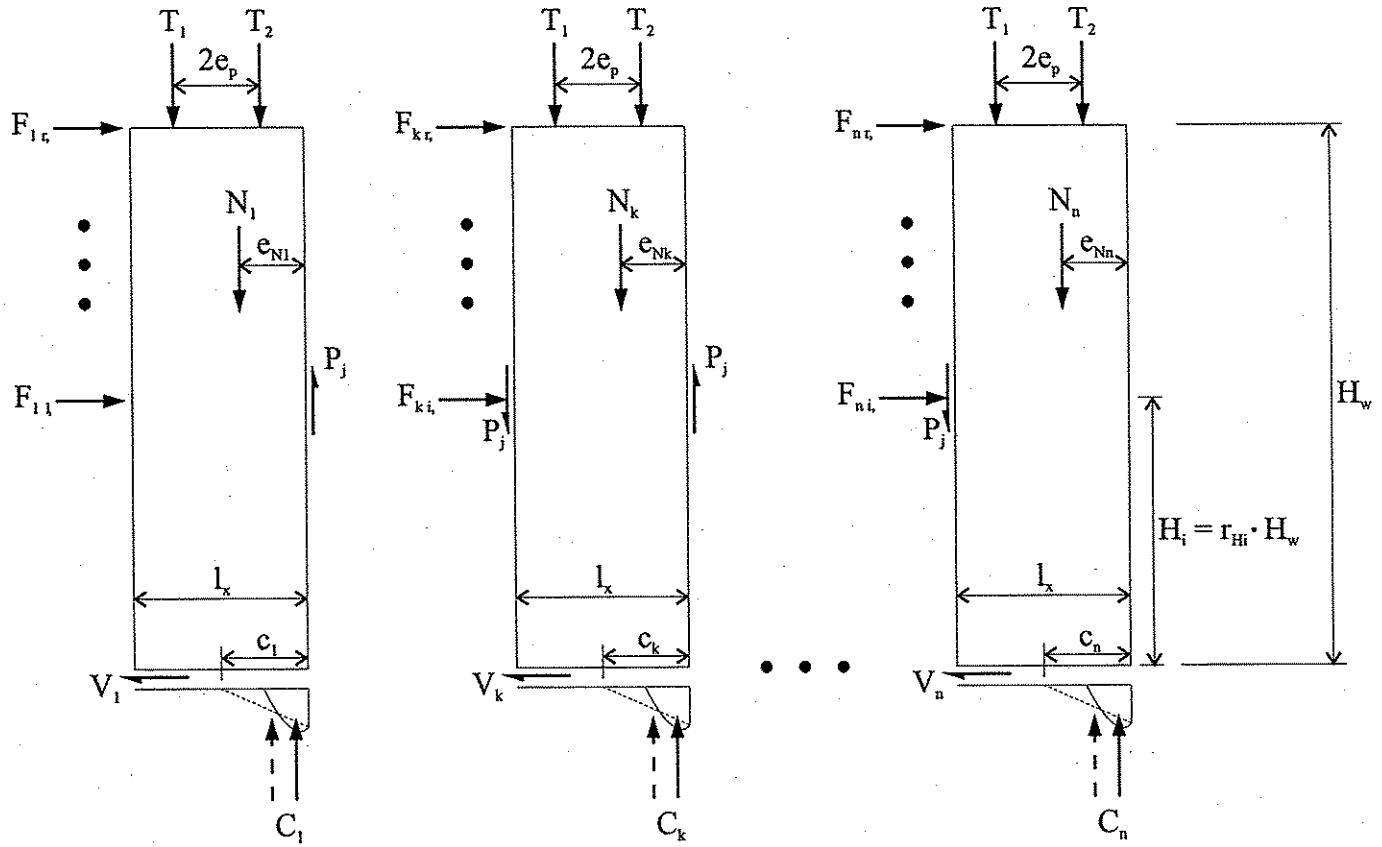


(a) left exterior panel (b) arbirary interior panel (c) right exterior panel

Figure 2.4 Forces on each panel of an unbonded post-tensioned precast concrete wall.

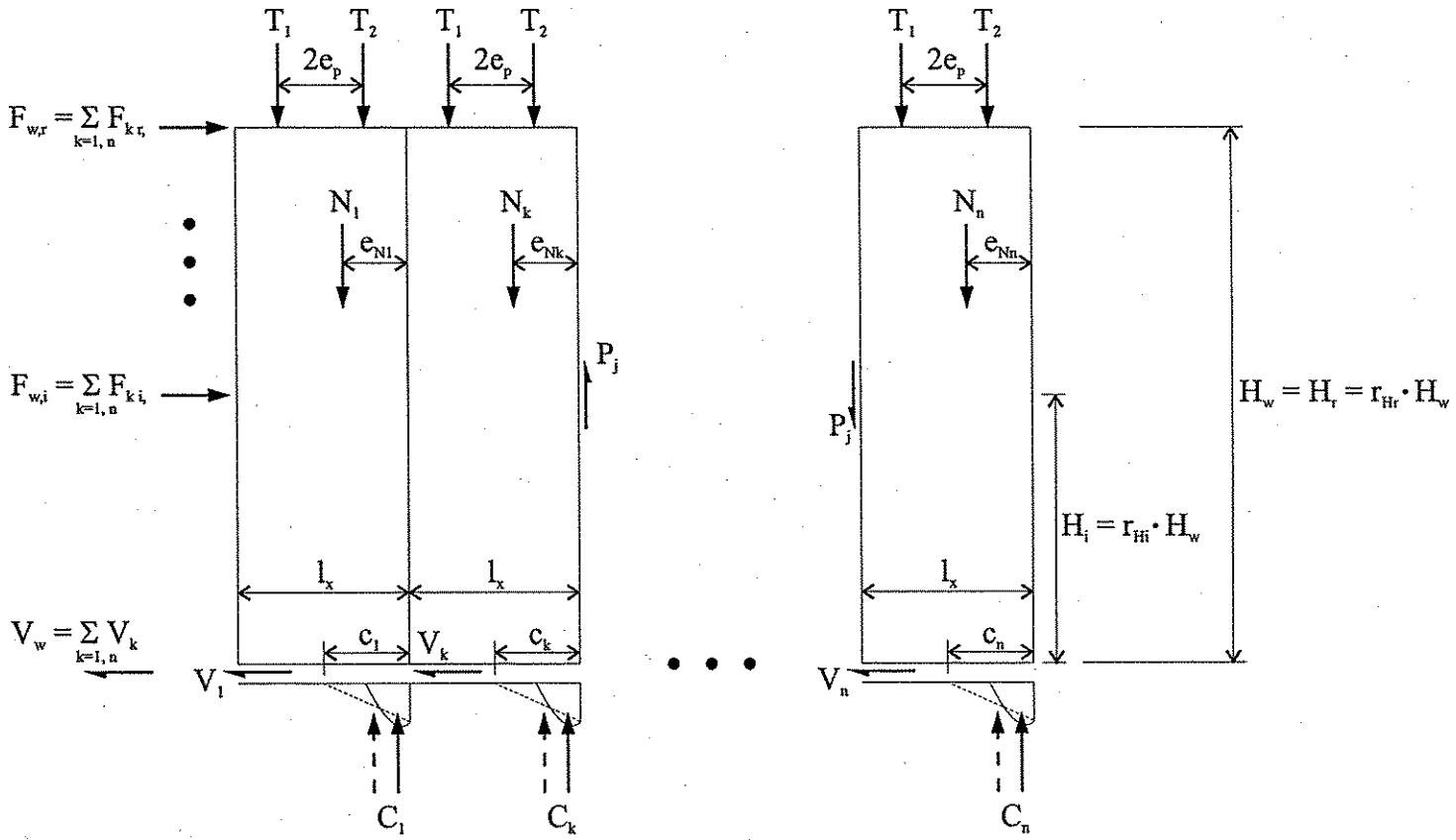


(a) left exterior and arbitrary interior panels (b) right exterior panel

Figure 2.5 Forces on an unbonded post-tensioned precast concrete wall with multiple panels.

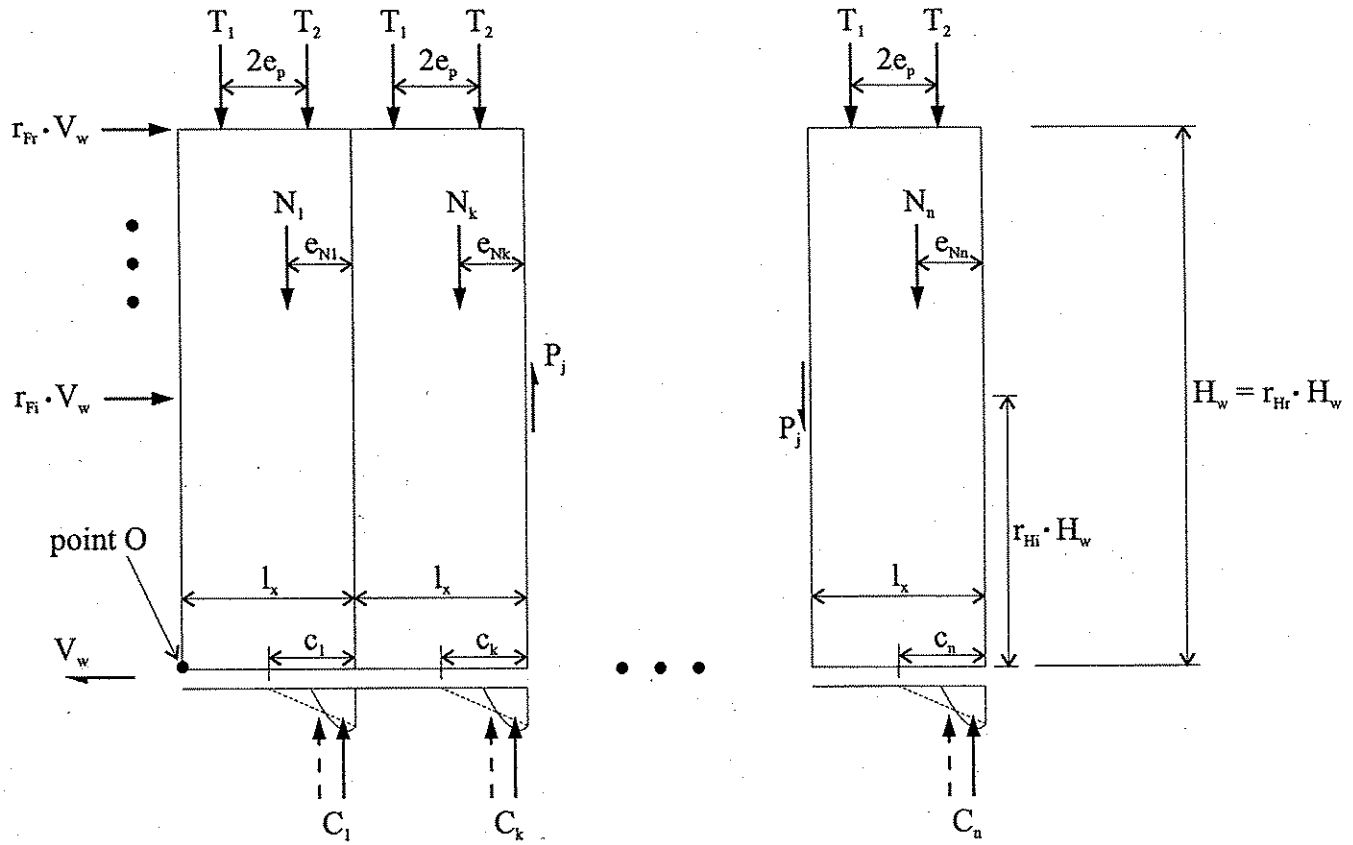


(a) left exterior and arbitrary interior panels (b) right exterior panel

Figure 2.6 Forces on an unbonded post-tensioned precast concrete wall with multiple panels.

# CHAPTER 3

# EXPECTED LATERAL LOAD BEHAVIOR OF UNBONDED POST-TENSIONED PRECAST WALLS

This chapter describes the expected lateral load behavior of an unbonded post-tensioned precast wall with vertical joints and ductile vertical joint connectors. As explained in Section 3.1, the expected lateral load behavior can be idealized as a tri-linear plot of base shear versus roof displacement. Section 3.1 presents this tri-linear idealization. Closed-form expressions to estimate the various base-shear-roof-displacement capacities that define the key points on this tri-linear idealization are derived in Section 3.2. Section 3.3 presents an evaluation of the accuracy of the base-shear-roof-displacement idealization.

## 3.1 TRI-LINEAR IDEALIZATION OF THE BASE-SHEAR-ROOF-DISPLACEMENT BEHAVIOR

This section presents the tri-linear idealization of the base-shear-roof-displacement behavior of an unbonded post-tensioned precast wall with ductile vertical joint connectors.

### 3.1.1 Structure limit states

Design of a building structure requires consideration of different limit states for the members and connections of the structure. A limit state is defined by a level of force (stress) or deformation (strain) in the structural member or connection, and may be considered to represent a level of damage in the member or connection. Each limit state has a corresponding force or deformation value.

The limit states considered for the unbonded post-tensioned precast concrete wall described in Chapter 2 are introduced using the idealized base-shear-roof-displacement relationship of the wall under monotonic lateral load shown in Figure 3.1. The limit states are: (1) decompression at the base of the wall; (2) yielding of vertical joint connectors; (3) significant reduction in lateral stiffness (i.e., softening) due to gap opening in flexure along the panel-to-foundation connections; (4) yielding of post-tensioning steel; (5) peak base shear; (6) loss of prestress under cyclic lateral load due to inelastic straining of post-tensioning steel; and (7) crushing of spiral confined concrete. These limit states are described below. Limit states 3, 4, and 7 define the key points on the idealized base-shear-roof-displacement relationship shown in Figure 3.1.

*Decompression*

Decompression at the base of the wall occurs when the overturning moment at the base of the wall results in decompression of part of the wall. Decompression is accompanied by the initiation of gap opening along the panel-to-foundation connection. Since the wall is comprised of multiple panels, decompression of the wall is defined as the first occurrence of decompression of any wall panel. Under a specified lateral load distribution (e.g. triangular), decompression of the wall can be related to a specific level of base shear and roof displacement, $V_{dec}$ and $\Delta_{dec}$ respectively.

*Yielding (linear limit) of vertical joint connectors*

The walls treated in this study employ ductile vertical joint connectors that are made of steel. Yielding of the vertical joint connectors occurs when the maximum strain in the connectors reaches the linear limit strain of the steel. The base shear and roof displacement corresponding to the linear limit strain of the vertical joint connectors are designated $V_{llj}$ and $\Delta_{llj}$ respectively.

*Significant reduction in lateral stiffness - effective linear limit*

The point on the base-shear-roof-displacement response of the wall when the lateral stiffness of the wall begins to reduce significantly is called the effective linear limit. This reduction in lateral stiffness (called softening) is caused by significant gap opening along the panel-to-foundation connections. The base shear and roof displacement corresponding to the effective linear limit are denoted as $V_{ell}$ and $\Delta_{ell}$ respectively. Softening usually occurs in a smooth and continuous manner in a precast wall with unbonded post-tensioned horizontal joints which open in flexure (Kurama et al. 1996). Hence, the term *effective* linear limit is used to describe this point on the base-shear-roof-displacement relationship.

*Yielding (linear limit) of post-tensioning steel*

Yielding of the post-tensioning steel occurs when the maximum strain in the steel reaches the linear limit of the steel. For the walls considered in this study, the post-tensioning steel in all the panels does not yield simultaneously. Thus, the linear limit strain of post-tensioning steel is defined as the first occurrence of yielding in the post-tensioning steel. The base shear and roof displacement corresponding to the linear limit strain of the post-tensioning steel are denoted as $V_{llp}$ and $\Delta_{llp}$ respectively. Due to unbonding, the linear limit strain of post-tensioning steel is usually reached after the effective linear limit of the base-shear-roof-displacement relationship is reached (and thus after significant softening in the base-shear-roof-displacement relationship occurs) (Kurama et al. 1996).

*Peak base shear*

The base shear capacity is the peak base shear resistance of the wall. For walls considered in this study, the base shear capacity is intended to be controlled by axial-flexural behavior at the base of the walls, rather than by shear sliding. Thus, at this limit state, the overturning capacity of a wall controls the base shear capacity. The idealized base-shear-roof-displacement relationship shown in Figure 3.1 neglects strain hardening effects in the post-tensioning steel. As a result, the base shear capacity of the wall is reached at the last occurrence of yielding in the post-tensioning steel. It is assumed that the base shear at the last occurrence of yielding in the post-tensioning steel is very close to the base shear at the first occurrence of yielding in the post-tensioning steel. Therefore, the peak base shear corresponds to $V_{llp}$, and the corresponding roof displacement is denoted as $\Delta_{llp}$.

*Loss of prestress*

Prestress in an unbonded post-tensioned wall subjected to cyclic lateral load can be reduced when the linear limit strain of the post-tensioning steel is exceeded. This is illustrated in Figure 3.2, which shows a typical prestressing steel stress-strain relationship. Let the initial

stress in the steel be $f_{pi}$. As long as the steel strain remains in the linear-elastic range during cyclic lateral loading of the wall, no loss of prestress will result (ignoring inelastic deformations which may occur in the concrete in a highly-stressed wall). If the steel strain exceeds the elastic limit, such as point 2 in Figure 3.2, some prestress will be lost after the lateral load is removed, since the steel follows an elastic unloading path parallel to the initial elastic path as it unloads from point 2. Hence, after the lateral load is removed from the wall, the prestress is reduced from $f_{pi}$ to a residual value $f_{pr}$. Upon unloading from an even larger inelastic strain, such as point 3 in Figure 3.2, the entire prestress may be lost.

***Crushing of spiral confined concrete***

Crushing of spiral confined concrete occurs when the ultimate compressive strain of the spiral confined concrete is reached. Based on the concrete confinement model developed by Mander et al. (1988a, 1988b), crushing of the spiral confined concrete occurs at an ultimate concrete compressive strain $\varepsilon_{cu}$ which is reached when the spiral reinforcement fractures. Significant loss of lateral load and gravity load resistance is expected to occur when crushing of the spiral confined concrete occurs. The base shear and roof displacement corresponding to crushing of the spiral confined concrete are denoted as $V_{csc}$ and $\Delta_{csc}$ respectively.

### 3.1.2 Idealized base-shear-roof-displacement behavior

Figure 3.1 shows the idealized base-shear-roof-displacement behavior of an unbonded post-tensioned precast concrete wall subjected to monotonic lateral load. As noted earlier, the trilinear idealization of the wall response is defined by three key structure limit states: the effective linear limit (ELL); yielding of the post-tensioning steel in tension (LLP); and crushing of spiral confined concrete (CSC).

## 3.2 ESTIMATION OF BASE-SHEAR-ROOF-DISPLACEMENT CAPACITIES

This section derives expressions which are used to estimate the base shear and roof displacement capacities corresponding to the points ELL and LLP in Figure 3.1. The expressions are derived for an unbonded post-tensioned precast wall with n panels, r stories, and eccentric axial forces as described in Chapter 2. In addition, the base shear and roof displacement capacities corresponding to points ELL and LLP in Figure 3.1 are derived for the specific case of the prototype wall (discussed in Chapter 5), which has three panels, two stories, and concentric axial forces.

### 3.2.1 Derivation of an expression to estimate the base shear corresponding to the effective linear limit state, $V_{ell}$

Figure 3.3(a) shows the total force in the post-tensioning steel, $P_i$ and the gravity load, N acting on a panel. $P_i$ is the force in the steel after shortening of the panel has occurred due to the post-tensioning and the application of gravity load. $C_i$ is the concrete compression stress resultant in equilibrium with $P_i$ and N. $P_i$ and N are assumed to remain constant in the development that follows. Hence, $C_i$ also remains constant.

Figure 3.3(b) shows the forces acting on a panel at decompression. The moment at the base of the panel when decompression begins is referred to as the decompression moment, $M_{dec}$.

Assuming a linear stress distribution exists in the region of contact between the panel and the base, the base moment is $2M_{dec}$ when the gap opening has propagated to the center of the panel (Figure 3.3(c)). Finally, for the idealized case of the compression resultant at the edge of the panel, the base moment is $3M_{dec}$ (Figure 3.3(d)).

Kurama et al. (1996) found that the effective linear limit of the base-shear-roof-displacement relationship of an unbonded post-tensioned precast wall with horizontal joints occurs when the base moment is between $2M_{dec}$ and $3M_{dec}$ (i.e., between the two distributions of stress shown in Figures 3.3(c) and 3.3(d). The linear limit is controlled by gap opening and/or concrete softening due to the bending moment at the base of the wall. Taking the effective linear limit due to gap opening at a base moment equal to $2.5M_{dec}$, and assuming a linear stress distribution at the base, the depth of the compression region is one fourth of the panel length ($0.25\ l_x$) (Figure 3.3(e)). This result can be applied to a precast wall with vertical joints and with a horizontal joint at the base which is reinforced with only unbonded post-tensioning steel (Figure 2.1).

Assuming that the depths of the compression regions of the middle panels, and the average depth of the compression regions of the two exterior panels are $0.25\ l_x$, and summing moments about the extreme tension edge of the base of the left exterior panel (point O in Figure 2.6) the base shear corresponding to the effective linear limit state, $V_{ell}$ can be estimated for a wall with n panels, r stories, and eccentric axial forces by

$$V_{ell} = \frac{A_{ell} + B_{ell} + \sum_{k=2,n-1} C_{ell_k}}{H_w \sum_{i=1,r} (r_{H_i} \cdot r_{F_i})} \tag{3.1}$$

where

$$A_{ell} = -T_1(\frac{l_x}{2} - e_p) - T_2(\frac{l_x}{2} + e_p) - N_1(l_x - e_{N_1}) + C_1(l_x - \frac{c_1}{3})$$

$$B_{ell} = -T_1\left[(n-1)l_x + \frac{l_x}{2} - e_p\right] - T_2\left[(n-1)l_x + \frac{l_x}{2} + e_p\right] - N_n\left(n \cdot l_x - e_{N_n}\right) + C_n\left(n \cdot l_x - \frac{c_n}{3}\right)$$

$$C_{ell_k} = -T_1\left[(k-1)l_x + \frac{l_x}{2} - e_p\right] - T_2\left[(k-1)l_x + \frac{l_x}{2} + e_p\right] - N_k\left(k \cdot l_x - e_{N_k}\right) + C_k\left(k \cdot l_x - \frac{c_k}{3}\right)$$

$$c_1 = \frac{l_x\sqrt{C_1}}{2\left(\sqrt{C_1} + \sqrt{C_n}\right)}$$

$$c_n = \frac{l_x\sqrt{C_n}}{2\left(\sqrt{C_1} + \sqrt{C_n}\right)}$$

$$c_k = \frac{l_x\sqrt{C_k}}{2\left(\sqrt{C_1} + \sqrt{C_n}\right)}$$

$$C_1 = N_1 + T_1 + T_2 - P_j$$

$C_n = N_n + T_1 + T_2 + P_j$

$C_k = N_k + T_1 + T_2$

$P_j = P_{llj}$

$T_1 = T_{1i}$

and $T_2 = T_{2i}$.

$A_{ell}$, $B_{ell}$, and $C_{ell_k}$ represent the sum of moments about point O in Figure 2.6 for the left exterior panel (panel 1), the right exterior panel (panel n), and an interior panel (panel k), respectively which, when added over all the panels, is in equilibrium with the overturning moment caused by the applied lateral loads. For a wall with one panel, $B_{ell}$ and $\Sigma C_{ell_k}$ are zero. For a wall with only two panels, $\Sigma C_{ell_k}$ is zero (no interior panels). A wall with three or more panels involves $A_{ell}$, $B_{ell}$, and $\Sigma C_{ell_k}$.

The following discussion explains how the term in the denominator of Equation 3.1 is derived. First, the lateral force on the wall at each floor level, $F_{w,i}$ (shown in Figure 2.5) is taken as the sum of the panel forces, $F_{k,i}$ on that floor level (Figure 2.4). The lateral force on the wall at each floor level is then expressed as a fraction of the total base shear of the wall, $V_w$ by Equation 2.3, where $V_w = V_{ell}$ (see Figure 2.6). Similarly, the total force on the wall at the roof level can be expressed as a fraction of the total base shear of the wall by Equation 2.2, where $V_w = V_{ell}$. The height of each floor level and the height of the roof level, measured from the base of the wall, are expressed as a fraction of the total wall height, $H_w$ by Equation 2.1, where i=1 to r and $r_{Hr}$=1. Summing moments about point O in Figure 2.6, the overturning moment caused by the applied lateral loads that is in equilibrium with $A_{ell}$, $B_{ell}$, and $\Sigma C_{ell_k}$ is written as

$$M_{ell} = \sum_{i=1,r} \left(H_w \cdot r_{H_i}\right) \cdot \left(r_{F_i} \cdot V_{ell}\right) \tag{3.2}$$

From equilibrium, Equation 3.2 is equal to the sum of $A_{ell}$, $B_{ell}$, and $\Sigma C_{ell_k}$. Thus, factoring $V_{ell}$ from Equation 3.2 and dividing through by the summation term yields Equation 3.1. As noted in Chapter 2, the value of $r_{Fi}$ in Equations 3.1 and 3.2 are determined from the vertical distribution of seismic forces as per NEHRP (1994).

In Equation 3.1, $T_1$ and $T_2$ are assumed to be equal to the initial prestressing force on the steel, $T_{1i}$ and $T_{2i}$, respectively, which are the same for all panels. $P_{llj}$ is the total shear force in the vertical joint connectors at linear limit strain. The forces in the connectors are assumed to be the connector yield force when the effective linear limit state of the wall due to gap opening is reached because at this state the gap at the tension side of the panels has opened significantly, producing relative vertical displacements between adjacent panels that are large enough to yield the connectors. Note that if vertical joint connectors with very large yield displacements are utilized, this assumption may not be valid.

For the prototype wall, which has two stories, and three panels having the same geometry, the same gravity forces N acting at the center of each panel, and the same forces $T_1$ and $T_2$ each equal to half the total initial prestress force on each panel, Equation 3.1 becomes

$$V_{ell} = \frac{l_x\left[\sqrt{C_1}\left(13P_{llj}+8C_2\right)+\sqrt{C_3}\left(11P_{llj}+8C_2\right)-\sqrt{C_2}\cdot C_2\right]}{6H_w\left[r_{H_1}\left(1-r_{F_r}\right)+r_{F_r}\right]\left(\sqrt{C_1}+\sqrt{C_3}\right)} \tag{3.3}$$

where

$C_1 = N + P_i - P_{llj}$

$C_2 = P_i + N$

and $C_3 = P_i + N + P_{llj}$.

$C_1$, $C_2$ and $C_3$ are the concrete compression resultants at the base of the left exterior panel (panel 1), the middle panel (panel 2), and the right exterior panel (panel 3), respectively, which are in static equilibrium with the axial force N, total prestress force on a panel $P_i$, and vertical joint yield shear force $P_{llj}$.

### 3.2.2 Derivation of an expression to estimate the roof displacement corresponding to the effective linear limit state, $\Delta_{ell}$

To derive an expression to estimate the roof displacement corresponding to the effective linear limit state, $\Delta_{ell}$, the wall is modeled as a cantilever beam subjected to lateral loads at each floor level along the height of the wall, and concentrated moments caused by eccentric axial forces. The uncracked elastic section properties of the wall are obtained by calculating the properties of one panel and multiplying them by the total number of panels, n in the wall. The resulting bending and shear deformations are then computed. The stiffness of the vertical joint connectors is assumed to be zero in the analysis because they are assumed to have yielded at $\Delta_{ell}$. Gap opening at the base of the wall is neglected, since $\Delta_{ell}$ is an estimate of the roof displacement at which gap opening begins to appreciably affect the lateral stiffness of the wall.

An elastic analysis of a wall with r stories, n panels of the same geometry with eccentric gravity load axial forces on each panel that can vary along the height of the wall, and lateral loads applied at each floor level gives the following estimation of the roof displacement corresponding to the effective linear limit state:

$$\Delta_{ell} = \Delta_{F_r} + \Delta_{S_r} + \Delta_{N_r} + \Delta_{P_r} \tag{3.4}$$

where

$$\Delta_{F_r} = \sum_{i=1,r} \frac{1}{2\cdot E_c \cdot I_w}\left(r_{F_i}\cdot V_{ell}\right)\left(r_{H_i}\cdot H_w\right)^2\left[H_w\left(1-\frac{1}{3}r_{H_i}\right)\right]$$

$$\Delta_{S_r} = \sum_{i=1,r} \frac{1}{G_c \cdot A'_w}\left(r_{F_i}\cdot V_{ell}\cdot r_{H_i}\cdot H_w\right)$$

$$\Delta_{N_r} = \sum_{i=1,r} \frac{1}{E_c \cdot I_w}\cdot M_{w,i}(r_{H_i}\cdot H_w)\cdot H_w\left(1-\frac{1}{2}r_{H_i}\right)$$

$$\Delta_{P_r} = \frac{n \cdot e_p (T_2 - T_1) \cdot H_w^{\,2}}{2 \cdot E_c \cdot I_w}$$

$T_1 = T_{1i}$
and $T_2 = T_{2i}$.

$\Delta_{Fr}$ is the roof deflection of the wall in flexure due to lateral forces. $\Delta_{Fr}$ is obtained using the principle of superposition (i.e., successively applying a concentrated lateral load, $r_{Fi} \cdot V_{ell}$, along the height of the wall and adding the corresponding roof deflections). The roof deflection of the wall due to elastic shear deformations, similarly obtained using the principle of superposition, is denoted as $\Delta_{Sr}$. $\Delta_{Nr}$ is the roof deflection of the wall in flexure due to the eccentric gravity load axial forces. The term $M_{w,i}$ in the $\Delta_{Nr}$ equation represents a concentrated wall moment at floor level i, which is derived using a wall as shown in Figure 2.4. The total gravity load of each panel, $N_k$ is represented by a gravity load at each floor level, $N_{k,i}$ and a gravity load at the roof level, $N_{k,r}$. The eccentricities at which the gravity loads are applied, $e_{Nk}$, measured from the right edge of the panels are the same along the height of a given panel, but may vary from panel to panel. The eccentric normal force at each level can be replaced by the normal force acting at the center of the panel, plus a concentrated moment measured positive in the clockwise direction. Summing all the panel concentrated moments due to eccentric gravity loads across all panels at a particular floor level yields a concentrated moment in the wall at that level. In general, the concentrated wall moment at floor level i is given by

$$M_{w,i} = \sum_{k=1,n} N_{k,i} \left( \frac{l_x}{2} - e_{N_k} \right) \tag{3.5}$$

Similarly, the concentrated wall moment at the roof level (level r) is given by

$$M_{w,r} = \sum_{k=1,n} N_{k,r} \left( \frac{l_x}{2} - e_{N_k} \right) \tag{3.6}$$

In Equation 3.4, $\Delta_{Pr}$ is the roof deflection of the wall caused by the application of different initial prestressing forces on the post-tensioning steel to the left and to the right of each panel, denoted by $T_{1i}$ and $T_{2i}$, respectively. The initial prestressing forces, $T_{1i}$ and $T_{2i}$, are the same for all panels. The moment produced by the unbalanced prestressing forces on a panel is added over the panels and is applied to the wall as a concentrated moment at the roof level because, since the post-tensioning steel is unbonded over the entire height of the wall, the wall is subjected to a constant moment over its entire height.

$V_{ell}$ in Equation 3.4 is found from Equation 3.1. $G_c$ is the shear modulus of concrete, $A'_w$ the effective shear area of the wall, $E_c$ the elastic modulus of concrete, and $I_w$ the second area moment of the uncracked transformed section of the wall.
Note that $V_{ell}$ is based on gap opening in flexure along the base of the wall, while $\Delta_{ell}$ is calculated from elastic deformations of the wall without considering gap opening. The estimate of $\Delta_{ell}$ is considered to be reasonable because the effect of gap opening on the lateral displacement of the wall is small until $V_{ell}$ is reached.

For the prototype wall described in Chapter 5, which has two stories, and three panels with the same geometry, the same gravity forces, N acting at the center of each panel, and the same forces $T_1$ and $T_2$ each equal to half the total initial prestress force on each panel, Equation 3.4 becomes

$$\Delta_{ell} = \Delta_{F_r} + \Delta_{S_r} \tag{3.7}$$

where

$$\Delta_{F_r} = \frac{1}{2 \cdot E_c \cdot I_w}\left[\left(1 - r_{F_r}\right) \cdot V_{ell}\left(r_{H_1} \cdot H_w\right)^2\left(H_w\left(1 - \frac{1}{3} r_{H_1}\right)\right) + \left(r_{F_r} \cdot V_{ell} \cdot H_w{}^2 \cdot \left(\frac{2}{3} H_w\right)\right)\right]$$

and $\Delta_{S_r} = \frac{1}{G_c \cdot A'_w}\left[\left(1 - r_{F_r}\right) \cdot V_{ell} \cdot r_{H_1} \cdot H_w + r_{F_r} \cdot V_{ell} \cdot H_w\right]$.

$\Delta_{Fr}$ is the roof deflection of the wall in flexure due to lateral forces and $\Delta_{Sr}$ is the roof deflection of the wall due to elastic shear deformations. $V_{ell}$ in Equation 3.7 corresponds to that computed from Equation 3.3.

### 3.2.3 Derivation of an expression to estimate the base shear corresponding to the linear limit strain of the post-tensioning steel, $V_{llp}$

Figure 2.4 shows the wall for which an expression is derived to estimate the base shear corresponding to the linear limit strain of the post-tensioning steel, $V_{llp}$. The wall consists of n panels, r floors, and eccentric axial forces, $N_k$. To derive an expression for $V_{llp}$, the lateral forces acting on each panel along the height (shown in Figure 2.4) are expressed as a fraction of the total base shear of the panel, $V_k$ where k = 1 to n, by Equation 2.3, where the term $V_w$ is replaced by $V_k$ (see Figure 3.4). Similarly, the total force on each panel at the roof level can be expressed as a fraction of the total base shear of the panel by Equation 2.2, where $V_w$ is replaced by $V_k$. It is assumed that $r_{Fi}$ is constant for all panels at a given floor level. The height of each floor level and the height of the roof level, measured from the base of the wall, are expressed as a fraction of the total wall height, $H_w$ by Equation 2.1, where i = 1 to r and $r_{Hr} = 1$.

The concrete compression stress resultant in each panel is assumed to be located at a distance $l_x/30$ from the right edge of each panel. Moment equilibrium is established for the panels by summing the moments about the compression edge of the base of each panel (point O for each panel in Figure 3.4). Next, the moment expressions for each of the panels are added together, replacing the sum of the panel shears at the base ($\Sigma V_k$, where k = 1 to n) with the base shear of the wall, $V_w$, which is denoted by $V_{llp}$ for this limit state. Solving for $V_{llp}$ yields the following estimate of the base shear corresponding to the linear limit strain of the post-tensioning steel:

$$V_{llp} = \frac{1}{H_w \sum_{i=1,r}\left(r_{H_i} \cdot r_{F_i}\right)}\left[A_{llp} + B_{llp} + \sum_{k=2,n-1} C_{llp_k}\right] \tag{3.8}$$

where

$$A_{llp} = \left(\frac{l_x + 2e_p}{2}\right)T_1 + \left(\frac{l_x - 2e_p}{2}\right)T_2 + e_{N_1} \cdot N_1 - \frac{l_x}{30}C_1$$

$$B_{llp} = \left(\frac{l_x + 2e_p}{2}\right)T_1 + \left(\frac{l_x - 2e_p}{2}\right)T_2 + e_{N_n} \cdot N_n + l_x \cdot P_j - \frac{l_x}{30}C_n$$

$$C_{llp_k} = \left(\frac{l_x + 2e_p}{2}\right)T_1 + \left(\frac{l_x - 2e_p}{2}\right)T_2 + e_{N_k} \cdot N_k + l_x \cdot P_j - \frac{l_x}{30}C_k$$

$$C_1 = N_1 + T_1 + T_2 - P_j$$

$$C_n = N_n + T_1 + T_2 + P_j$$

$$C_k = N_k + T_1 + T_2$$

$$P_j = P_{llj}$$

$$T_1 = T_{llp}$$

and $T_2 = T_{2i}$.

$A_{llp}$, $B_{llp}$, and $C_{llp_k}$ represent the sum of moments about the compression edge of the base of the left exterior panel (panel 1), the right exterior panel (panel n), and an interior panel (panel k), respectively which, when added over all the panels, is in equilibrium with the overturning moment caused by the applied lateral loads, defined by Equation 3.2 with $M_{ell}$ and $V_{ell}$ replaced by $M_{llp}$ and $V_{llp}$, respectively for this limit state.
For a wall with one panel, $B_{llp}$ and $\Sigma C_{llp_k}$ are zero. For a wall with only two panels, $\Sigma C_{llp_k}$ is zero (no interior panels). A wall with three or more panels involves $A_{llp}$, $B_{llp}$, and $\Sigma C_{llp_k}$.

In Equation 3.8, $C_1$, $C_n$, and $C_k$ are the concrete compression resultants at the base of the left exterior panel, the right exterior panel, and the middle panels, respectively. These forces are in static equilibrium with the axial force, $N_k$ where k = 1 to n, prestress forces, $T_1$ and $T_2$, and vertical joint shear force, $P_j$. $P_{llj}$ is the total shear force in the vertical joint connectors at linear limit strain. $T_{llp}$ represents the force in the post-tensioning steel when it reaches its linear-limit strain. $T_{2i}$ represents the initial prestressing force in the post-tensioning steel.

Under the set of lateral loads shown in Figure 3.4, the post-tensioning steel located toward the left face of the panels are at a tensile load of $T_{llp}$, while the steel toward the right face are assumed to remain at the initial prestress force, $T_{2i}$. Since $T_{llp}$ is larger than $T_{1i}$, the concrete compression stress resultants, $C_1$, $C_n$, and $C_k$ are larger in Equation 3.8 than in Equation 3.1.

For the prototype wall, composed of two-stories, three panels having the same geometry, and the same gravity forces, N acting at the center of each panel, the base shear corresponding to the linear limit strain of the post-tensioning steel, $V_{llp}$ is estimated by

$$V_{llp} = \frac{3\left(\frac{l_x + 2e_p}{2}\right)T_1 + 3\left(\frac{l_x - 2e_p}{2}\right)T_2 + 3\left(\frac{l_x}{2}\right)N + 2l_x \cdot P_j - 3\left(\frac{l_x}{30}\right)C_2}{H_w\left(r_{H_1} \cdot r_{F_1} + r_{H_r} \cdot r_{F_r}\right)} \qquad (3.9)$$

where

$C_2 = T_1 + T_2 + N$

$P_j = P_{llj}$

$T_1 = T_{llp}$

and $T_2 = T_{2i}$.

$C_2$ is the concrete compression resultant at the base of the interior panel (panel 2). $P_{llj}$, $T_{llp}$, and $T_{2i}$ were defined previously. As noted in Chapter 2, the values $r_{Fl}$ and $r_{Fr}$ in Equations 3.8 and 3.9 are determined from the vertical distribution of seismic forces as per NEHRP (1994).

### 3.2.4 Derivation of an expression to estimate the roof displacement corresponding to the linear limit strain of the post-tensioning steel, $\Delta_{llp}$

Consider an unbonded post-tensioned precast concrete panel shown in Figure 2.4. After the application of post-tensioning and gravity force, the panels undergo elastic shortening. The initial prestress levels in the post-tensioning at this point are denoted as $f_{pi}$. When the panel is displaced horizontally at the roof level to its effective linear limit state ($\Delta_{ell}$), the stresses in the post-tensioning steel on the tension side are assumed to remain at $f_{pi}$. Displacing the roof beyond $\Delta_{ell}$ results in gap opening along the base of the panel until the post-tensioning steel yields. Thus, the roof displacement when the post-tensioning steel reaches the linear limit strain is expressed as

$$\Delta_{llp} = \Delta_{ell} + \Delta_{go} \tag{3.10}$$

where $\Delta_{go}$ is the roof displacement due to gap opening at the base of the panel. $\Delta_{ell}$ is computed from Equation 3.4 and $\Delta_{go}$ is computed as follows:

$$\Delta_{go} = \frac{2H_w{}^2\left(f_{pl} - f_{pi}\right)}{E_p\left(l_x + 2e_p\right)} \tag{3.11}$$

$E_p$ is the modulus of elasticity of the post-tensioning steel and $f_{pl}$ is the stress corresponding to the linear limit strain on the stress-strain relationship of the post-tensioning steel. Equation 3.11 is developed by establishing a kinematic relationship between the horizontal displacement of a panel at the roof level ($\Delta_{go}$) and the vertical displacement at the location of the post-tensioning steel at the tension face of the panel ($\Delta_v$) as the panel pivots rigidly about a lower corner point. $\Delta_v$ is expressed as the product of the wall height and the change in strain in the post-tensioning steel.

## 3.3 EVALUATION OF THE BASE-SHEAR-ROOF-DISPLACEMENT IDEALIZATION

The accuracy of the tri-linear base-shear-roof-displacement idealization is briefly examined here by comparing the response parameters estimated for the prototype wall, using this idealization, to analytical results from a fiber model of the same wall. The fiber model was created using the DRAIN-2DX program (Prakash and Powell 1993). Further comparisons between the estimated values that define key points on the tri-linear response and the fiber

model results are presented in Chapter 7. The prototype wall treated in the comparison presented here has three panels, two stories, and concentrically applied axial loads. The prototype wall is described in Chapter 5, and the fiber model of the wall is explained in detail in Chapter 6.

Figure 3.5 compares the base-shear-roof displacement response of the prototype wall obtained from the fiber model analysis to the tri-linear idealization (shown as a dotted line). Figure 3.5 shows that the tri-linear idealization provides a good approximation of the key response parameters of the wall. The effective linear limit point (ELL) is accurately positioned where the lateral stiffness of the wall begins to reduce significantly due to gap opening along the panel-to-foundation connections. In addition, the point corresponding to the linear limit strain of the post-tensioning steel (LLP) is in good agreement with the fiber model prediction of the first occurrence of yielding in the post-tensioning steel. Chapter 7 presents an evaluation of the influence of several design parameters on the behavior of the prototype wall under monotonic lateral loads. In this design parameter study, parameters including the total shear area of connectors across each vertical joint, initial stress in post-tensioning, and area of post-tensioning steel are varied over a range of values to gain insight into the impact of these parameters on the response of the wall. Comparisons are made in Chapter 7 between the estimated capacities, computed using the closed-form expressions derived in this chapter, and the fiber model results for the different cases considered.

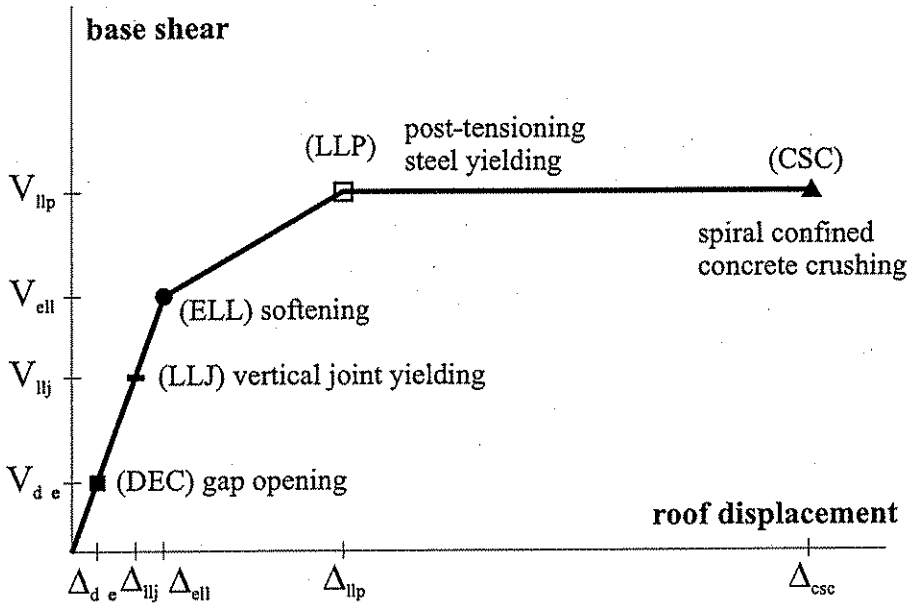


Figure 3.1 Structure limit states.

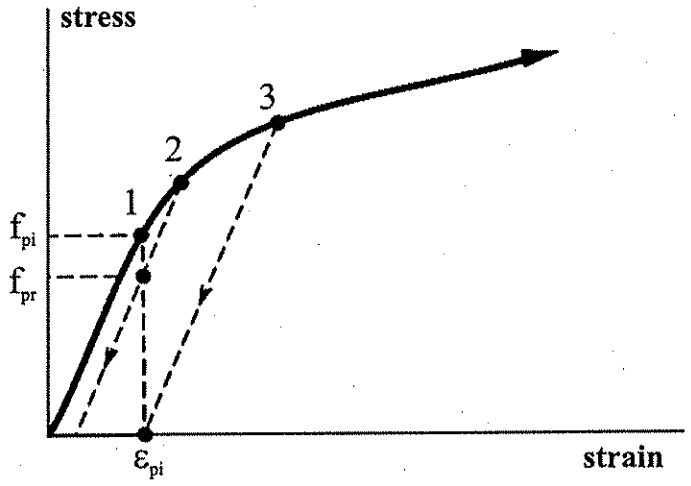


Figure 3.2 Prestress loss due to inelastic response (Kurama et al. 1997).

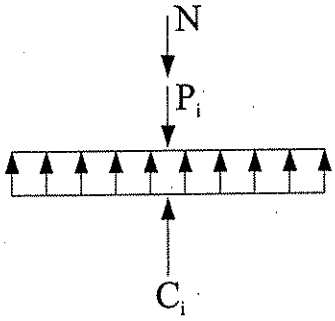


(a) stress distribution before application of lateral load

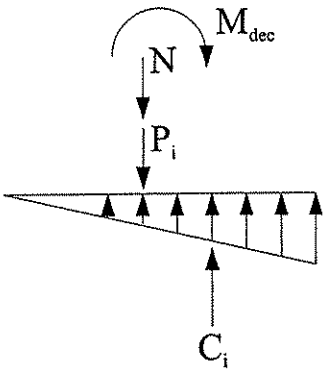


(b) stress distribution at $M_{dec}$

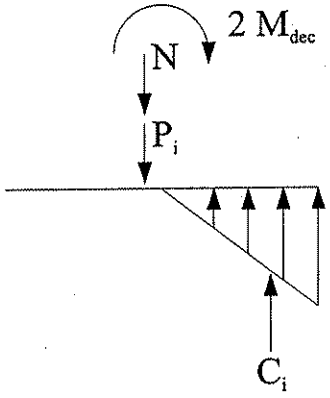


(c) stress distribution at $2M_{dec}$

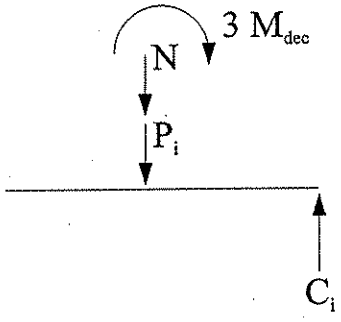


(d) stress distribution at $3M_{dec}$

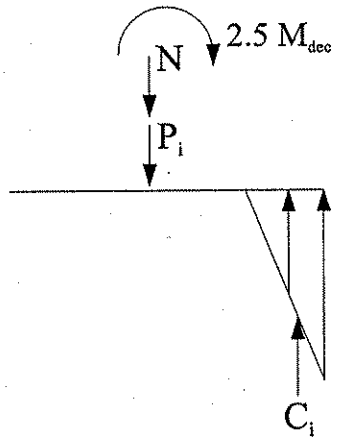


(e) stress distribution at 2.5 $M_{dec}$ (ELL)

Figure 3.3 Stress distribution at the base of a panel at different loading stages (adapted from Kurama et al. 1997).

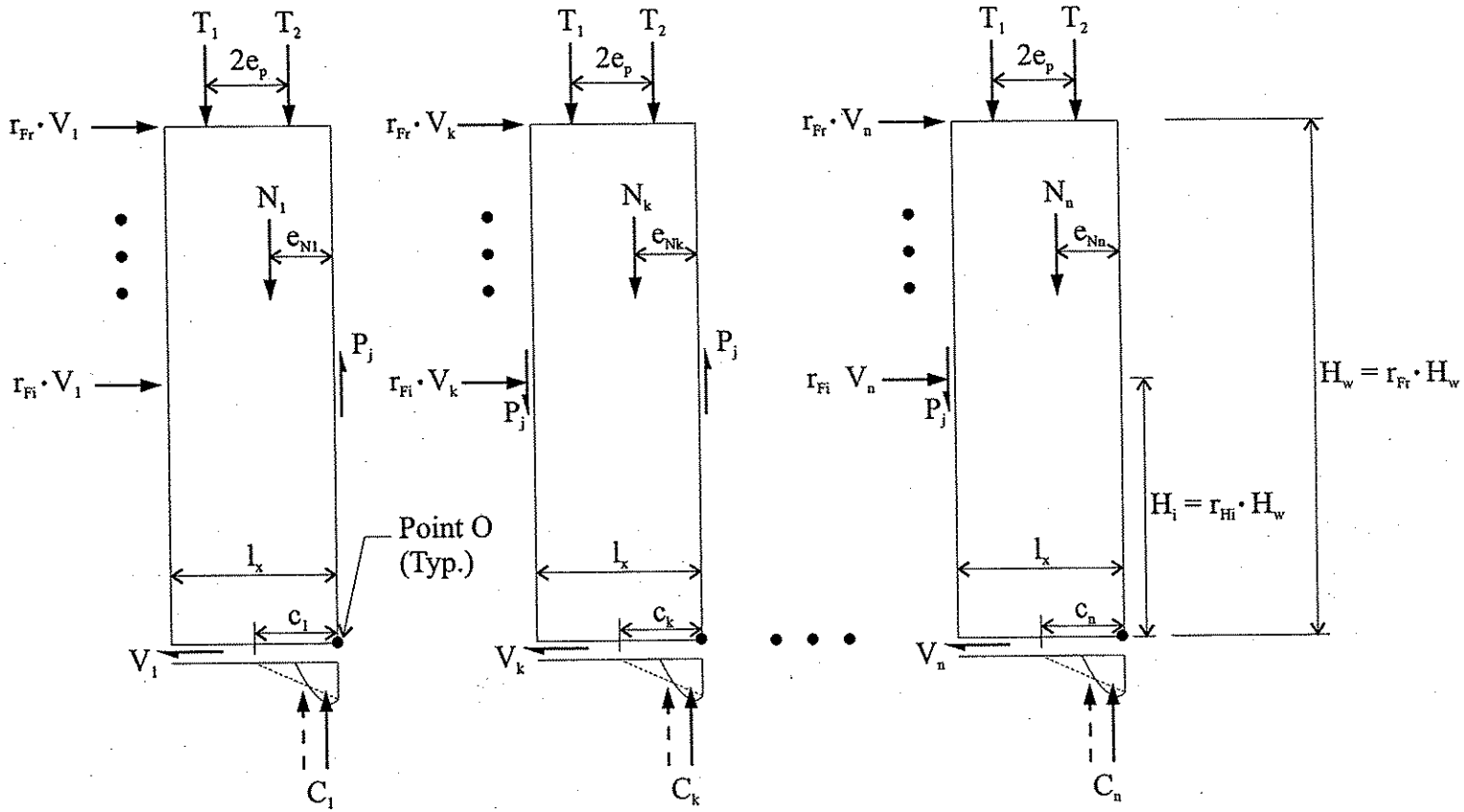


Figure 3.4 Free body diagram used to derive $V_{ilp}$.

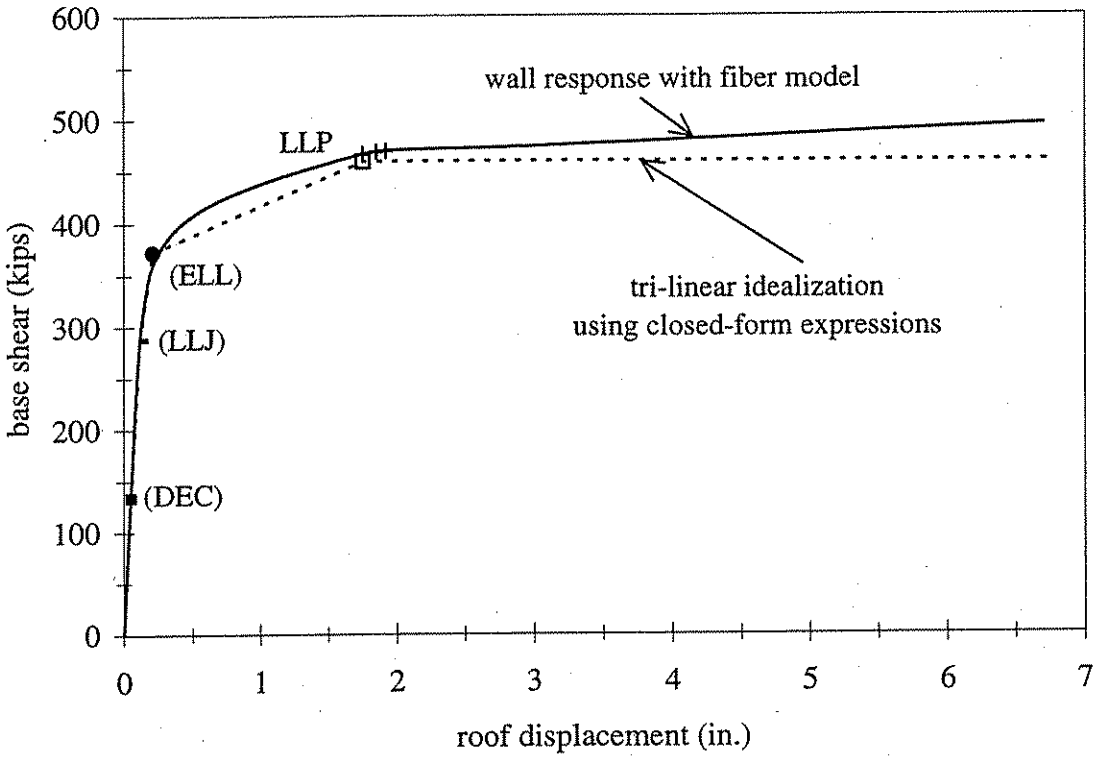


Figure 3.5 Accuracy of tri-linear idealization for PW1.

# Chapter 4

# PROPOSED SEISMIC DESIGN OF BUILDINGS WITH UNBONDED POST-TENSIONED PRECAST CONCRETE WALLS

This chapter proposes a seismic design approach for building structures with unbonded post-tensioned precast walls with vertical joints and ductile joint connectors as the primary lateral load resisting system. Section 4.1 discusses the proposed design approach. The design criteria used to control the axial-flexural behavior of a wall are presented in Section 4.2. Section 4.3 discusses the estimation of design capacities and Section 4.4 discusses the estimation of design demands.

## 4.1 OVERVIEW OF PROPOSED DESIGN APPROACH

The proposed design approach is a performance-based design approach which allows the designer to specify and predict the performance (degree of damage) of a building for a specified level of ground motion intensity. The performance-based design requires identifying performance (damage) levels, structure limit states and capacities, seismic demand levels, structure demands, and establishing design objectives and design criteria.

### 4.1.1 Performance levels

The design approach considers two performance levels which are defined in terms of the maximum damage expected in various structural and non-structural elements during a ground motion. The performance levels are: (1) the *immediate occupancy* performance level, and (2) the *collapse prevention* performance level. The immediate occupancy performance level refers to a post-earthquake state in which only limited structural and non-structural damage occurs. The structure responds to the ground motion for the most part in an elastic manner with limited cracking and yielding of structural members. The collapse prevention performance level refers to a post-earthquake damage state where the structure sustains considerable damage and is on the verge of partial or total collapse, but does not collapse.

### 4.1.2 Structure limit states and capacities

The structure limit states and capacities describe the damage in various structural and non-structural elements of a building. Structure limit states and capacities include limit states and capacities for unbonded post-tensioned precast walls, gravity load resisting frames, and non-structural elements. The limit states for unbonded post-tensioned precast concrete walls with vertical joint connectors are: (1) decompression at the base of the wall; (2) yielding of vertical joint connectors; (3) significant reduction in lateral stiffness (i.e., softening) due to gap opening in flexure along the panel-to-foundation connections; (4) yielding of post-tensioning steel; (5) peak base shear; (6) loss of prestress under cyclic lateral load due to inelastic straining of post-tensioning steel; and (7) crushing of spiral confined concrete. As described in Chapter 3, limit states 3, 4, and 7 define the key points on the tri-linear idealization of the lateral load behavior of an unbonded post-tensioned precast wall. The wall capacities corresponding to limit states 3 and 4 are estimated using the closed-form expressions presented in Chapter 3. Since a closed-form expression has not been developed for limit state 7, the wall

capacity corresponding to this limit state is obtained from a nonlinear static push-over analysis of a fiber model of the wall under combined lateral and gravity loads.

The limit state for the gravity load resisting frames is significant loss of gravity load resistance. Kurama et al. assume that gravity load resisting frames can be designed to sustain a roof drift of 2.5%. The same assumption is made in this research.

The limit states for non-structural elements are: (1) initiation of damage to the non-structural elements; and (2) damage to basic access and life safety systems. Damage to non-structural elements occurs when the story drift (i.e., relative displacement between adjacent floors) exceeds a certain level. In this research, the story drift is expressed as a percentage (i.e., story drift divided by the story height) as explained in Section 4.4.3. Freeman (1977) indicates that damage to non-structural elements initiates at a story drift of 0.25%, while damage requiring repair occurs at a story drift of 0.5% to 1%. NEHRP (1994) includes a limit on story drift to keep the basic access and life safety systems operable during and after a ground motion. For building structures, the limit on story drift is 2.5%. In this report, the NEHRP limit on story drift is adopted.

### 4.1.3 Relationship between performance levels and structure limit states

The relationship between the performance levels and the structure limit states identified above is described using the idealized base-shear-roof-displacement relationship shown in Figure 4.1. The immediate occupancy performance level is reached when yielding of the post-tensioning steel occurs (at a roof displacement of $\Delta_{llp}$). The collapse prevention performance level is reached when crushing of spiral confined concrete occurs (at a roof displacement of $\Delta_{csc}$).

### 4.1.4 Seismic demand levels

Seismic demand levels are generally defined in terms of ground motion levels with selected return periods for a given site. The proposed design approach considers two levels of ground motion; a design level ground motion and a survival level ground motion. This is the same approach used in earlier work by Kurama et al. (1997). The design level ground motion is the same as the NEHRP (1994) design ground motion, which has a 90% probability of not being exceeded in 50 years (corresponding to approximately a 500-year return period). The survival level ground motion has a 90% probability of not being exceeded in 250 years, corresponding to approximately a 2500-year return period (Kurama et al. 1997).

### 4.1.5 Structure demands

Structure demands quantify roof displacement, story drift, and base shear demands for the seismic demand levels described above. For buildings with unbonded post-tensioned precast walls as the primary lateral load resisting system, structure base shear demands are established in terms of wall base shear demands. For the design level ground motion, the demands considered for unbonded post-tensioned walls include the design base shear demand, $V_d$ (governed by axial-flexural behavior), the maximum roof displacement demand, $\Delta_d$ and the maximum story drift demand, $\delta_d$. For the survival level ground motion, the demands are the

maximum roof displacement demand, $\Delta_s$ and the maximum base shear demand, $V_{max}$. Estimation of the structure demands is described in Section 4.4.

### 4.1.6 Design objectives

Performance-based design requires design objectives to relate the expected performance levels to the seismic demand levels described above. The proposed design approach for buildings with unbonded post-tensioned precast walls has two objectives: (1) to achieve the immediate occupancy performance level under the design level ground motion; and (2) to achieve the collapse prevention performance level under the survival level ground motion. These objectives are illustrated in Figure 4.2.

### 4.1.7 Required performance under the design level ground motion

For the design level ground motion, the required performance of an unbonded post-tensioned precast wall is as follows: (1) the wall responds in a nonlinear-elastic manner, with the nonlinear response primarily due to gap opening along the panel-to-foundation connections, and partially from nonlinear behavior of concrete in compression; (2) the vertical joint connectors yield in shear; (3) the post-tensioning steel remains linear-elastic; (4) the wall panels remain nearly linear-elastic with minimal cracking, and with nonlinear behavior in compression and spalling of cover concrete near the base at the compression edge of the panels; (5) shear slip of the panels along the panel-to-foundation connections does not occur; and (6) the resistance of the wall to gravity and lateral loads does not deteriorate. Since the immediate occupancy performance level is reached when the linear limit strain of the post-tensioning steel is reached (at $\Delta_{llp}$), the first objective is achieved if $\Delta_{llp}$ is not exceeded under the design level ground motion (Figure 4.2).

### 4.1.8 Required performance under the survival level ground motion

For the survival level ground motion, the required performance of an unbonded post-tensioned precast wall is as follows: (1) axial-flexural compression failure in the wall panels does not occur; (2) post-tensioning steel yields, but the nonlinear strains in the steel are small because the steel is unbonded; (3) loss of prestress occurs as a result of inelastic straining in the post-tensioning steel; (4) the lateral stiffness of the wall deteriorates due to the loss of prestress, but the base shear capacity is maintained; (5) due to post-tensioning, the wall has a self-centering capability resulting in minimal residual post-ground-motion lateral displacements; and (6) shear slip along the panel-to-foundation connections does not occur. Since the collapse prevention performance level is reached when crushing of the spiral confined concrete is reached (at $\Delta_{csc}$), the second objective is achieved if $\Delta_{csc}$ is not exceeded under the survival level ground motion (Figure 4.2).

Performance based design requires seismic design criteria to compare structure capacities with structure demands. The design objectives are achieved if the structure capacities exceed the structure demands. For a structure with unbonded post-tensioned precast walls the design criteria is represented in terms of wall demands and wall capacities as described in detail in Section 4.2.

## 4.2 SEISMIC DESIGN CRITERIA

This section describes the design criteria that are used to control the axial-flexural behavior of unbonded post-tensioned precast walls with vertical joint connectors. The estimation of design capacities is covered in Section 4.3, and Section 4.4 discusses the estimation of design demands.

### 4.2.1 Softening

The first criterion of the design approach controls softening of an unbonded post-tensioned precast wall under lateral load. This criterion prevents a premature reduction in lateral stiffness of the wall. Accordingly, the base shear capacity (as governed by axial-flexural behavior) corresponding to the onset of a significant reduction in lateral stiffness, $V_{ell}$ should be larger than the base shear demand specified in NEHRP (referred to as the design base shear demand, $V_d$). That is,

$$V_{ell} > V_d = \frac{Q_d}{R} \tag{4.1}$$

The design base shear demand, $V_d$ is determined using the equivalent lateral force procedure in NEHRP (1994) and is equal to the linear-elastic base shear demand for the design level ground motion, $Q_d$ divided by a response modification coefficient, R (equal to 4.5 for bearing wall systems) in accordance with the NEHRP provisions (Figure 4.3).

### 4.2.2 Base moment capacity

The second criterion of the design approach controls the base moment capacity (as governed by axial-flexural behavior) of the wall. The structure demands in NEHRP are quantified in terms of base shear under equivalent lateral forces. Thus, the moment capacity of the wall is quantified in terms of the base shear capacity of the wall (as governed by axial-flexural behavior). The base shear capacity of an unbonded post-tensioned precast wall corresponds to the base shear at yielding of the post-tensioning steel (i.e., $V_{llp}$), as shown in Figure 4.1. According to the design criterion, $V_{llp}$ should be larger than the design base shear demand. A capacity reduction factor, $\Phi_f$ (equal to 0.75) is applied to $V_d$ as required by the ACI 318 Code (American Concrete Institute 1995). Thus, according to the second criterion,

$$\Phi_f V_{llp} > V_d = \frac{Q_d}{R} \tag{4.2}$$

### 4.2.3 Yielding of post-tensioning steel

The third criterion of the design approach controls yielding of the post-tensioning steel. According to this criterion, the roof displacement corresponding to yielding of the post-tensioning steel, $\Delta_{llp}$ should be larger than the roof displacement demand for the design level ground motion, $\Delta_d$. That is,

$$\Delta_{llp} > \Delta_d \tag{4.3}$$

### 4.2.4 Gap closure at the base

The fourth design criterion controls the minimum level of initial prestress force on a panel, $P_i$ to ensure that the gap which develops at the base of the panels due to lateral loads closes after the removal of the lateral loads. Figure 4.4 shows five possible displacement states that are can develop during rocking of a rigid interior panel with flexural reinforcement, eccentric axial force, and equal prestress forces on groups of post-tensioning steel: (1) undisplaced position with full contact at the base of the panel; (2) gap opening with contact at the right end of the panel, yielding of the vertical joint connectors, and yielding of the post-tensioning steel to the left; (3) undisplaced position with full contact at the base of the panel, and a reduction in prestress of the post-tensioning steel to the left where $\Phi_{gc}$ is the initial prestress reduction factor (assumed to be 0.75); (4) gap opening with contact at the left end of the panel and yielding of the post-tensioning steel to the right; (5) undisplaced position with full contact at the base of the panel (provided $P_i$ is large enough), and a reduction in prestress of the post-tensioning steel to the right. Summing moments about point O in displaced state 5 of Figure 4.4 gives the following expression:

$$\Phi_{gc}\left(P_i \cdot \frac{l_x}{2}\right) + N(l_x - e_N) \geq P_{lij} \cdot l_x \tag{4.4}$$

where: $l_x$ is the length of the panel; N is the total axial load on a panel; $e_N$ is the eccentricity of the axial load N measured from the right edge of the panel; and $P_{lij}$ is the total shear force in the vertical joint connectors at yield. The left terms in Equation 4.4 represent the moments that force the gap to close after the removal of lateral loads, whereas the term on the right side of the equation represents the moment that causes the gap at the base to open.

### 4.2.5 Story drift

The fifth design criterion controls the maximum story drift under the design level ground motion to control the lateral stiffness of the walls and to maintain basic access and life safety systems operable. According to this criterion, the allowable story drift, $\delta_{all}$ should be larger than the estimated maximum story drift demand for the design level ground motion, $\delta_d$. Thus,

$$\delta_{all} \geq \delta_d \tag{4.5}$$

### 4.2.6 Crushing of spiral confined concrete

The sixth design criterion controls crushing of spiral confined concrete. According to this criterion, the roof displacement capacity corresponding to crushing of spiral confined concrete, $\Delta_{csc}$ should be larger than the roof displacement demand for the survival level ground motion, $\Delta_s$. Thus,

$$\Delta_{csc} \geq \Delta_s \tag{4.6}$$

### 4.2.7 Other criteria

A criterion is needed to control the length and height of the spiral confined concrete region near the base of the panels. This criterion is developed by Kurama et al. (1997) for unbonded post-tensioned walls with horizontal connections, but is not considered in this study. Another criterion is required to prevent shear slip along the panel-to-foundation connections under the

action of earthquake loads. This criterion (developed by Kurama et al. 1997) requires an estimation of wall demands that are obtained through dynamic analyses. Since this study does not include dynamic analyses, the shear slip criterion is not considered.

## 4.3 ESTIMATION OF DESIGN CAPACITIES

The previous section described the design criteria that are used to control the behavior of a wall. This section describes how the capacity of each of the limit states included in the design criteria is calculated.

### 4.3.1 Softening

The base shear capacity (as governed by axial-flexural behavior) corresponding to the effective linear limit state, $V_{ell}$ of an unbonded post-tensioned precast wall with vertical joint connectors is calculated using Equation 3.1. Equation 3.1 applies to a wall with numerous panels and floor levels, and eccentric axial forces. For the specific case of the prototype wall described in Chapter 5, $V_{ell}$ is calculated using Equation 3.3.

### 4.3.2 Base moment capacity

As noted in Section 4.2.2, the base moment capacity of the wall is quantified in terms of the base shear capacity of the wall. Thus, the base shear capacity, $V_{llp}$ of an unbonded post-tensioned precast wall with vertical joint connectors is computed from Equation 3.8. Equation 3.8 applies to a wall with numerous panels and floor levels, and eccentric axial forces. For the specific case of the prototype wall described in Chapter 5, $V_{llp}$ is calculated using Equation 3.9.

### 4.3.3 Yielding of post-tensioning steel

The roof displacement corresponding to yielding of the post-tensioning steel, $\Delta_{llp}$ of an unbonded post-tensioned precast wall with vertical joint connectors is calculated using Equation 3.10.

### 4.3.4 Story drift

The maximum allowable story drift for the design level earthquake, $\delta_{all}$ is equal to 2.5% based on NEHRP (1994). This value is applicable to buildings four stories or less in height with interior walls, partitions, ceilings, and exterior wall systems that have been designed to accommodate the story drifts.

### 4.3.5 Crushing of spiral confined concrete

A closed form expression has not been developed to estimate the roof displacement capacity corresponding to crushing of spiral confined concrete ($\Delta_{csc}$). Further, detailing requirements have been specified to ensure that the sixth design criterion is met. Therefore, $\Delta_{csc}$ is determined from a nonlinear static push-over analysis of a fiber model of a wall under combined lateral and gravity loads. The distribution of the lateral loads over the height of the wall is determined from the equivalent lateral force procedure in NEHRP. The gravity loads (i.e., dead and live loads) are determined from the load combinations in NEHRP.

## 4.4. ESTIMATION OF DESIGN DEMANDS

Section 4.2 described the design criteria that are used to control the behavior of a wall. Section 4.3 described how the capacity of each limit state treated in the design criteria is calculated. This section describes the estimation of design demands, which are compared with the design capacities (Section 4.3) to check the design criteria given in Section 4.2. The design approach as described here treats buildings with no *plan* or *vertical* structural irregularities (discussed in NEHRP, 1994). Thus, the methods described here are not applicable to structures classified as *irregular* by NEHRP.

### 4.4.1 Design base shear demand for the design level ground motion

The wall design base shear demand for the design level ground motion, $V_d$ is estimated by distributing a structure design base shear demand, $V^s_d$ between the unbonded post-tensioned precast walls and other lateral load resisting members in a structure. The structure design base shear demand, $V^s_d$ depends on the properties of the structure, the seismicity of the region where the building is located, and the soil profile at the building site, and is given by

$$V_d^s = WC_s \tag{4.10}$$

In Equation 4.10, W is the seismic weight of the structure, which is comprised of the building self-weight and dead load only (live load is excluded). Partition loads of 20 psf, which are part of the live loads used in the design of a building as per UBC 1994, are included in the seismic weight computation. $C_s$ is the seismic response coefficient defined in NEHRP (1994). The seismic response coefficient depends on the fundamental period of the structure T, the site soil profile, and the design peak ground acceleration, and is calculated as

$$C_s = \frac{1.2C_v}{RT^{2/3}} \le \frac{2.5C_a}{R} \tag{4.11}$$

where R is the response modification factor (equal to 4.5 for bearing wall systems) in accordance with NEHRP (1994). $C_v$ and $C_a$ are seismic coefficients introduced in the 1994 edition of NEHRP and are calculated as $C_v=A_vF_v$ and $C_a=A_aF_a$. $A_v$ is a dimensionless coefficient representing the effective peak velocity-related acceleration, and $A_a$ is a dimensionless coefficient representing the effective peak acceleration. $A_v$ and $A_a$ depend on the seismicity of the site where the structure is located, and are determined using maps included in the NEHRP provisions. This report considers regions of the U.S. with $A_v=A_a=0.4$ (i.e., regions with "high seismicity"). $F_v$ and $F_a$ are the velocity-based site coefficient and the acceleration-based site coefficient, respectively. $F_v$ and $F_a$ depend on the site conditions and the shaking intensity (i.e., $A_v$ and $A_a$, respectively).

In Equation 4.11, T represents the fundamental period (1$^{st}$ mode period) of the structure in the direction of the unbonded post-tensioned precast walls. The fundamental period can be determined from an eigenvalue analysis (using DRAIN-2DX, for example), or from approximate methods such as Rayleigh's method. Use of a large value for T is unconservative. Therefore, NEHRP places an upper limit on T, equal to $C_uT_a$, where $C_u$ is a function of the seismic coefficient $C_v$ and increases with decreasing levels of seismicity. The approximate fundamental period is computed as $T_a = C_Th_n^{3/4}$, where $h_n$ is the height of the structure. $C_T$ depends on the type of construction and is taken as 0.02 according to NEHRP (1994) for all

building systems that are not moment resisting- or eccentrically braced steel frames. In this report, the fundamental period T corresponds to the approximate fundamental period given in NEHRP (i.e., $T_a$).

Once the structure design base shear demand $V^s_d$ is obtained, the wall design base shear demand, $V_d$ is calculated. The portion of the structure base shear demand that is resisted by a wall depends on the distribution of mass and stiffness in the plan of the structure. According to NEHRP, *applied* torsion exists if the center of mass and the center of stiffness in a building do not coincide over the height. This report considers only regular building structures (i.e., no applied torsion). However, *accidental* torsion may be introduced during a ground motion due to a number of factors including differences between estimated and actual stiffness of the lateral load resisting members and different degrees of stiffness degradation of lateral load resisting members during inelastic response. For this reason NEHRP includes the effect of *accidental* torsion, calculated as the product of the structure base shear and the *accidental eccentricity* which is 5% of the dimension of the structure perpendicular to the direction of the structure base shear.

In Chapter 5, the above procedure is applied to the prototype structure in Figure 5.1. The following assumptions are made: (1) the structure has no plan or vertical irregularities; (2) the floor and roof diaphragms are rigid; (3) all lateral forces acting on the structure are in the E-W direction; (4) the lateral stiffnesses of the walls in the N-S direction and of the frames are neglected; and (5) all the walls in the E-W direction have the same initial lateral stiffness, $k_{wi}$. From these assumptions, the wall design base shear demand $V_d$ can be calculated as

$$V_d = \frac{V_d^s}{w} + V_{d,acc} \tag{4.12}$$

The ratio $V^s_d/w$ represents the wall base shear demand due to story translations induced by the ground motion, where $V^s_d$ is the structure design base shear demand and w is the number of walls in the E-W direction. $V_{d,acc}$ is the wall base shear due to story twist caused by *accidental* torsion. $V_{d,acc}$ is calculated as follows for a wall in the E-W direction:

$$V_{d,acc} = \frac{k_{wi} e_1 \left(V_d^s \cdot e_{acc}\right)}{w \cdot k_{wi} e_1^2} = \frac{V_d^s \cdot e_{acc}}{w \cdot e_1} \tag{4.13}$$

where $e_1$ is the distance perpendicular to the walls from the center of resistance of the structure, and $e_{acc}$ is the *accidental* eccentricity in the direction perpendicular to the E-W direction (i.e., the N-S direction).

### 4.4.2 Maximum wall roof displacement demands

The maximum wall roof displacement demands for the design level and the survival level ground motions, $\Delta_d$ and $\Delta_s$, are assumed to be equal to the linear-elastic roof displacement demands under these ground motions. In the context of the NEHRP-based design procedure, the linear-elastic roof displacement demands are calculated by dividing the wall linear-elastic base shear demands, $Q_d$ and $Q_s$ (for the design and survival level ground motions, respectively) by the wall initial (linear-elastic) lateral stiffness (Figure 4.3). The wall initial lateral

stiffness can be approximated as $k_{wi}=V_{ell}/\Delta_{ell}$ where $V_{ell}$ is calculated using Equation 3.1 and $\Delta_{ell}$ is calculated using Equation 3.4. The wall linear-elastic base shear demand for the design level ground motion, $Q_d$ is equal to the product of the wall design base shear demand, $V_d$ and the response modification coefficient, R (equal to 4.5 as defined in NEHRP). The wall linear-elastic base shear demand for the survival level ground motion, $Q_s$ is set equal to 2.5 times the wall linear-elastic base shear demand for the design level ground motion, $Q_d$.

### 4.4.3 Maximum story drift demand for the design level ground motion

The maximum story drift demand for the design level ground motion, $\delta_d$ is determined by

$$\delta_d(\%) = C_d \cdot \frac{\delta_{xe}}{h} \tag{4.14}$$

where h is the story height, $C_d$ is the deflection amplification factor (equal to 4 for bearing wall systems) in accordance with NEHRP (1994), and $\delta_{xe}$ is the story drift (i.e., the difference between the lateral deflections of the floor level above and below the story under consideration) determined by an elastic analysis of the wall under the NEHRP distribution of equivalent lateral forces. The lateral deflection of a wall with r stories, n panels of the same geometry, eccentric axial forces on each panel that can vary along the height of the wall, and lateral loads applied at each floor level, can be computed for an arbitrary floor level j by

$$\Delta_j = \Delta_{F_j} + \Delta_{S_j} + \Delta_{N_j} + \Delta_{P_j} \tag{4.15}$$

where

$$\Delta_{F_j} = \sum_{i=1,j} \frac{1}{6E_c \cdot I_w} \cdot r_{F_i} \cdot V_d \cdot r_{H_i}^2 \cdot H_w^3 \left(3r_{H_j} - r_{H_i}\right) + \sum_{i=j+1,r} \frac{1}{6E_c \cdot I_w} \cdot r_{F_i} \cdot V_d \cdot r_{H_j}^2 \cdot H_w^3 \left(3r_{H_i} - r_{H_j}\right)$$

$$\Delta_{S_j} = \sum_{i=1,j} \frac{r_{F_i} \cdot V_d \cdot r_{H_i} \cdot H_w}{G_c \cdot A'_w} + \sum_{i=j+1,r} \frac{r_{F_i} \cdot V_d \cdot r_{H_j} \cdot H_w}{G_c \cdot A'_w}$$

$$\Delta_{N_j} = \sum_{i=1,j} \frac{1}{E_c \cdot I_w} \cdot M_{w,i}\left(r_{H_i} \cdot H_w\right) \cdot H_w \left(r_{H_j} - \frac{r_{H_i}}{2}\right) + \sum_{i=j+1,r} \frac{1}{2 \cdot E_c \cdot I_w} \cdot M_{w,i}\left(r_{H_j} \cdot H_w\right)^2$$

$$\Delta_{P_j} = \frac{n \cdot e_p (T_2 - T_1) \cdot \left(r_{H_j} \cdot H_w\right)^2}{2 \cdot E_c \cdot I_w}$$

$T_1 = T_{1i}$

and $T_2 = T_{2i}$.

Equation 4.15 is derived for a wall as described in Chapter 2 in the same manner as the roof displacement corresponding to the effective linear limit state, $\Delta_{ell}$ was derived in Section 3.2.2. $\Delta_{Fj}$ is the deflection of the wall at floor j in flexure due to lateral forces. $\Delta_{Fj}$ is obtained using the principle of superposition (i.e., successively applying a concentrated lateral load, $r_{Fi} \cdot V_d$, along the height of the wall and adding the corresponding deflections of floor j). The first summation term in the $\Delta_{Fj}$ equation represents the total lateral deflection of floor j caused by lateral loads applied at floor j and at all the floor levels below it. The second summation term in the $\Delta_{Fj}$ equation represents the total lateral deflection of floor j caused by lateral loads applied at the floor levels above floor j. Thus, estimating the roof deflection re-

quires only the first summation term. The deflection of the wall at floor j due to elastic shear deformations, obtained using the principle of superposition, is denoted as $\Delta_{Sj}$. $\Delta_{Nj}$ is the deflection of the wall at floor j in flexure due to eccentrically applied axial forces. The term $M_{w,i}$ in the $\Delta_{Nj}$ equation represents a concentrated wall moment applied at floor level i which is calculated using Equation 3.5. The origin of $M_{w,i}$ is discussed in detail in Section 3.2.2. $\Delta_{Pj}$ is the deflection of the wall at floor j caused by the application of different initial prestressing forces on the post-tensioning steel to the left and to the right of each panel, denoted by $T_{1i}$ and $T_{2i}$, respectively. The initial prestressing forces, $T_{1i}$ and $T_{2i}$, are the same for all the panels. The moment produced by the unbalanced prestressing forces on a panel is added over the panels and is applied to the wall as a concentrated moment at the roof level because, since the post-tensioning steel is unbonded over the entire height of the wall, the wall is subjected to a constant moment over its entire height. $V_d$ is the design base shear demand calculated using Equation 4.12. $G_c$ is the shear modulus of concrete, $A'_w$ the effective shear area of the wall, $E_c$ the elastic modulus of concrete, and $I_w$ the moment of inertia of the uncracked transformed section of the wall.

For the particular case of the prototype wall described in Chapter 5, composed of two stories, three panels with the same geometry, the same gravity forces, N acting at the center of each panel, and the same forces $T_1$ and $T_2$ each equal to half the total initial prestress force on a panel, Equation 4.15 becomes

$$\Delta_r = \Delta_{F_r} + \Delta_{S_r} \tag{4.16}$$

for the roof deflection and

$$\Delta_1 = \Delta_{F_1} + \Delta_{S_1} \tag{4.17}$$

for the deflection of the first floor, where

$$\Delta_{Fr} = \frac{1}{6 \cdot E_c \cdot I_w} \cdot V_d \cdot H_w^3 \left(3r_{F_1} \cdot r_{H_1}^2 \cdot r_{H_r} - r_{F_1} \cdot r_{H_1}^3 + 2r_{F_r} \cdot r_{H_r}^3\right)$$

$$\Delta_{S_r} = V_d \cdot H_w \frac{\left(r_{F_1} \cdot r_{H_1} + r_{F_r} \cdot r_{H_r}\right)}{G_c \cdot A'_w}$$

$$\Delta_{F_1} = \frac{1}{6 \cdot E_c \cdot I_w} \cdot V_d \cdot r_{H_1}^2 \cdot H_w^3 \left(2r_{F_1} \cdot r_{H_1} + 3r_{F_r} \cdot r_{H_r} - r_{F_r} \cdot r_{H_1}\right)$$

and $\Delta_{S_1} = V_d \cdot r_{H_1} \cdot H_w \frac{\left(r_{F_1} + r_{F_r}\right)}{G_c \cdot A'_w}$.

$\Delta_{Fr}$ and $\Delta_{F1}$ are the deflections of the roof and the first floor level, respectively in flexure due to lateral forces. $\Delta_{Sr}$ and $\Delta_{S1}$ are the deflections of the roof and the first floor level, respectively due to elastic shear deformations of the prototype wall.

### 4.4.4 Roof displacement capacity corresponding to crushing of spiral confined concrete

In lieu of a closed-form expression, the roof displacement capacity corresponding to crushing of the spiral confined concrete, $\Delta_{csc}$ is determined by performing a nonlinear static push-over

analysis of a fiber wall model of the wall using DRAIN-2DX under the NEHRP distribution of equivalent lateral forces.

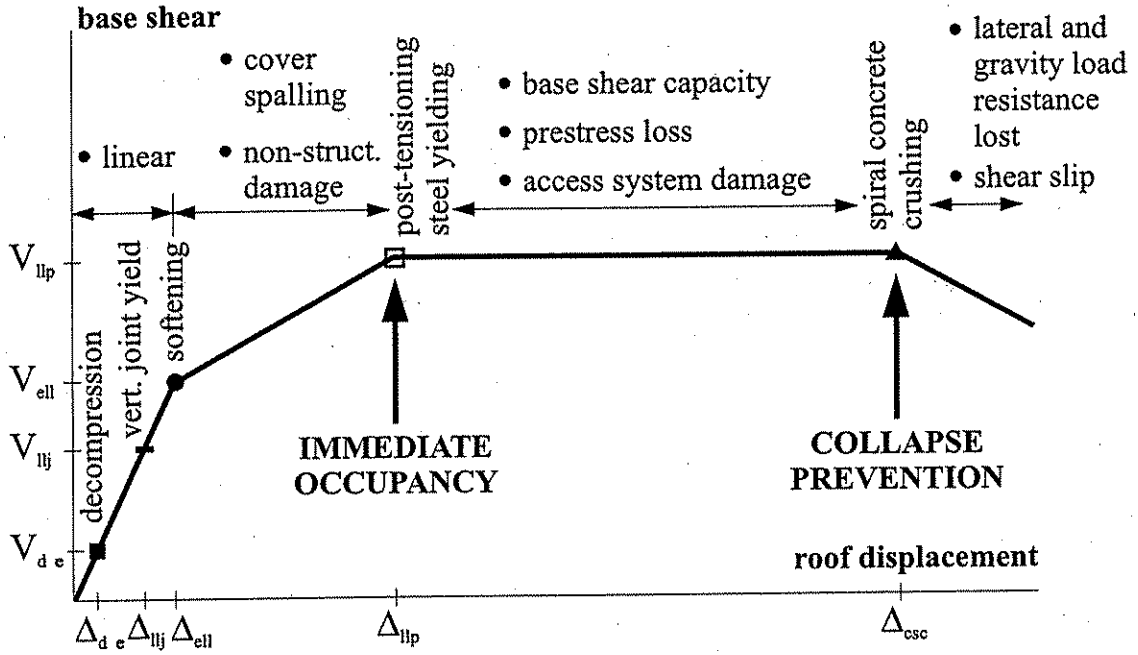


Figure 4.1 Structure limit states and expected performance levels (adapted from Kurama et al. 1997).

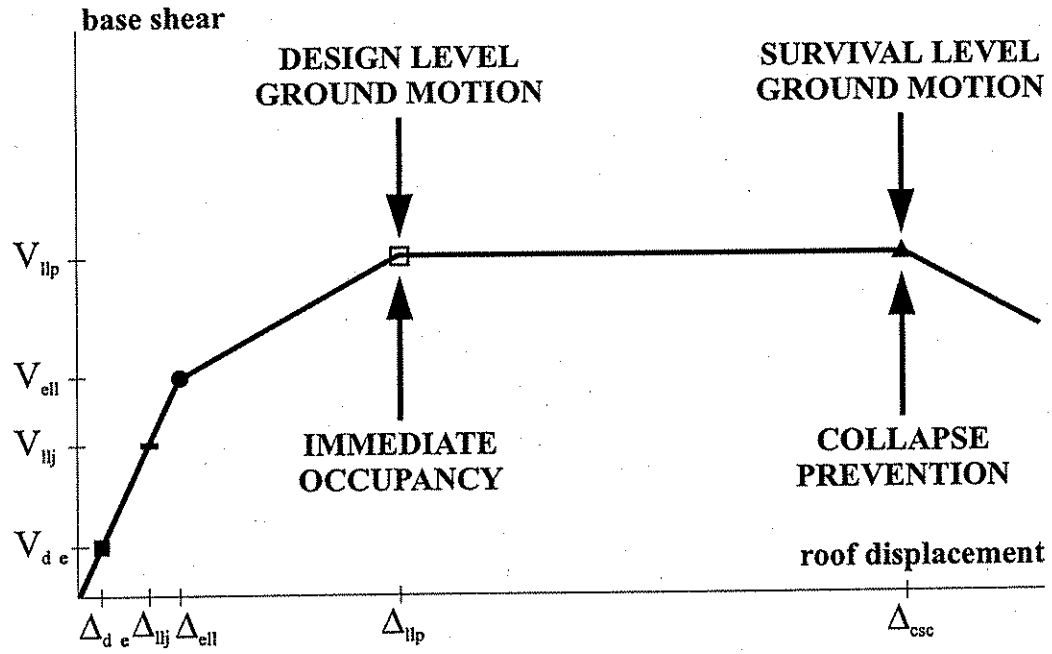


Figure 4.2 Objectives of the proposed design approach (adapted from Kurama et al. 1997).

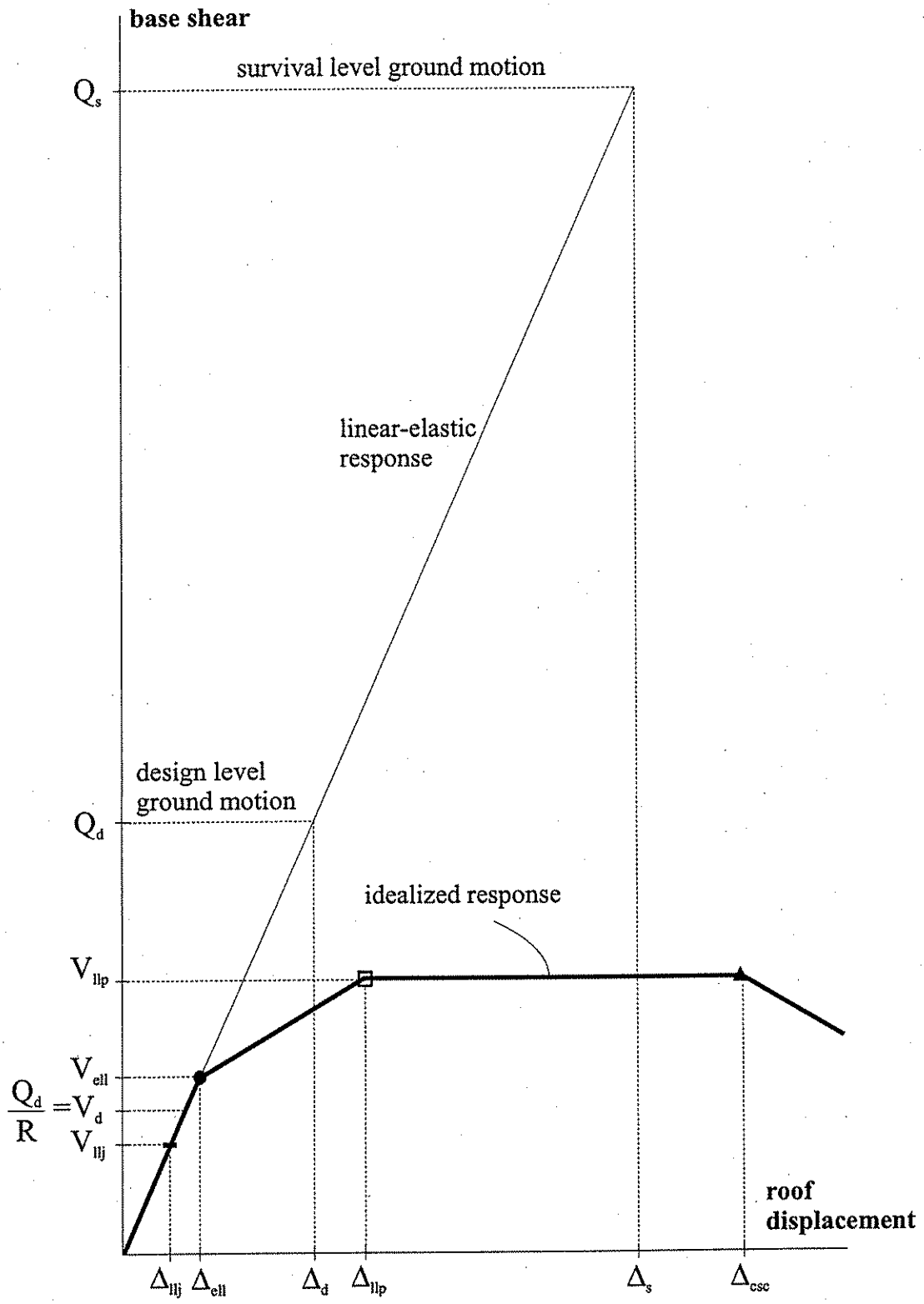


Figure 4.3 Design criteria to control axial-flexure behavior (adapted from Kurama et al. 1997).

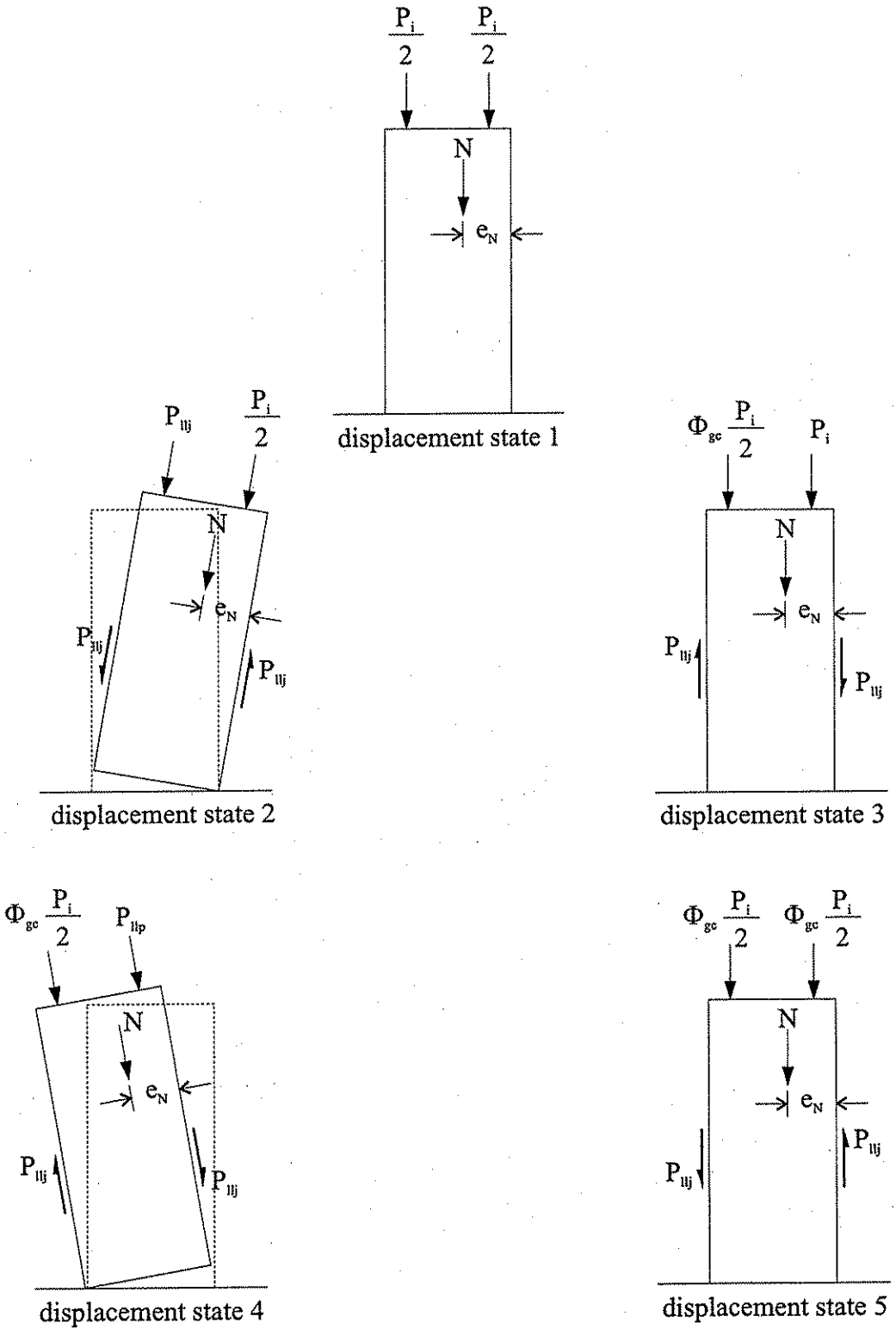


Figure 4.4 Five displacement states of a rocking panel.

# Chapter 5

# DESIGN OF THE PROTOTYPE WALL

This chapter describes the design of a prototype wall using the design approach presented in Chapter 4. Section 5.1 summarizes general properties of the prototype structure for which the prototype wall was designed. Section 5.2 describes the prototype wall, Section 5.3 identifies wall capacities and demands considered in the seismic design of the wall.

## 5.1 THE PROTOTYPE STRUCTURE

This section describes the general configuration of the prototype structure and how it was selected. This section also identifies the structural members of the prototype structure and gives a summary of the gravity loads used in the design of the structure.

### 5.1.1 Building layout

The precast concrete building treated in this study is a two-story office building with a plan view as shown in Figure 5.1. The building has a footprint of 230 ft. x 120 ft. and is 28 ft. tall. The building plan includes 7 bays in the east-west (E-W) and 3 bays in the north-south (N-S) direction. The lateral load resistance is provided by unbonded post-tensioned precast walls in both the E-W and N-S directions. The gravity loads are carried by the walls, and also by gravity load resisting frames which are not part of the lateral load resisting system. The floor system is comprised of double tees that span in the N-S direction at the center of the building and in the E-W direction at the east and west wings of the building. The double tees span between L-shaped beams around the periphery of the building and either walls, inverted tee beams or L-shaped beams in the interior. Double tees also span between walls and between inverted tee beams at the center of the building.

This research concentrates on the seismic behavior of the proposed system in the E-W direction only. Hence, each of the walls considered in this study supports the reactions of six double tees (see Figure 5.1).

***Selection of the building layout***

Kurama et al. (1997) give a number of recommendations for selecting a building layout based on Phase I of the PRESSS program and an advisory panel comprised of PRESSS researchers, practicing engineers, and architects. These recommendations, which were considered when selecting the building layout of the prototype structure shown in Figure 5.1, are as follows:

1. Building layouts with centers of mass and rigidity that are close together or coincident are preferred because the torsional effects of earthquakes are reduced.

2. To provide better overall torsional resistance, the walls should be distributed properly within the building layout, as close to the periphery of the building as possible.

3. To decrease the in-plane deformations of the diaphragm, the lateral stiffness of the building should be uniformly distributed in each direction. Furthermore, particularly for buildings in regions of high seismicity, the use of several walls rather than only a few walls reduces the forces that are transferred to the foundations, simplifying the design of the foundations (Paulay and Priestley 1992).

4. Supporting moderate levels of gravity loads with the walls is beneficial to the lateral load behavior of the wall. This issue is discussed more fully below.

5. Design of office buildings requires the consideration of several architectural requirements. These include preferences about the arrangement and dimensions of available open space for offices, lobbies, corridors, elevator shafts, staircases, and utility rooms.

As noted in item 4 above, the lateral load behavior of walls is improved when they support moderate levels of gravity loads. This is because: (1) together with post-tensioning, gravity loads provide a stabilizing force on the rocking of the walls by delaying gap opening during loading and forcing gaps to close during unloading, thereby contributing to self-centering behavior under cyclic loading; (2) gravity loads increase the shear slip capacity of horizontal connections (e.g., panel-to-foundation connections) by increasing the compression force across the connections; (3) gravity loads increase axial-flexural strength and reduce the demand for flexural reinforcement; and (4) gravity loads simplify the design of foundations to resist the overturning moments that develop at the base (Kurama et al., 1996).

### 5.1.2 Structural members of the prototype structure

This section describes the structural members of the prototype structure other than the unbonded post-tensioned precast walls. The structural members include the floor and roof members, and gravity load resisting frame members. The members were selected using the PCI Design Handbook for Precast and Prestressed Concrete (Prestressed Concrete Institute, 1992) to obtain an estimate of the gravity loads on the walls and the seismic weight, W of the prototype structure.

The floor system is comprised of 10 ft. wide by 24 in. deep double tees with 2 in. thick cast-in-place normal weight concrete topping (designation 10DT24+2). The roof system is comprised of the same double tees as the floor system, but without the 2 in. thick concrete topping (designation 10DT24). The span for all floor and roof double tees is 40 ft.

The gravity load resisting frame is composed of inverted tee beams that are 30 in. wide and 36 in. deep (designation 30IT36). The gravity load resisting frame is also composed of two 40 ft. long interior L-shaped beams that are 24 in. wide and 36 in. deep (designation 24LB36).

### 5.1.3 Gravity loads

A summary of the gravity loads used in the design of the prototype structure is given below.

*Floor loads*

| | |
|---|---|
| dead load | concrete structure weight + 20 psf |
| live load | 80 psf |

*Roof loads*

| | |
|---|---|
| dead load | concrete structure weight + 25 psf |
| live load | 40 psf |

The concrete structure weight includes the weight of the precast elements (150 pcf) and the weight of the 2 in. thick cast-in-place normal weight concrete topping where applicable (i.e., in the floor double tees only). A superimposed dead load of 20 psf is added to the floor loads to account for the weight of mechanical, heating, and electrical systems as well as plumbing equipment, floor finishes (e.g., carpet), ceilings, and insulation. The floor live load of 80 psf includes code required loads for office space and partitions per UBC 1994.

## 5.2 THE PROTOTYPE WALL

The prototype wall considered in this study is shown in Figure 5.2 and its properties are summarized in Table 5.1. The prototype wall is composed of three full-height precast concrete panels that are 9 ft. long, 28 ft. tall, and 1 ft. thick. Thus, the $l_x/t_x$ aspect ratio for each panel is 28/1 = 28, and the $H_w/l_x$ aspect ratio for each panel is 28/9 = 3.1 (for the prototype wall, the height of the wall panels is the height of the wall, $H_w$). The panels are connected by four steel plates, one plate at each vertical joint. The plates are 3 in. by 0.375 in. thick, and 4 inches long. The total area of steel across each vertical joint, $A_j$ is 4.50 $in^2$. The floor and roof loads are transferred to the wall through the stems of three 10 ft.-wide double tees located on each side of the wall. The stem loads on the wall due to the floor and roof dead loads (determined from the tributary area of each panel) are shown in Figure 5.2. Each load considers the effect of two double tees on the wall panel (one on each side of the wall). It is noted that the width of the double tees (10 ft.) differs from the length of each panel (9 ft.). Thus, an eccentricity of 12 in., measured from the stem resultant force (i.e., the center of the double tee) to the centerline of the panel, is introduced in the two exterior panels of the prototype wall (Figure 5.2).

Figures 5.3 and 5.4 show the reinforcement for a typical panel of the prototype wall. The flexural reinforcement consists of two groups of post-tensioning steel located on either side of the panel centerline. The eccentricity of post-tensioning steel, $e_p$ taken from the centerline of the panel to the centroid of a group of post-tensioning steel, is equal to 27 in. (i.e., $2e_p = 54$ in.). Each post-tensioning bar has a diameter of 9/8 in., and a cross-sectional area of 1.00 $in^2$. The post-tensioning steel is placed in 2.125 in. diameter ducts and is unbonded over the entire wall height. The post-tensioning steel is prestressed to 60% of its ultimate strength (i.e., $f_{pi} = 0.60\, f_{pu}$). This is the assumed value of prestress, after losses, used in this research.
As shown in Figures 5.3 and 5.4, the panel has three pairs of interlocking spirals at the corners near the base to provide confinement to the concrete. The spirals are provided over a length of 27 in. (0.25 $l_x$) near each end of the panel, and over a height of 168 in. (0.5 $H_w$) above the base of the panel. The spirals are 9.35 in. in diameter (center-to-center) and have a 1.75 in. pitch. The spirals are made of 5/8 in. diameter reinforcement with a yield strength of

60 ksi. The ratio of the volume of spiral reinforcement to the volume of confined concrete, $\rho_{sp}$ is 7.5%.

The panel has one sheet of welded wire mesh on each face, as shown in Figure 5.4. The mesh has a wire diameter of 0.264 in. (corresponding to a wire area of 0.055 $in^2$), and has a longitudinal and transverse wire spacing of 4 in. (designation 4x4-W5.5xW5.5). The mesh is located on each face along the entire length and height of the panel. The concrete cover to the welded wire mesh is 3/4 in.

***Design material properties***

The specified compressive strength of the unconfined concrete ($f'_c$) used for the walls is 6000 psi. The concrete within the wall is subjected to various levels of confinement by the reinforcement. Accordingly, three types of concrete stress-strain relationships are defined for the panel in Figure 5.4 as follows: (1) unconfined (cover) concrete (i.e., concrete outside the mesh); (2) spiral confined concrete (i.e., concrete within the spirals); and (3) mesh confined concrete (i.e., concrete outside the spirals and inside the mesh). The compressive stress-strain relationships of the three types of concrete are estimated using the confinement model developed by Mander et al. (1988a, 1988b) and are shown in Figure 5.5.

The stress-strain relationship for the post-tensioning steel is shown in Figure 5.6. The linear limit stress of the post-tensioning steel, $f_{pl}$ is 120 ksi at a strain of $4.14 \times 10^{-3}$ in./in. and the ultimate strength $f_{pu}$ is 160 ksi at a strain of 0.04 in./in (Kurama et al. 1997).

The vertical joint connector plates are of ASTM A572 Grade 50 steel with special requirements per AISC Technical Bulletin #3, New Shape Material, dated March 3, 1997. This material has a specified upper limit on yield strength of 65 ksi, a minimum tensile strength of 65 ksi, and a specified maximum yield-to-tensile ratio of 0.85 (Modern Steel Construction, 1997). The following values are used in this research: tensile yield strength of 60 ksi, and shear yield strength of 36 ksi (approximately 0.6 times the tensile yield strength).

## 5.3 SEISMIC DESIGN OF THE PROTOTYPE WALL

This section describes the seismic design of the prototype wall. The wall is designed according to the design approach outlined in Chapter 4. Section 5.3.1 summarizes the design capacities of the prototype wall, and Section 5.3.2 summarizes the design demands for the prototype wall. Lastly, Section 5.3.3 compares the design capacities and demands in accordance with the seismic design criteria discussed in Section 4.2.

### 5.3.1 Prototype wall design capacities

The estimation of design capacities for an unbonded post-tensioned precast wall is discussed in Section 4.3. The design capacities are: (1) the base shear capacity (as governed by axial-flexural behavior) corresponding to the effective linear limit state, $V_{ell}$; (2) the base moment capacity (expressed in terms of the base shear capacity of the wall, $V_{llp}$); (3) the roof displacement capacity corresponding to yielding of the post-tensioning steel, $\Delta_{llp}$; (4) the gap closing capacity of the wall (expressed in terms of the initial prestress force on each panel, $P_i$); (5) the maximum allowable story drift, $\delta_{all}$ based on NEHRP (1994); and (6) the roof

displacement capacity corresponding to crushing of the spiral confined concrete, $\Delta_{csc}$. The prototype wall design capacities are summarized in Table 5.2.

### 5.3.2 Prototype wall demands

The estimation of demands for an unbonded post-tensioned precast wall is discussed in Section 4.4. The wall demands are: (1) the wall design base shear demand, $V_d$; (2) the maximum wall roof displacement demand for the design level ground motion; (3) the minimum prestress demand on a panel for gap closure at the base; (4) the maximum story drift demand for the design level ground motion; (5) the maximum wall roof displacement demand for the survival level ground motion; and (6) the roof displacement corresponding to crushing of the spiral confined concrete.

Estimation of the wall demands requires the estimation of various seismic properties and demands for the prototype structure. The seismic properties and demands for the prototype structure (shown in Table 5.3) include the estimated seismic weight (W), 1st mode period (T), structure design base shear demand ($V^s_d$), structure linear-elastic base shear demand for the design level ground motion ($Q^s_d$), and the structure linear-elastic base shear demand for the survival level ground motion ($Q^s_s$). For R equal to 4.5, and $Q_s$ equal to 2.5 times the wall linear-elastic base shear demand for the design level ground motion, $Q_d$, $Q^s_d = 4.5 \times V^s_d$ and $Q^s_s = 2.5 \times 4.5 \times V^s_d$.

The wall design base shear demand, $V_d$ for the prototype wall is determined from the structure design base shear demand as described in Section 4.4.1. Due to the symmetry in the plan layout of the prototype structure (see Figure 5.1), the center of mass and the center of stiffness of the building coincide. Thus, the applied eccentricity is zero. However, accidental eccentricity equal to 5% of the dimension of the structure in the direction perpendicular to the E-W walls (i.e., $e_{acc} = 0.05 \times 120$ ft. = 6 ft.) is considered in design. Thus, from Equation 4.12, the design base shear demand for the prototype wall is the sum of the wall base shear demand due to story translations induced by the ground motion and the wall base shear demand due to story twist caused by accidental torsion (i.e., $V_d$ = 268 kips + 80 kips = 348 kips). The wall design base shear demand is shown along with the other estimated demands for the prototype wall in Table 5.2.

### 5.3.3 Seismic design capacities versus demands for the prototype wall

Table 5.2 presents comparisons between estimated design capacities and demands (associated with the eight design criteria discussed in Section 4.2) for the prototype wall. Table 5.2 shows that all of the seismic design criteria discussed in Section 4.2 are satisfied by the prototype wall. Finally, comparisons between the estimated base shear and roof displacement capacities and base shear and roof displacement demands (based on design criteria 1, 2, 3, and 6) are shown for the prototype wall in Figure 5.7.

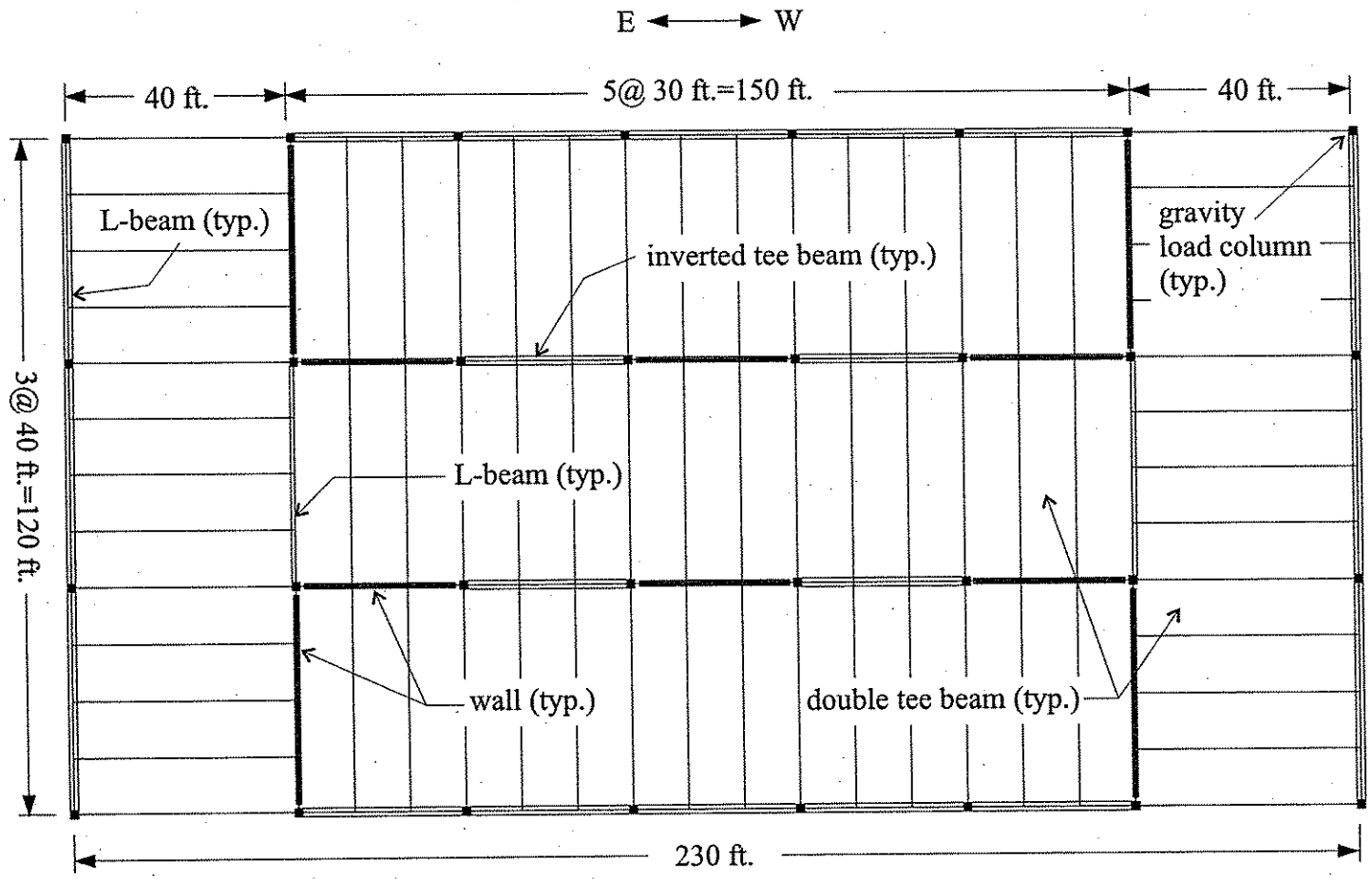


Figure 5.1. Plan view of the prototype structure.

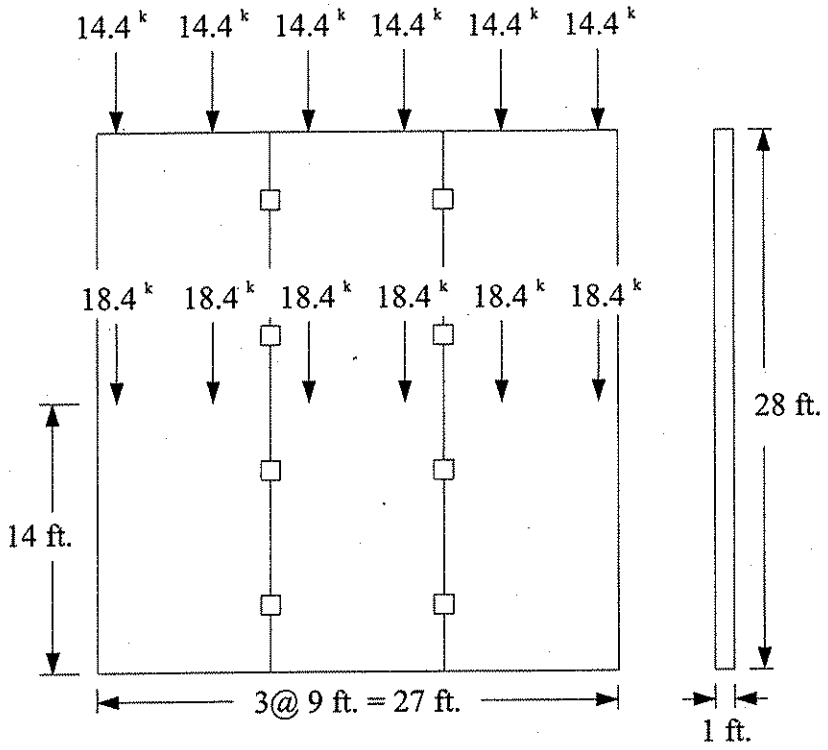


Figure 5.2. The prototype wall.

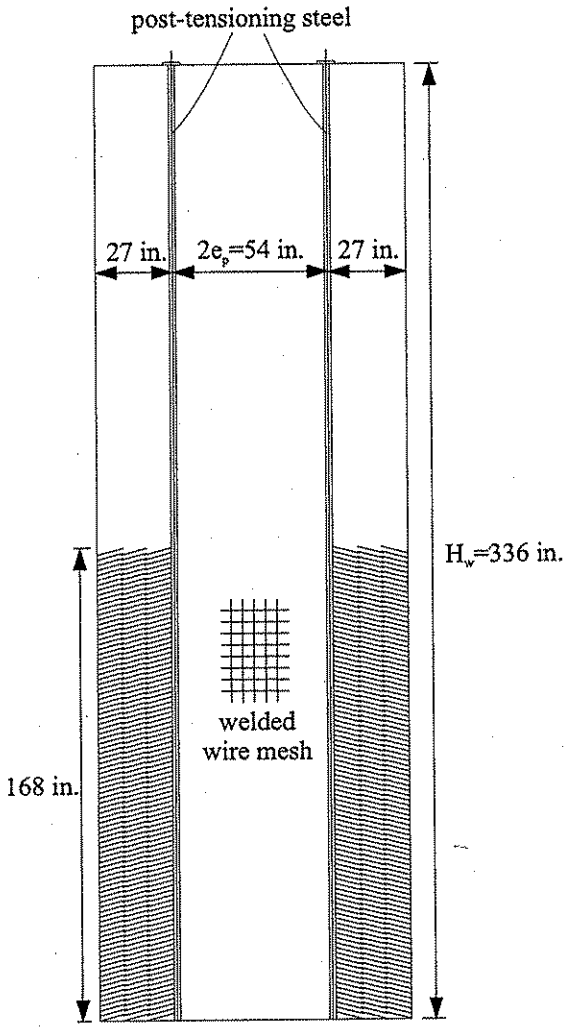


Figure 5.3. Elevation view of the prototype wall.

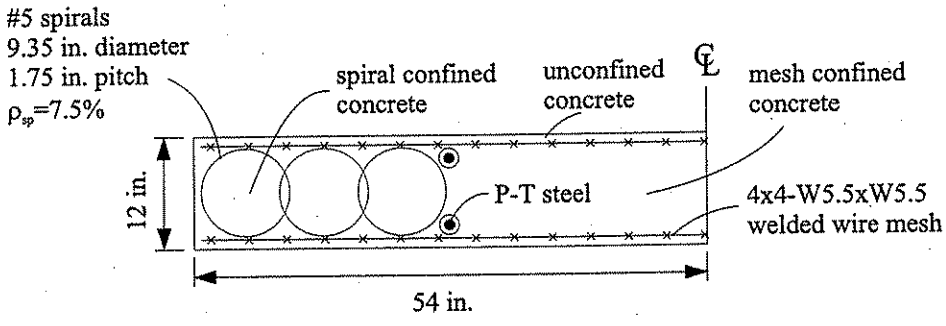


Figure 5.4. Cross-section of the prototype wall.

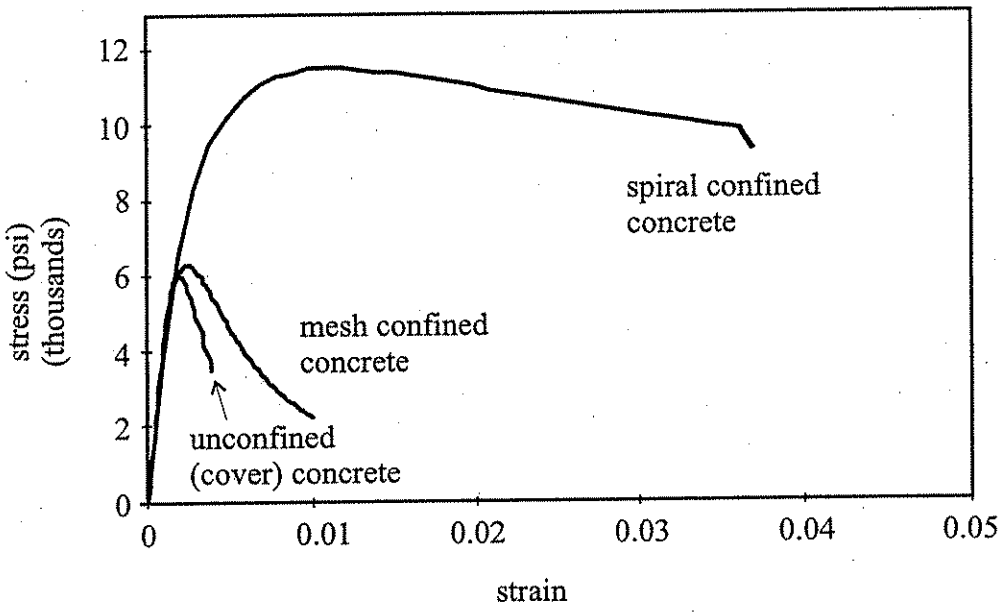


Figure 5.5 Concrete compressive stress-strain relationships for unconfined, mesh confined, and spiral confined concrete (Kurama et al. 1997).

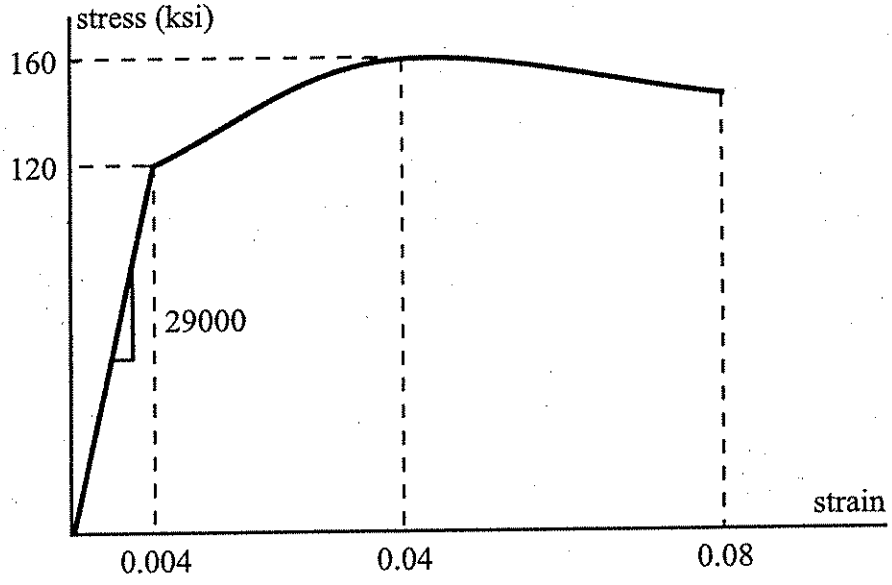


Figure 5.6 Stress-strain relationship for post-tensioning steel (adapted from Kurama et al. 1997).

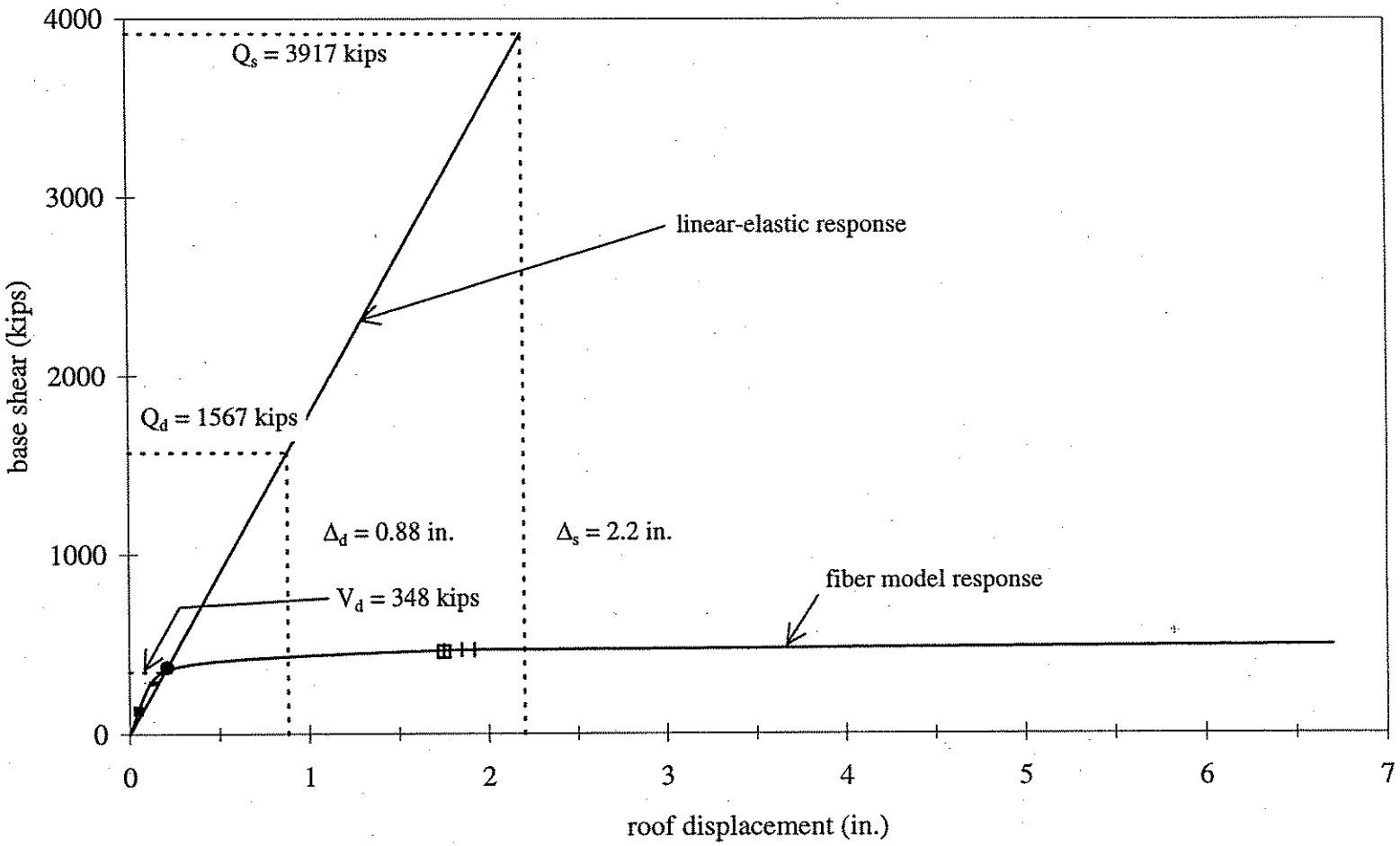


Figure 5.7 Base shear and roof displacement capacities and demands for the prototype wall.

Table 5.1. Properties of the prototype wall.

| $l_x$ (in.) | $l_w$ (in.) | $H_w$ (in.) | $t_w$ (in.) | $A_j$ ($in^2$) | $A_p$ ($in^2$) | $e_p$ (in.) | $f_{pi}/f_{pu}$ | $\rho_{sp}$ (%) |
|---|---|---|---|---|---|---|---|---|
| 108 | 324 | 336 | 12 | 4.5 | 4.0 | 27 | 0.6 | 7.5 |

Table 5.2 Estimated seismic capacities and demands for the prototype wall.

| | **Seismic Design Criteria** (Section 4.2) | **Capacity** | **Demand** |
|---|---|---|---|
| **Criterion 1** | $V_{ell} > V_d = Q_d/R$ (Eqn. 4.1) | $V_{ell}$ = 372 kips (Eqn. 3.3) | $V_d$ = 348 kips (Eqn. 4.12) |
| **Criterion 2** | $\Phi_f V_{llp} > V_d$ (Eqn. 4.2) | $\Phi_f$ = 0.75 $V_{llp}$ = 460 kips (Eqn. 3.9) | $V_d$ = 348 kips |
| **Criterion 3** | $\Delta_{llp} > \Delta_d$ (Eqn. 4.3) | $\Delta_{llp}$ = 1.8 in. (Eqn. 3.10) | $\Delta_d$ = 0.88 in. (Section 4.4.2) |
| **Criterion 4** | $\Phi_{gc}(P_i l_x/2) + N(l_x - e_N) \geq P_{llj} l_x$ (Eqn. 4.4) | 20,000 kip-ft. | 18,000 kip-ft. |
| **Criterion 5** | $\delta_{all} \geq \delta_d$ (Eqn. 4.5) | $\delta_{all}$ = 2.5% (NEHRP 1994) | $\delta_d$ = 0.3% (Eqn. 4.14) |
| **Criterion 6** | $\Delta_{csc} \geq \Delta_s$ (Eqn. 4.6) | * | $\Delta_s$ = 2.2 in. (Section 4.4.2) |

* Closed-form solution not developed. Results can be obtained from a nonlinear static push-over analysis. Values not shown in table because $\Delta_{csc}$ was not reached in analysis.

Table 5.3. Estimated seismic properties and demands for the prototype structure.

| **W (kips)** | **T (sec.)** | **$V^s_d$ (kips)** | **$Q^s_d$ (kips)** | **$Q^s_s$ (kips)** |
|---|---|---|---|---|
| 7289 | 0.24 | 1604 | 7218 | 18045 |

# Chapter 6

# ANALYTICAL MODELING OF UNBONDED POST-TENSIONED PRECAST WALLS

This chapter describes the analytical model that was developed to model the behavior of unbonded post-tensioned precast walls with vertical joints and ductile connectors. The model was developed using the DRAIN-2DX program (Prakash and Powell 1993) and uses the fiber element capabilities of the program. The model described in this chapter was used to conduct a series of monotonic and cyclic lateral load analyses (Chapter 7). The model can also be used for dynamic analyses, though such analyses are not included in this report. The analysis and modeling assumptions are discussed in Section 6.1. Section 6.2 identifies the various components of the wall and how they are modeled in the DRAIN-2DX program.

## 6.1 ANALYSIS AND MODELING ASSUMPTIONS

The analytical model was developed to study the seismic behavior of the prototype walls of the prototype precast structure described in Section 5.1. Attention focused on walls that provide lateral load resistance in the E-W direction of the structure. The model is developed to perform two-dimensional nonlinear analyses of isolated walls. The following assumptions are made for modeling and analyzing the walls under static monotonic and cyclic loads:

1. Seismic forces act in the direction of the walls.

2. The walls undergo in-plane axial, flexural, and shear deformations only. Torsional and out-of-plane deformations of the walls are not modeled.

3. The entire seismic force in the E-W direction of the prototype structure is resisted solely by the E-W walls.

4. Seismic forces at each floor and at the roof are transferred to the walls by the floor and roof diaphragms by adequate connections between the walls and the diaphragms. For in-plane forces, the floor and roof diaphragms are assumed to be rigid.

5. All walls undergo the same displacements at each floor level based on the rigid floor and roof diaphragm assumption.

6. Anchorages of the post-tensioning tendons remain fully effective during the seismic response of the walls.

7. Anchorages of the vertical joint connectors remain fully effective during the seismic response of the walls.

8. Elastic and inelastic deformations that may occur in the foundation or the supporting ground are not considered.

9. The walls are adequately braced against out-of-plane buckling.

## 6.2 THE PRECAST WALL MODEL

### 6.2.1 Overview

This section describes an analytical model developed using the DRAIN-2DX fiber element for the nonlinear inelastic axial-flexural behavior of unbonded post-tensioned precast walls. Figure 6.1(a) shows the elevation of a two-story precast wall with three panels, and the corresponding fiber wall model is shown in Figure 6.1(b). The axial-flexural behavior of the wall is modeled using fiber elements, beam-column elements, truss bar elements, and simple connection elements.

Fiber elements are used in the lower portion of the wall to model gap opening along the base of the panels. Fiber elements are also used to model the height of each panel that is reinforced with spirals, which in this case corresponds to $0.5H_w$. Beam-column elements are used to model the top half of the panels, where the strains developed in the concrete due to lateral loads are expected to remain in the linear-elastic range. The unbonded post-tensioning steel is modeled using truss elements (shown as dashed lines in Figure 6.1(b)) which are connected to the model at the ends of the unbonded length. A connection element is used to model the connection between adjacent panels. Finally, the displacements of various nodes in the model are slaved to provide the correct deformation of the wall. This is described more fully later in this chapter.

The fiber element is described briefly in Section 6.2.2. This is followed by descriptions of the various components of the model in Sections 6.2.3 through 6.2.5.

### 6.2.2 The fiber beam-column element in DRAIN-2DX

The fiber element in the DRAIN-2DX program (Prakash and Powell 1993) is a nonlinear inelastic element for modeling the axial-flexural behavior of steel, reinforced concrete, or composite steel-concrete beams and beam-columns. Kurama et al. describe the fiber beam-column element in detail and verify the axial-flexural behavior of the element. A brief review is presented here.

Figure 6.2(a) shows a reinforced concrete section with longitudinal steel, transverse ties, and spiral reinforcement. Because the regions of the concrete section have different levels of confinement (or no confinement) provided by the spirals and ties, the stress-strain relationships vary for each region (Figure 6.2(b)).

Figure 6.2(c) shows how the fiber beam-column element is used to model the reinforced concrete section by a series of steel and concrete fibers. Each fiber is characterized by a uniaxial material stress-strain relationship, an area, and a distance from a longitudinal reference axis.

Figure 6.2(d) shows a typical fiber element. The fiber element is divided into a number of fiber segments. The behavior of the fiber element is monitored at the midpoint of each fiber segment, which is represented by a fiber slice. The fiber slice has the properties of the fiber cross-section shown in Figure 6.2(c). The cross-sectional properties are assumed to be constant within each fiber segment, but may vary from fiber segment to fiber segment.

### 6.2.3 Modeling of wall panels

The concrete portions of the wall panels are modeled by fiber elements and beam-column elements along the height of the wall. As shown in Figure 6.1, the fiber elements and beam-column elements are located at the centerline of each panel.

Figure 6.3 shows a cross-section near the base of a typical panel of the wall shown in Figure 6.1(a). As shown in this figure, spiral reinforcement is provided near the ends of the panels to resist the large compressive strains that develop there as a result of gap opening. Typically a finer fiber discretization (in terms of the number of fiber elements, segments, and the number of fibers in the depth of the cross-section) is used near the base of the wall where the nonlinear deformations of the wall are expected to concentrate. Kurama et al. show that the length of the fiber segment closest to the base of the wall controls the nonlinear behavior of the wall under lateral loads. The length of the controlling fiber is set equal to the height of the wall region over which significant nonlinear behavior and crushing in concrete is expected to occur. In this research, the length of the controlling fiber segment near the base is assumed to be equal to the spiral-confined thickness of the wall cross-section (9.75 in.). This assumption is thought to be conservative (as far as estimated displacement capacities are concerned) because the height of the nonlinear wall region near the base is expected to be larger than the spiral-confined thickness of the wall cross-section (Kurama et al., 1996).

The spiral reinforcement and mesh reinforcement in the panels are modeled by including their effect on the compression stress-strain curves of the concrete in the panel. This is discussed further below. The spiral reinforcement and mesh reinforcement do not extend across the panel-to-foundation connection, because gap-opening is supposed to occur at this interface. Accordingly, these reinforcements do not extend across the panel-foundation interface in the model.

To ensure that the individual wall panels do not overlap in the wall model of Figure 6.1(b) when lateral forces are applied, a single rigid link modeled with a truss element (not shown) is set between the roof nodes of adjacent beam-column elements.

#### *Stress-strain relationship for concrete*

In a typical fiber model of the cross-section shown in Figure 6.3, three types of concrete fibers with different stress-strain relationships are identified: (1) unconfined (cover) concrete (i.e., concrete outside the welded wire mesh); (2) spiral-confined concrete (i.e., concrete within the spirals); and (3) mesh-confined concrete (i.e., concrete outside the spirals and inside the welded wire mesh).

The stress-strain relationships of the spiral-confined concrete and unconfined concrete are estimated using the concrete confinement model developed by Mander et al. (1988a, 1988b). Figure 6.4 shows how the smooth stress-strain relationships obtained from the confinement model are approximated using five linear segments for modeling with the fiber element of DRAIN-2DX. The fibers modeling the regions of mesh-confined concrete in Figure 6.3 are assumed to have the same stress-strain behavior as unconfined concrete fibers. This is based on similarities to previous work which showed that the lateral response of a wall is unaffected by modeling the stress-strain behavior of tie-confined concrete fibers with the stress-strain relationship of unconfined concrete (Kurama et al. 1997).

In the concrete stress-strain relationships of Figure 6.4, the tensile stiffness and tensile strength of concrete are neglected in order to model gap opening along the base-to-foundation connections (Kurama et al. 1996).

### 6.2.4 Modeling of post-tensioning steel

Figure 6.1(a) shows post-tensioning steel oriented vertically along both sides of each panel. This steel, modeled by truss elements, is anchored to the wall at the roof and at the base. The anchorages at the roof are modeled by slaving the displacements of the truss elements to the displacements of the beam-column elements modeling the top half of each panel. Slaving is used in the DRAIN-2DX program to cause the displacements of the slaved node to be determined by the displacements of the master node. In essence, the relative positions of the master node and slaved node become fixed by slaving. The displacements and rotation of the master node then determine the displacements and rotation of the slaved node. The three displacements (i.e., two translations and one rotation) of each truss node modeling an anchorage at the roof level are slaved to the displacements of the node modeling the top of the panels (i.e., the roof node of the beam-column element). The slaving, shown as bold lines in Figure 6.1(b), ensures that at the roof, the vertical and horizontal displacements of the truss elements are compatible with the displacements and rotation of the beam-column element. At the base, all nodes (except the truss nodes) are given a fixed boundary condition to model a rigid foundation.

The wall model shown in Figure 6.1(b) shows that each full-height group of post-tensioning steel is modeled by two truss elements connected by a node at mid-height. These mid-height nodes are used to ensure that the lateral displacements of the truss elements and the fiber elements are compatible. In an unbonded post-tensioned wall, the post-tensioning steel is located inside ducts in the wall panels. Consequently, the post-tensioning steel has nearly the same lateral displacements as the wall panels at any point over the height of the wall. To ensure that the lateral displacements of the truss elements are similar to those of the fiber elements, the lateral displacement of each mid-height truss node is slaved to the node connecting the fiber elements at the same floor level. Because the post-tensioning steel is unbonded over the height of the wall, the vertical displacements of the mid-height truss nodes are not slaved to the fiber element nodes.

*Stress-strain relationship of post-tensioning steel*

Figure 6.5(a) shows the stress-strain relationship of the post-tensioning steel. The stress corresponding to the linear limit strain of the post-tensioning steel and the ultimate strength of the post-tensioning steel are defined as $f_{pl}$ and $f_{pu}$ respectively. The smooth stress-strain relationship of the post-tensioning steel can be idealized by a trilinear relationship as shown in Figure 6.5(a). Since the DRAIN-2DX program uses a bilinear stress-strain relationship for truss elements, this research employed the bi-linear stress-strain relationship shown in Figure 6.5(b), where the yield strength of the truss elements ($f_{py}$) corresponds to the linear limit ($f_{pl}$) of the stress-strain relationship shown in Figure 6.5(a). Modeling the unbonded post-tensioning steel in this manner is satisfactory provided that the ultimate stress ($f_{pu}$) is not exceeded. For a well designed wall, this will be the case.

### 6.2.5 Modeling of vertical joint connectors

Figure 6.1(a) shows four vertical joint connectors located along the vertical joint between adjacent precast concrete panels. The two vertical joint connectors at each story are lumped at the mid-height of the story and modeled by one simple connection element as shown in Figure 6.1(b). The simple connection element in DRAIN-2DX is an inelastic element that can be used to model structural connections with rotational and/or translational flexibility (Prakash and Powell 1993). The element connects two nodes which must have identical coordinates (i.e., this is a zero-length element) and it can be used to connect either the rotational displacements or the translational displacements of the nodes. For a translational connection, the element can connect horizontal displacements or vertical displacements, but not inclined displacements (Prakash and Powell 1993).

For the fiber model shown in Figure 6.1(b), each simple connection element connects the vertical displacements of the nodes. The reason for connecting the vertical displacements can be explained using the idealized wall response of Figure 6.6. Figure 6.6(a) shows a two-panel wall in its undisplaced position. The wall has a vertical joint connector between nodes A and B, which have the same coordinates. As the wall is displaced laterally as shown in Figure 6.6(b), nodes A and B move vertically relative to eachother along the vertical joint of the wall. Thus, the connection element modeling a vertical joint connector behaves like a translational spring that acts in the direction of the local vertical axis of the element.

To achieve a relative vertical displacement between the two nodes of a simple connection element in the wall model (Figure 6.1(b)), the three displacements (two translations and one rotation) of one node of the connection element are slaved to the displacements of one of the adjacent fiber element (or beam-column element) node and the three displacements of the other node of the connection element are slaved to the displacements of the other adjacent fiber element (or beam-column element) node.

The DRAIN-2DX program requires the initial stiffness, strain hardening ratio, and yield force to be defined for the simple connection element. As noted above, the walls considered in this study have four vertical joint plates, which are modeled with two simple connection elements. Thus, each simple connection element models two vertical joint plates. The connection detail selected for the vertical joints is shown in Figure 2.2(g). The vertical joint plates

are welded to steel plates which are embedded in the concrete panels. The embedded plates are anchored to the panels with rebar. It may be possible for this connection detail to have imperfections in the welds, or for the anchorage hardware to slip as the wall is subjected to lateral loads. These imperfections will affect the connection by introducing some flexibility into it. Accordingly, for the walls considered in this study, the flexibility of each of the vertical joint plates is increased by 50% (i.e., $F_{vjp} = 1.5\ L_{pl} / G_{pl}\ A'_{pl}$). Since each simple connection element models two vertical joint plates, the initial shear stiffness of a simple connection element, $k_{i,sce}$ is given by

$$k_{i,sce} = 2\left(\frac{1}{3} \cdot \frac{G_{pl} \cdot A'_{pl}}{L_{pl}}\right) \tag{6.1}$$

where $G_{pl}$, $A_{pl}$, and $L_{pl}$ represent the shear modulus, the shear area, and the length of the connection plates across the vertical joint. The strain hardening ratio assigned to the simple connection element is 0.001. The yield force of the connection element is taken as the product of the vertical joint shear yield stress and the shear area of the steel in the vertical joint connection.

### 6.2.6 Modeling of loads

Three types of loads are included in the fiber model: (1) post-tensioning loads; (2) gravity loads; and (3) seismic loads. In the analyses of unbonded post-tensioned precast walls, the post-tensioning loads are applied first, followed by the gravity loads and the seismic loads, in that order.

***Post-tensioning loads***

In the fiber model, post-tensioning loads are modeled as tensile forces in the truss elements that model the post-tensioning steel. Upon application of the tensile forces in the truss elements, compression forces develop in the fiber elements and the beam-column elements (modeling the wall panels) to satisfy equilibrium. These compression forces cause the fiber elements, beam-column elements, and the truss elements to elastically undergo axial shortening. As a result of elastic shortening due to post-tensioning, some of the tensile force in the truss elements is lost. Thus, the required amount of total force applied to the truss elements in a panel, $P_t$ to achieve the desired level of total force in the post-tensioning steel after elastic shortening due to post-tensioning, $P_i'$ is given by Kurama et al. as

$$P_t = P_i' \left(1 + m\frac{A_p}{A_{xnet}}\right) \tag{6.2}$$

where m is the modular ratio, $A_p$ is the total cross-sectional area of post-tensioning steel in a panel, and $A_{xnet}$ is the net cross-sectional area of a panel (i.e., gross cross-sectional area minus the area of the post-tensioning ducts).

***Gravity loads***

Gravity loads consist of dead loads carried by the wall panels based on the appropriate tributary areas plus the self weight of the panels. The dead load on a wall panel is adjusted according to NEHRP (1994) to account for the effects of horizontal and vertical ground accelerations, where the effects of gravity counteract the seismic load. Thus, the gravity load on a

wall panel is reduced by $0.5C_aN$, where $C_a$ is a seismic coefficient introduced in the 1994 edition of NEHRP (see Section 4.4.1), and N is the dead load on a panel, including the panel self-weight. Figure 6.7(a) shows the gravity loads on a two-story precast wall similar to the prototype wall shown in Figure 5.2. The self-weight of the wall panels is modeled by concentrated forces applied at the mid-height of each story. As discussed in Section 5.2, floor and roof loads are transferred to the walls by double tees. In the fiber wall model, gravity loads transferred to the walls by double tees are modeled as concentrated forces applied at the ends of fiber elements and beam-column elements at each floor and roof level as shown in Figure 6.7(b). These concentrated forces represent the resultant of the stem loads for a given double tee. It is noted that the fiber wall model neglects the eccentricity of the double tee stem resultant loads present in the two exterior wall panels (see Section 5.2). This eccentricity was neglected so that the model corresponds with the simplified closed-form expressions of Chapter 3 that estimate the base-shear-roof-displacement capacities of the wall with concentric axial forces, and not with the general expressions which consider eccentric axial forces. This was done because the general expressions were not available at the time the model was created.

***Seismic loads***

The seismic loads considered in the static analyses are modeled by equivalent lateral loads determined from NEHRP (1994) applied on the fiber elements and beam-column elements at each floor level and roof level. This is shown for a two-story precast wall and the corresponding fiber wall model in Figure 6.8. Figure 6.8 shows a triangular lateral load distribution with the maximum load at the roof level.

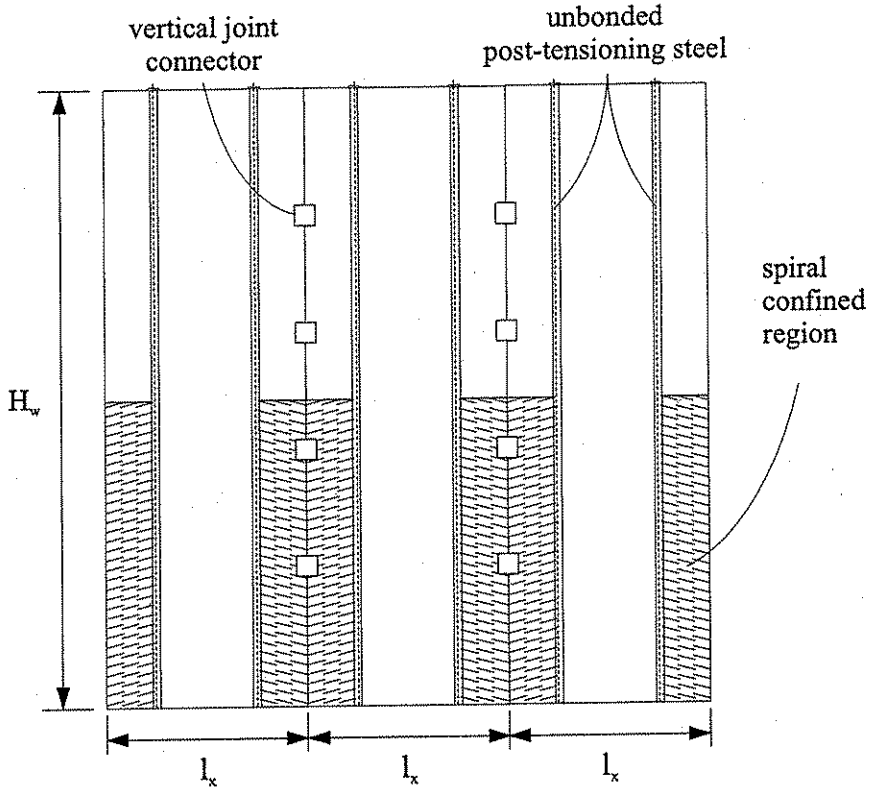


(a) precast wall

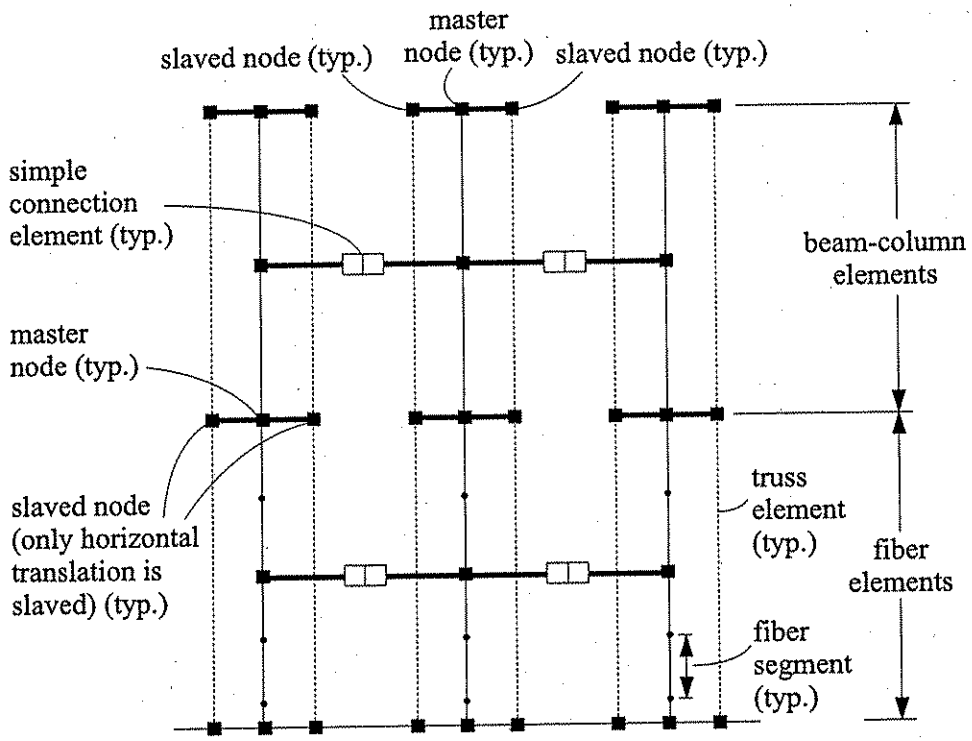


(b) fiber model

Figure 6.1 The fiber wall model.

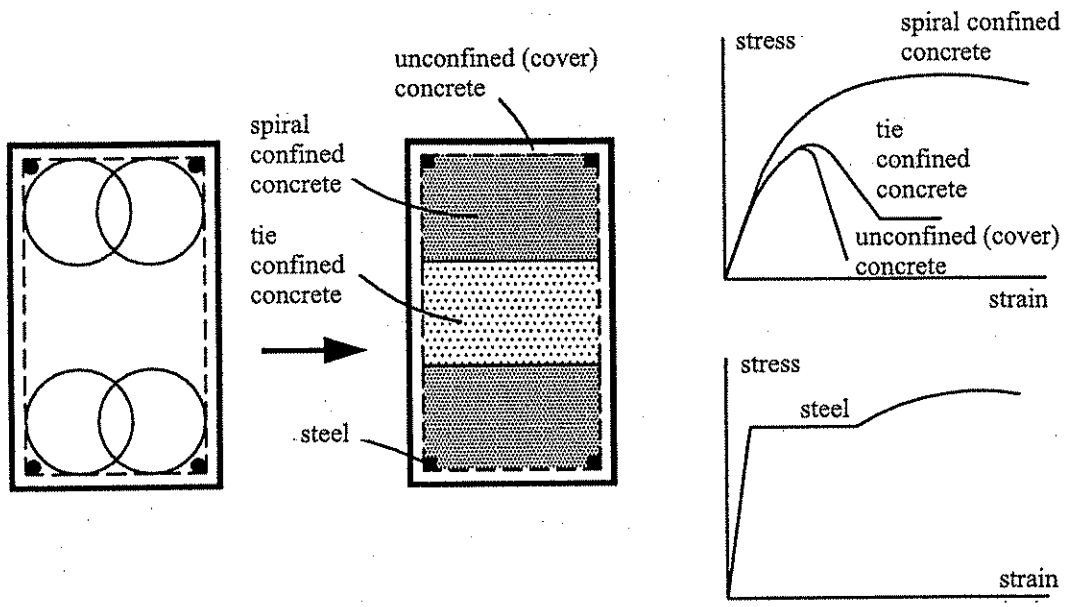


(a) reinforced concrete section

(b) regions of the section with different stress-strain behavior

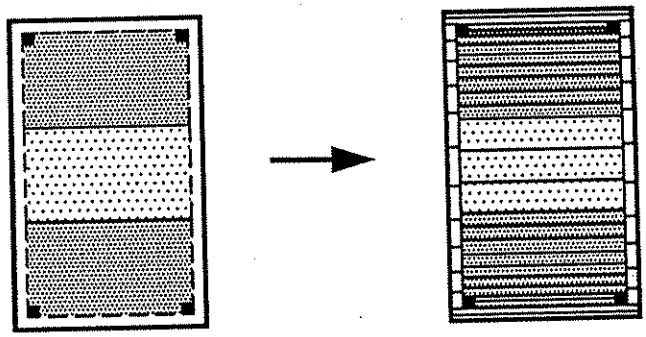

(c) idealization of the section

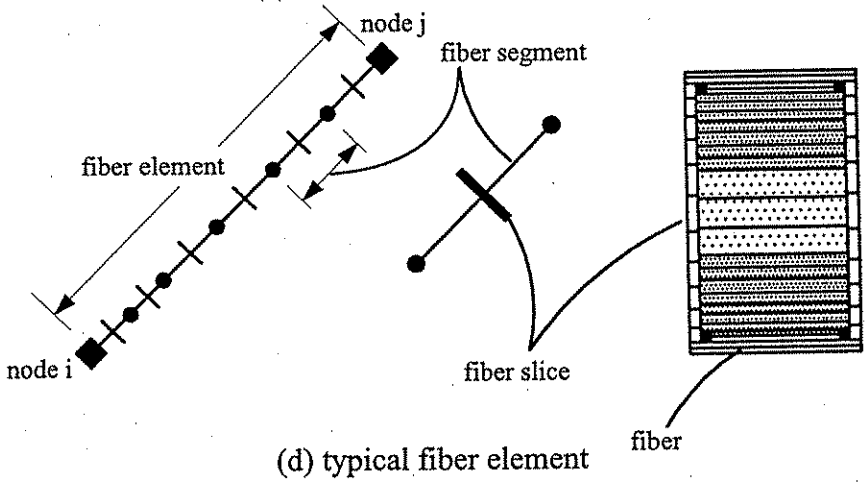


(d) typical fiber element

Figure 6.2 The fiber beam-column element in DRAIN-2DX (adapted from Kurama et al. 1997).

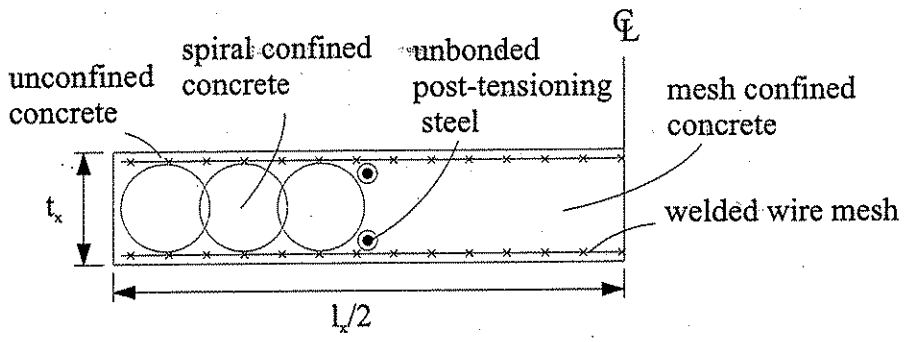


Figure 6.3 Typical cross-section of a panel near the base of the wall.

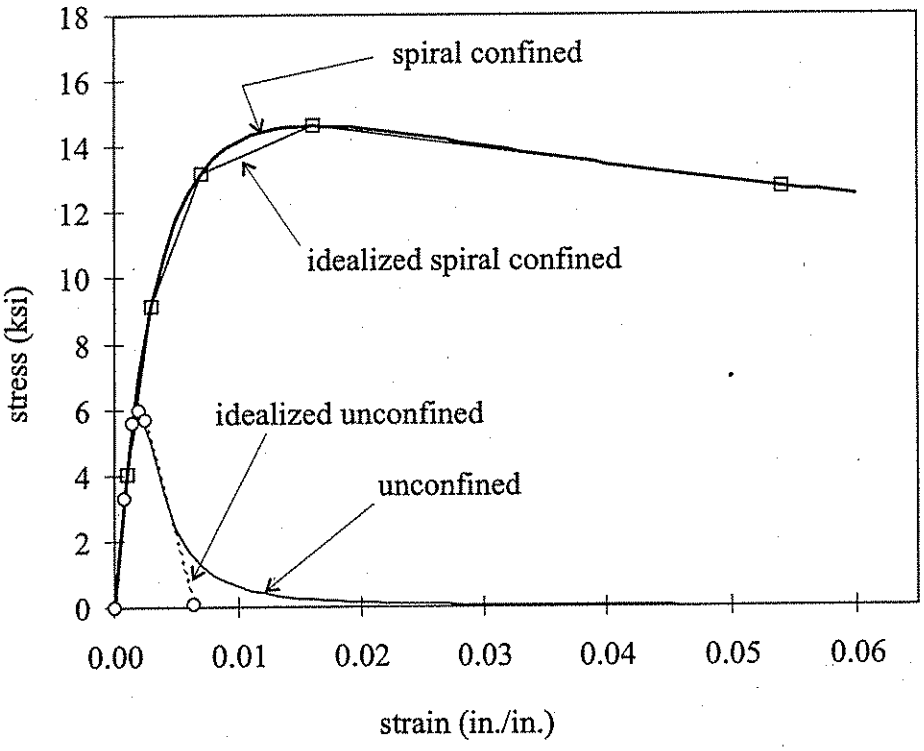


Figure 6.4 Concrete compressive stress-strain relationships for spiral confined and unconfined concrete.

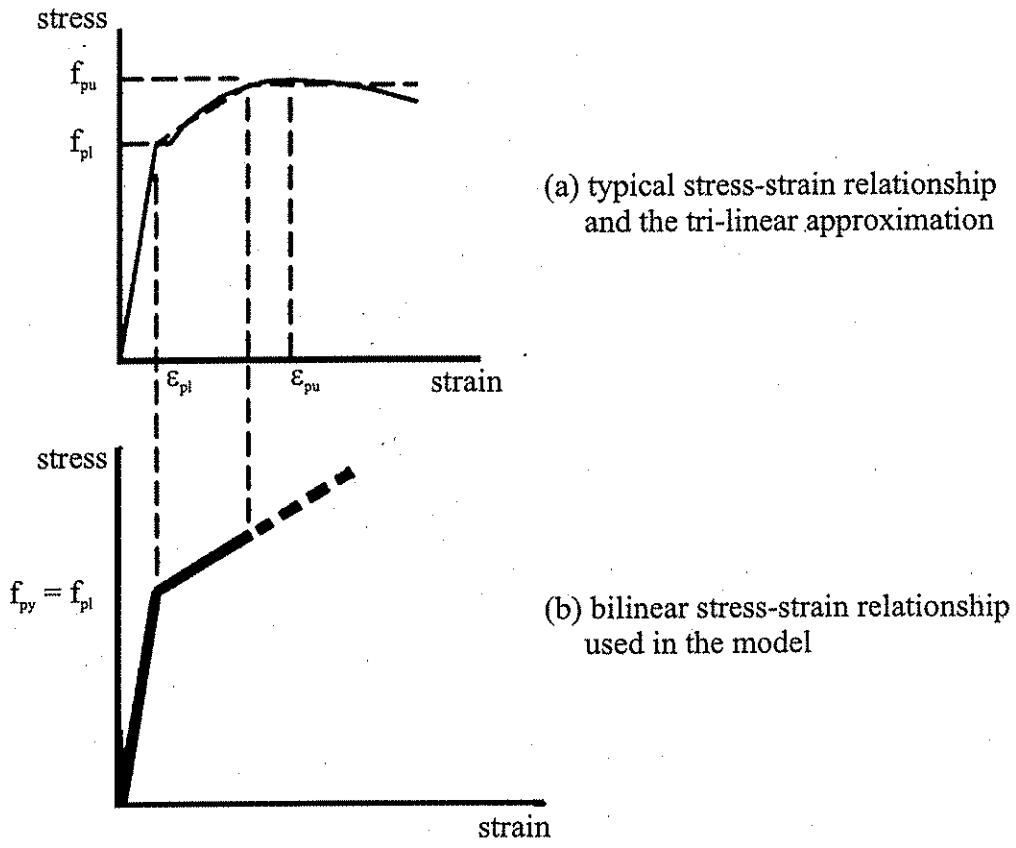


Figure 6.5 Modeling of the stress-strain relationship of the post-tensioning steel (Kurama et al. 1997).

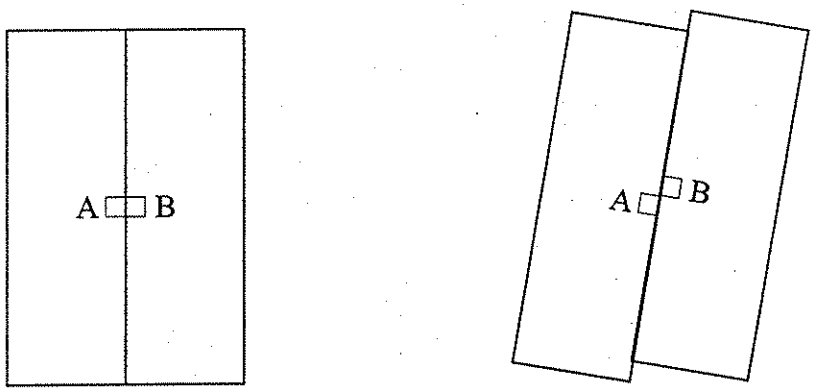


Figure 6.6 Relative vertical displacement at joint connection.

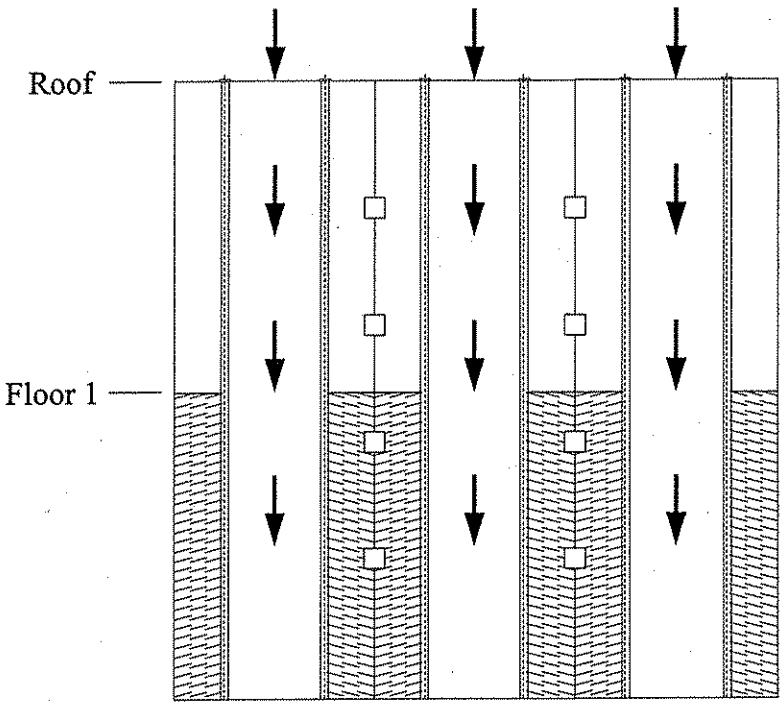


(a) precast wall

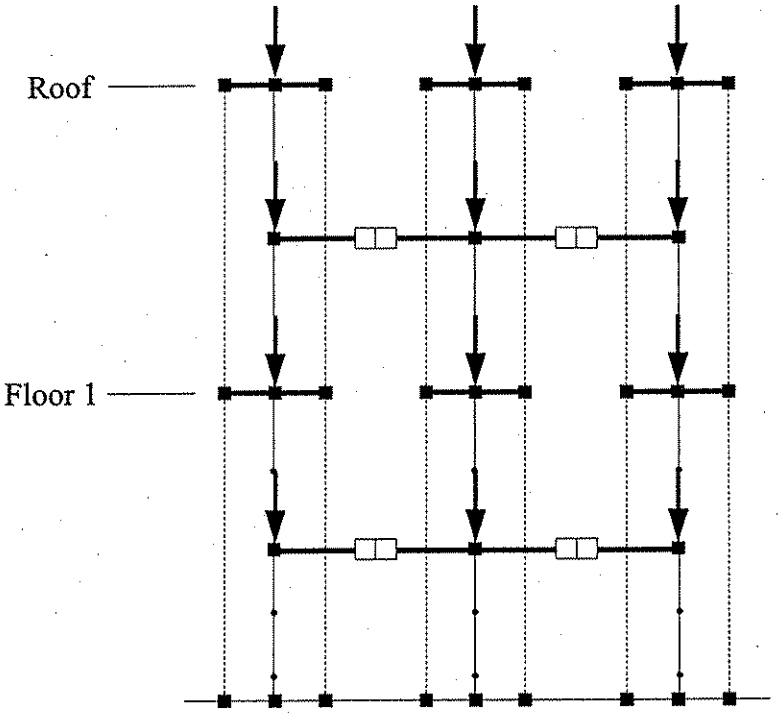


(b) fiber model

Figure 6.7 Modeling of gravity loads.

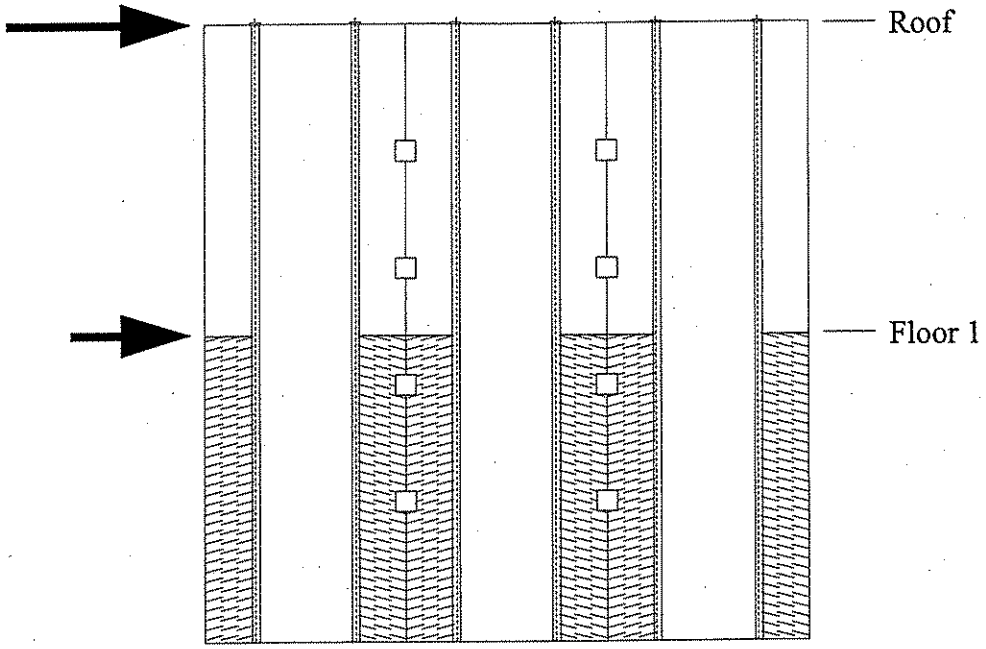


(a) precast wall

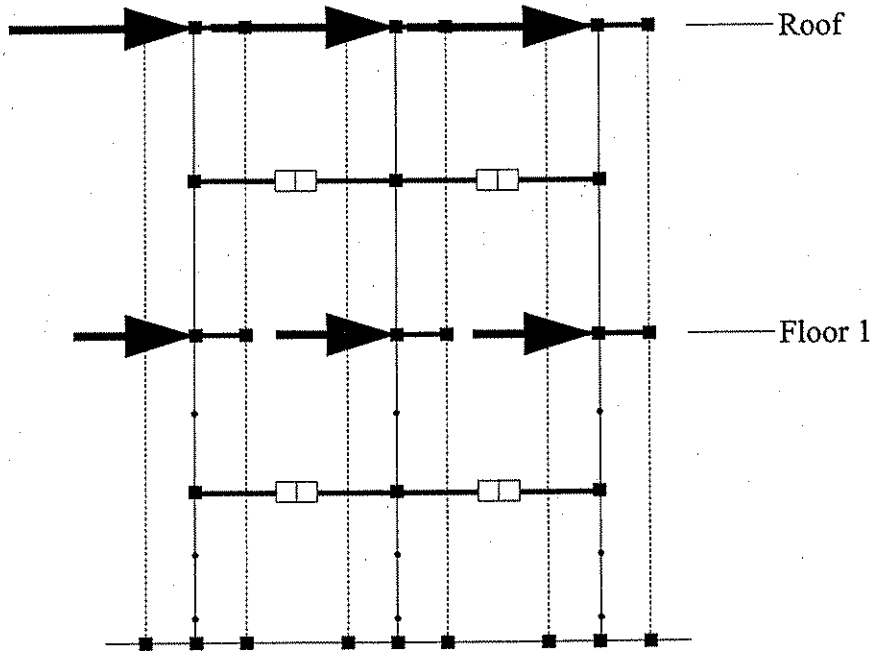


(b) fiber model

Figure 6.8 Modeling of seismic loads.

# Chapter 7

# STATIC ANALYSIS OF UNBONDED POST-TENSIONED PRECAST WALLS

This chapter presents the results of a series of monotonic and cyclic static analyses of unbonded post-tensioned precast walls. Much of the chapter focuses on an evaluation of the effect of several structural design parameters on the lateral load response of the prototype unbonded post-tensioned precast wall described in Section 5.2. The analyses treat a total of 18 different walls– the prototype wall and 17 other walls that include a systematic variation of properties from the prototype wall. The structural design parameters that are evaluated in the design parameter study are described in Section 7.1. Section 7.2 identifies the response quantities that are used to describe the lateral load response of the walls. The results of the design parameter study under monotonic lateral loads are given in Section 7.3 and discussed in Section 7.4. The relationship between the structural design parameters and the seismic design criteria (given in Chapter 4) is discussed in Section 7.5.

Three walls treated in the monotonic lateral load analyses were also analyzed under the action of cyclic static lateral loads. Section 7.6 presents and discusses the results of these analyses.

## 7.1 STRUCTURAL DESIGN PARAMETERS INVESTIGATED IN THE STUDY

The effect of four structural design parameters on the static nonlinear lateral load response of the prototype wall was investigated. The four design parameters are: (1) total shear area of connectors across a vertical joint, $A_j$ (referred to as the area of vertical joint connectors); (2) initial stress in the post-tensioning steel after elastic shortening due to post-tensioning and gravity load (referred to as the initial stress in the post-tensioning steel) with variable $A_p$ (where $A_p$ is the total area of post-tensioning steel in a panel) to produce a constant prestress force in the post-tensioning steel, $P_i$; (3) initial stress in the post-tensioning steel with constant $A_p$ and variable $P_i$; and (4) total area of post-tensioning steel in a panel, $A_p$ with constant $f_{pi}$ and variable $P_i$.

The study of each design parameter is called a parameter investigation. In each parameter investigation, the lateral load responses of a series of walls which are a variation of the prototype wall are studied. A total of 18 walls are treated in this study. The prototype wall is referred to as PW1, and the remaining walls are numbered 2 through 18.

### 7.1.1 Area of vertical joint connectors

The objective of this parameter investigation is to determine the effect of varying the total shear area of connectors across a vertical joint, $A_j$. Five walls (including PW1) are considered, as shown in Table 7.1. This table gives the following information for each wall: (1) the number of post-tensioning bars in each panel, $N_b$ and the diameter of each bar; (2) total area of post-tensioning steel in a panel, $A_p$; (3) initial stress in the post-tensioning steel, $f_{pi} = P_i/A_p$; (4) total force in the post-tensioning steel of a panel after elastic shortening due to

post-tensioning and gravity load, $P_i$; (5) gravity load on a panel, N (reduced by $0.5C_aN$ as discussed in Section 6.2.6); (6) area of vertical joint connectors across a single joint between two panels, $A_j$; (7) linear limit force of vertical joint connectors, $P_{llj} = f_{llj}A_j$ (where $f_{llj}$ is the shear yield strength of the vertical joint connectors); (8) stress in a concrete panel due to $P_i$, $f_{ci,P} = P_i/A_{x,net}$ (where $A_{x,net}$ is the net cross-sectional area of a panel); (9) stress in a concrete panel due to N, $f_{ci,N} = N/A_{x,net}$; and (10) initial stress in a concrete panel, $f_{ci} = f_{ci,P} + f_{ci,N}$. The stress $f_{ci,P}$ is also referred to as the initial stress in the concrete due to post-tensioning, and the stress $f_{ci,N}$ is also referred to as the initial stress in the concrete due to gravity load.

### 7.1.2 Initial stress in post-tensioning steel with variable $A_p$

The objective of this parameter investigation is to determine the effect of varying both the initial stress in the post-tensioning steel, $f_{pi}$ and the total area of post-tensioning steel in a panel, $A_p$ such that $P_i$ and $f_{ci,P}$ remain constant. As shown in Table 7.2, five walls (including PW1) are considered in this parameter investigation. Table 7.2 is organized in the same manner that Table 7.1 is organized.

### 7.1.3 Initial stress in post-tensioning steel with constant $A_p$

The objective of this parameter investigation is to determine the effect of varying the initial stress in the post-tensioning steel, $f_{pi}$, while keeping the total area of post-tensioning steel in a panel, $A_p$ constant. By varying $f_{pi}$ and keeping $A_p$ constant, the initial stress in a concrete panel after elastic shortening due to post-tensioning and gravity load, $f_{ci}$ varies in the parameter investigation. Five walls (including PW1) are included in this parameter investigation, as shown in Table 7.3. The organization of Table 7.3 is the same as the organization of Table 7.1.

### 7.1.4 Area of post-tensioning steel

The objective of this parameter investigation is to determine the effect of varying the total area of post-tensioning steel in each panel, $A_p$. Varying $A_p$ while keeping the initial stress in the post-tensioning steel, $f_{pi}$ constant varies the initial stress in a concrete panel after elastic shortening due to post-tensioning and gravity load, $f_{ci}$. Table 7.4 shows that six walls (including PW1) are considered in this parameter investigation. Table 7.4 is organized in the same manner that Table 7.1 is organized.

## 7.2 ANALYSIS RESPONSE QUANTITIES

The analysis response quantities examined in the design parameter study include base shear and roof displacement quantities that are used to describe the base-shear-roof-displacement response of the walls. The response quantities are obtained in one of two ways: (1) from nonlinear lateral load analyses using the fiber model and the DRAIN-2DX program; or (2) from closed-form expressions which were developed in Chapter 3. The response quantities are: (1) base shear and roof displacement corresponding to initial gap opening (i.e., decompression) at the base of the wall ($V_{dec}$ and $\Delta_{dec}$, respectively); (2) base shear and roof displacement at which the vertical joint connectors reach their linear limit strain ($V_{llj}$ and $\Delta_{llj}$, respectively); (3) base shear and roof displacement at which the effective linear limit of the base-shear-roof-displacement relationship is reached ($V_{ell}$ and $\Delta_{ell}$, respectively); (4) base

shear and roof displacement corresponding to the linear limit strain of the post-tensioning steel ($V_{llp}$ and $\Delta_{llp}$, respectively); and (5) base shear corresponding to the peak base shear, $V_{max}$. In addition to the base shear and roof displacement quantities listed above, the effect of the design parameters on the initial lateral stiffness of the walls is investigated.

The analysis response quantities listed above are described in the sections that follow. How these response quantities are determined for the walls in the design parameter study is also discussed.

### 7.2.1 Decompression

The structure limit state corresponding to decompression at the base of the wall is discussed in Section 3.1.1. Since the wall is comprised of three panels, decompression of the wall is defined as the first occurrence of decompression of a wall panel. The base shear and roof displacement corresponding to decompression at the base of the wall are denoted by $V_{dec}$ and $\Delta_{dec}$, respectively. These response quantities are determined from nonlinear lateral load analyses using the fiber model.

### 7.2.2 Linear limit strain of vertical joint connectors

The structure limit state corresponding to the linear limit strain of the vertical joint connectors is discussed in Section 3.1.1. This limit state is defined by the first occurrence of yielding of the vertical joint connectors. The base shear and roof displacement corresponding to the linear limit strain of vertical joint connectors are denoted by $V_{llj}$ and $\Delta_{llj}$, respectively. These response quantities are determined from nonlinear lateral load analyses using the fiber model.

### 7.2.3 Effective linear limit of base-shear-roof-displacement relationship

The structure limit state corresponding to the effective linear limit of the base-shear-roof-displacement relationship is discussed in Section 3.1.1. The base shear and roof displacement corresponding to the effective linear limit are denoted by $V_{ell}$ and $\Delta_{ell}$, respectively. $V_{ell}$ is estimated using Equation 3.3, and $\Delta_{ell}$ is estimated using Equation 3.7 for the walls considered in the design parameter study.

### 7.2.4 Linear limit strain of post-tensioning steel

The structure limit state corresponding to the linear limit strain of post-tensioning steel is discussed in Section 3.1.1. This limit state is defined by the first occurrence of yielding of the post-tensioning steel. The base shear and roof displacement corresponding to the linear limit strain of the post-tensioning steel are denoted by $V_{llp}$ and $\Delta_{llp}$, respectively. $V_{llp}$ is estimated using Equation 3.9, and $\Delta_{llp}$ is estimated using Equation 3.10 for the walls considered in the design parameter study.

### 7.2.5 Peak base shear

The peak base shear capacity of the walls is discussed in Section 3.1.1. The peak base shear capacity is defined as the base shear corresponding to the first occurrence of yielding of the post-tensioning steel. Thus, the peak base shear corresponds to $V_{llp}$. As shown later, the

value of $V_{llp}$ estimated from Equation 3.9 differs somewhat from the value of $V_{llp}$ predicted from the fiber model. One of these values of $V_{llp}$ must be assigned to $V_{max}$. Since later in this chapter, the base shear response obtained for the walls from nonlinear lateral load analyses (using the fiber model) are normalized with respect to the maximum base shear of the prototype wall (PW1), the maximum base shear $V_{max}$ is assigned the value of $V_{llp}$ obtained from the fiber model in order to maintain the integrity of the data.

### 7.2.6 Lateral stiffness of the walls

The initial lateral stiffness, $k_{wi}$ of each wall is calculated from the slope of the linear-elastic portion of the base-shear-roof-displacement relationship as $k_{wi}=V_{ell}/\Delta_{ell}$, where $V_{ell}$ and $\Delta_{ell}$ are estimated using Equations 3.3 and 3.7, respectively for each of the walls considered in the design parameter study. Kurama et al. define the initial lateral stiffness of an unbonded post-tensioned precast wall with horizontal joints as $k_{wi}=V_{dec}/\Delta_{dec}$, where $V_{dec}$ and $\Delta_{dec}$ are the base shear and roof displacement corresponding to decompression at the base of the wall and are predicted from nonlinear lateral load analysis (using the fiber model). Kurama et al. define the initial stiffness of a wall in this way because a closed-form expression was not developed for defining the initial slope of the base-shear-roof-displacement response of a wall. Thus, it is possible to define the initial lateral stiffness of the walls considered in the design parameter study as $k_{wi} = V_{ell}/\Delta_{ell}$ or as $k_{wi} = V_{dec}/\Delta_{dec}$. In this report, the former ($k_{wi} = V_{ell}/\Delta_{ell}$) is used to estimate the initial stiffness of the walls. The initial lateral stiffnesses of the walls, $k_{wi}$ obtained using the closed-form expression and fiber model, are compared later.

## 7.3 PRESENTATION OF THE RESULTS OF THE DESIGN PARAMETER STUDY

Results of the design parameter study are presented in four ways: (1) an individual plot of base shear versus roof displacement for each of the 18 walls treated in the study; (2) tables that summarize the analysis response quantities; (3) plots of base shear versus roof drift for each parameter investigation; and (4) plots of relationships between the analysis response quantities and the design parameters.

### 7.3.1 Base-shear-roof-displacement relationships

The base-shear-roof-displacement response obtained from the lateral load analysis of each of the 18 walls treated in the design parameter study are shown in Figure 7.1(a) through (r). The analysis response quantities described in Section 7.2 are indicated on the plots using the following markers:

1. Decompression, obtained from fiber model analysis, ■.

2. Linear limit strain of vertical joint connectors, obtained from fiber model analysis, ▪.

3. Effective linear limit of base-shear-roof-displacement relationship, estimated from Equations 3.3 and 3.7, •.

4. Linear limit strain of post-tensioning steel, estimated from Equations 3.3 and 3.7, □.

5. Linear limit strain of post-tensioning steel, obtained from fiber model analysis, +.

As discussed in Chapter 3, the lateral load behavior of an unbonded post-tensioned precast wall can be idealized by a tri-linear approximation which is defined by the effective linear limit point (•) and the point on the base-shear-roof-displacement response corresponding to the linear limit strain of post-tensioning steel (□). Both of these points are computed using the closed-form expressions of Chapter 3. Thus, Figure 7.1 shows the accuracy of the tri-linear idealization of the base-shear-roof-displacement behavior of the walls obtained with the closed-form expressions of Chapter 3. Figure 7.1 shows that, in general, excellent agreement is obtained between the closed-form results of Chapter 3 and the fiber model analysis results. This is discussed further in Section 7.4.

The following roof displacement and base shear demands are shown for the prototype wall, PW1 in Figure 7.1(a): (1) roof displacement demand for the design level ground motion, $\Delta_d$ = 0.88 in.; (2) roof displacement demand for the survival level ground motion, $\Delta_s$ = 2.2 in.; (3) wall design base shear demand, $V_d$ = 348 kips; and (4) the minimum required base shear capacity of the walls, $V_d/\Phi_f$ = 464 kips. These same wall demands are shown on all of the plots of Figure 7.1 to show whether the response of each wall satisfies criterion 1, 2, 3, and 6 of the seismic design criteria discussed in Section 4.2. It is noted here that not all walls were intended to satisfy all criteria.

### 7.3.2 Tables of analysis response quantities

For each of the structural design parameters identified in Section 7.1 (Tables 7.1 through 7.4), the values of the analysis response quantities that are indicated on the base-shear-roof-displacement relationships of the walls (Figure 7.1) are summarized in Tables 7.5 through 7.8.

### 7.3.3 Base-shear-roof-drift relationships

The base-shear-roof-drift relationships obtained from the lateral load analyses of the walls are shown in Figures 7.2 through 7.5 for each of the four structural design parameters identified in Section 7.1. In each figure, the base shear values are normalized with respect to the peak base shear resistance (i.e., base shear capacity) of the prototype wall PW1 (467 kips). The roof drift, in percent, is obtained by normalizing the roof displacement values with respect to the height of the wall (336 in.). Figures 7.2 through 7.5 were generated to show the effect of each design parameter on the base-shear-roof-drift responses of the walls.

### 7.3.4 Relationships between structural design parameters and analysis response quantities

Relationships between the structural design parameters (Tables 7.1 through 7.4) and the analysis response quantities (Tables 7.5 through 7.8) are plotted in Figures 7.6 through 7.13. Each figure shows the effect of one of the design parameters identified in Section 7.1 on the

base shear and roof drift response quantities identified in Section 7.2. The axes are normalized as explained in Section 7.3.3 to yield normalized base shear and roof drift values. All plots of normalized base shear are plotted to the same value of 1.8, and all plots of roof drift are plotted to the same value of 1.5 percent.

In Figures 7.6 and 7.7, the area of vertical joint connectors, $A_j$ is normalized with respect to the area of vertical joint connectors of the prototype wall (PW1), $A_{j,pw1}$ (4.50 $in^2$). In Figures 7.8 through 7.11, the initial stress in the post-tensioning steel, $f_{pi}$ is normalized with respect to the ultimate strength of the post-tensioning steel, $f_{pu}$ (160 ksi). In Figures 7.12 and 7.13, the area of post-tensioning steel is normalized with respect to the area of post-tensioning steel of PW1, $A_{p,pw1}$ (4.00 $in^2$). Figures 7.6 through 7.13 show discrete points (■, ▪, +) which were obtained from nonlinear lateral load analyses of the walls using the fiber model. The closed-form expressions derived in Chapter 3, which estimate the base shear and roof displacement response quantities $V_{ell}$, $V_{llp}$, $\Delta_{ell}$, and $\Delta_{llp}$, are also normalized as explained in Section 7.3.3, and are plotted in the figures.

It is noted that a precise linear limit point cannot be easily defined for unbonded post-tensioned precast walls with horizontal joints that open in flexure because, as discussed in Section 3.1.1, the reduction in lateral stiffness usually occurs in a smooth and continuous manner. Therefore, discrete points that define the linear limit on the base-shear-roof-displacement response of the walls are not shown in Figures 7.1(a) through (r) because they cannot be obtained from the fiber model analyses.

## 7.4 DISCUSSION OF THE RESULTS OF THE DESIGN PARAMETER STUDY

The accuracy of the tri-linear idealization of the base-shear-roof-displacement response of the walls is examined first in Section 7.4.1. Sections 7.4.2 through 7.4.5 discuss the effect of each structural design parameter on the base-shear-roof-drift response quantities. Finally, a discussion of the effect of the design parameters on the initial lateral stiffness of the walls is given in Section 7.4.6.

### 7.4.1 Accuracy of the tri-linear idealization

As stated earlier, the lateral load behavior of an unbonded post-tensioned precast wall can be idealized by a tri-linear approximation which is defined by two key points: (1) the effective linear limit point (estimated from Equations 3.3 and 3.7, and represented by • in Figure 7.1); and (2) the point on the base-shear-roof-displacement response corresponding to the linear limit strain of post-tensioning steel (estimated from Equations 3.9 and 3.10, and represented by □ in Figure 7.1).

Figure 7.1 shows that, in general, excellent agreement is obtained between the estimated values that define the key points of the tri-linear idealization of the lateral load behavior of the walls and the predicted behavior obtained using fiber model analyses. Figure 7.1 shows that, for all of the walls treated in this study, the effective linear limit point (•) is located in the region where the initial lateral stiffness of the walls begins to reduce significantly due to gap opening along the panel-to-foundation connections. In Figure 7.1, the symbol + defines the

point on the base-shear-roof-displacement response when yielding in tension first occurs in the post-tensioning steel of each panel, obtained from the fiber model analysis. Thus, Figure 7.1 also shows that, for all of the walls treated in this study, the point corresponding to the linear limit strain of the post-tensioning steel (□) is in good agreement with the first occurrence of yielding in the post-tensioning steel, obtained in the fiber model analysis.

The above findings are confirmed by the base shear and roof displacement values corresponding to these points given in Tables 7.5 through 7.8. Therefore, it is concluded that the estimated capacities of Section 3.2 establish a tri-linear idealization of the base-shear-roof-displacement response of unbonded post-tensioned precast concrete walls with vertical joint connectors that accurately represents the lateral load response predicted with the fiber model of the same walls.

### 7.4.2 Effect of shear area of vertical joint connectors on the base shear and roof drift response quantities

Figure 7.2 shows the effect of varying the shear area of vertical joint connectors on the base-shear-roof-drift response of the walls. Figures 7.6 and 7.7 show the effect of the shear area of vertical joint connectors on the wall base shear and roof drift response quantities. Following is a discussion of the effect of shear area of vertical joint connectors on key response quantities for the walls.

*Decompression*

Figure 7.6 shows that as the shear area of the vertical joint connectors, $A_j$ is increased, the base shear resistance to the first occurrence of decompression of a wall panel, $V_{dec}$ increases very slightly. Figure 7.7 shows that the roof drift corresponding to this limit state, $\Delta_{dec}/H_w$ is unaffected by $A_j$. Thus, the initiation of gap opening along the panel-to-foundation connections occurs in a wall at a slightly higher base shear, but at the same roof drift as $A_j$ is increased. This occurs because an increase in $A_j$ increases the initial joint stiffness, which in turn increases the initial wall stiffness, $k_{wi}$.

*Linear limit strain of vertical joint connectors*

Figure 7.6 shows that increasing the total shear area across a vertical joint, $A_j$ increases the base shear corresponding to the linear limit strain of the vertical joint connectors, $V_{llj}$. This is shown by Equation 3.8, where the wall base shear is directly proportional to the yield force in the vertical joint connectors, $P_{llj}$. Since $P_{llj}$ is proportional to $A_j$, increasing $A_j$ increases the wall base shear corresponding to yielding of the vertical joint connectors, $V_{llj}$. Figure 7.7 shows that increasing the area of vertical joint connectors has no effect on the roof drift corresponding to the linear limit strain of the vertical joint connectors, $\Delta_{llj}/H_w$.

*Effective linear limit*

Figure 7.6 shows that as the area of the vertical joint connectors, $A_j$ is increased, the base shear corresponding to the effective linear limit, $V_{ell}$ increases. This occurs because the force in the vertical joint connectors, $P_j$ is directly proportional to $V_{ell}$ (Equation 3.1). Thus, increasing $A_j$ increases the shear force necessary to yield the vertical joints, $P_{llj}$, which causes

$V_{ell}$ to increase. Figure 7.7 shows that increasing $A_j$ has no effect on the roof drift corresponding to the effective linear limit, $\Delta_{ell}/H_w$.

*Linear limit strain of post-tensioning steel*
Figure 7.6 shows that increasing the area of vertical joint connectors, $A_j$ increases the base shear corresponding to the linear limit strain of the post-tensioning steel, $V_{llp}$. This occurs because the force in the vertical joint connectors, $P_j$ is directly proportional to $V_{llp}$ (Equation 3.8). Thus, increasing $A_j$ increases the shear force necessary to yield the vertical joints, $P_{llj}$, which causes $V_{llp}$ to increase. Figure 7.7 shows that increasing $A_j$ has no effect on the roof drift corresponding to the linear limit strain of the post-tensioning steel, $\Delta_{llp}/H_w$.

*Summary of parameter investigation*
Increasing the area of vertical joint connectors, $A_j$ increases the wall base shear response quantities ($V_{dec}$, $V_{llj}$, $V_{ell}$, and $V_{llp}$), but has no effect on the wall roof drift response quantities ($\Delta_{dec}/H_w$, $\Delta_{llj}/H_w$, $\Delta_{ell}/H_w$, and $\Delta_{llp}/H_w$). This is reflected in Figure 7.2, which shows the effect of $A_j$ on the base-shear-roof-drift response of the walls considered in this parameter investigation. It can be seen that increasing $A_j$ increases the initial lateral stiffness of a wall by increasing the effective linear limit point (not shown), as well as the base shear capacity of a wall. The general shape of the base-shear-roof-drift response is the same for all of the walls considered in this parameter investigation.

### 7.4.3 Effect of initial stress in post-tensioning steel with variable $A_p$ and constant $P_i$ on the base shear and roof drift response quantities

Figure 7.3 shows the effect of varying the initial stress in the post-tensioning steel, $f_{pi}$ on the base-shear-roof-drift response of the walls. The area of post-tensioning steel, $A_p$ is varied such that the total force in post-tensioning steel on a panel, $P_i$ remains constant. The effect of $f_{pi}$ with variable $A_p$ and constant $P_i$ on the wall base shear and roof drift response quantities is shown in Figures 7.8 and 7.9, respectively and is discussed in the following sections.

*Decompression*
Figures 7.8 and 7.9 show that the base shear and roof drift corresponding to the first occurrence of decompression of a wall panel, $V_{dec}$ and $\Delta_{dec}/H_w$, respectively are not affected by the initial stress in the post-tensioning steel, for the case of constant $P_i$. The initiation of gap opening along the panel-to-foundation connections is unaffected because the initial force in the post-tensioning steel remains the same.

*Linear limit strain of vertical joint connectors*
Figures 7.8 and 7.9 show that the base shear and roof drift corresponding to the linear-limit strain of the vertical joint connectors, $V_{llj}$ and $\Delta_{llj}/H_w$, respectively are not influenced by the initial stress in the post-tensioning steel, $f_{pi}$ for the case of constant $P_i$.

*Effective linear limit*
Equations 3.3 and 3.7 indicate that the base shear and roof drift corresponding to the effective linear limit, $V_{ell}$ and $\Delta_{ell}/H_w$, respectively are not influenced by the initial stress in the post-

tensioning steel for the case of constant $P_i$. This finding is plotted in Figures 7.8 and 7.9. This finding is also supported by the fiber model results plotted on Figure 7.3, which shows that all walls treated in this parametric investigation exhibit the same behavior up to the point which could reasonably be identified as the effective linear limit.

*Linear limit strain of post-tensioning steel*

Figures 7.8 and 7.9 show that increasing the initial stress in the post-tensioning steel, $f_{pi}$ while decreasing the area of post-tensioning steel, $A_p$ significantly reduces the base shear and roof drift corresponding to the linear limit strain of the post-tensioning steel, $V_{llp}$ and $\Delta_{llp}/H_w$, respectively. These figures also illustrate the good agreement obtained between the estimated values obtained from the closed-form expressions of Chapter 3 and the predicted values obtained from the fiber model analyses.

*Summary of parameter investigation*

Changing the initial stress in the post-tensioning steel, $f_{pi}$ while varying $A_p$ to provide constant $P_i$ has no effect on the following base shear and roof drift response quantities: $V_{dec}$, $\Delta_{dec}/H_w$, $V_{llj}$, $\Delta_{llj}/H_w$, $V_{ell}$, and $\Delta_{ell}/H_w$. As $f_{pi}$ is increased and $A_p$ is decreased, the base shear and roof drift corresponding to the linear limit strain of the post-tensioning steel, $V_{llp}$ and $\Delta_{llp}/H_w$ are significantly reduced. As shown in Figure 7.3, the walls exhibit the same base-shear-roof-drift response until the effective linear limit point is reached. At this point, the walls with more post-tensioning steel and a lower initial prestress display a greater range of roof drift over which gap-opening along the panel-to-foundation connections occurs before yielding of the post-tensioning steel occurs. This increase in drift over which gap-opening behavior occurs is accompanied by an increase in the base shear capacity of the walls. On the other hand, the walls that have less post-tensioning steel and larger prestressing levels exhibit less drift over which gap-opening behavior occurs, exhibit a reduction in base shear capacity, and exhibit reduced stiffness after the effective linear limit is reached.

### 7.4.4 Effect of initial stress in post-tensioning steel with constant $A_p$ and variable $P_i$ on the base shear and roof drift response quantities

Figure 7.4 shows the effect of varying the initial stress in the post-tensioning steel, $f_{pi}$, on the base-shear-roof-drift response of the walls. The area of post-tensioning steel, $A_p$ is kept constant so that the total force in post-tensioning steel on a panel, $P_i$ varies. The effect of $f_{pi}$ with constant $A_p$ and variable $P_i$ on the wall base shear and roof drift response quantities is shown in Figures 7.10 and 7.11 and is discussed in the following sections.

*Decompression*

Figure 7.10 shows that the initial stress in the post-tensioning steel, $f_{pi}$ affects the base shear corresponding to the first occurrence of decompression of a wall panel, $V_{dec}$. As $f_{pi}$ increases, $V_{dec}$ increases. This follows from the fact that as the post-tensioning force in the panels is increased, it generates a larger clamping force between the panel-to-foundation connections, and thus a larger horizontal force is required on the wall to cause a panel to decompress. This same result is also shown by the fiber model results plotted in Figure 7.4. Figure 7.11

shows that the roof drift corresponding to the first occurrence of decompression of a wall panel, $\Delta_{dec}/H_w$ is unaffected by the initial stress in the post-tensioning steel, $f_{pi}$.

***Linear limit strain of vertical joint connectors***
Figures 7.10 shows that the base shear corresponding to the linear limit strain of the vertical joint connectors, $V_{llj}$ exhibits a slight increase as $f_{pi}$ increases. However, as shown in Figure 7.11, increasing $f_{pi}$ has no effect on the roof drift corresponding to the linear limit strain of the vertical joint connectors, $\Delta_{llj}/H_w$.

***Effective linear limit***
Figure 7.10 shows that the base shear corresponding to the effective linear limit, $V_{ell}$ increases with increasing $f_{pi}$. However, as shown in Figure 7.11, the roof drift corresponding to the effective linear limit, $\Delta_{ell}/H_w$ is largely unaffected by $f_{pi}$. These same findings are shown in the fiber model results plotted in Figure 7.4.

***Linear limit strain of post-tensioning steel***
Figure 7.10 shows that increasing the initial stress in the post-tensioning steel, $f_{pi}$ has no significant effect on the base shear corresponding to the linear limit strain of the post-tensioning steel, $V_{llp}$. This same finding is shown by the fiber model results in Figure 7.4. This is because the base shear (base moment) is determined mostly by the total area of post-tensioning steel (see Figure 7.5 for comparison). The initial stress in the post-tensioning steel has little effect on the base moment capacity. As shown in Figure 7.11, increasing $f_{pi}$ significantly decreases the roof drift corresponding to the linear limit strain of the post-tensioning steel, $\Delta_{llp}/H_w$. This occurs because as the initial stress in the post-tensioning steel is increased, the initial strain in the steel is also increased. As a result, a smaller gap along the panel-to-foundation connections (and thus a smaller roof drift) is required for the steel to reach the yield strain.

***Summary of parameter investigation***
Increasing the initial stress in the post-tensioning steel, $f_{pi}$ with constant $A_p$ and variable $P_i$ increases $V_{dec}$, $V_{llj}$, and $V_{ell}$, decreases $\Delta_{llp}/H_w$, and does not significantly affect $\Delta_{dec}/H_w$, $\Delta_{llj}/H_w$, $\Delta_{ell}/H_w$ or $V_{llp}$.

### 7.4.5 Effect of area of post-tensioning steel on the base shear and roof drift response quantities

Figure 7.5 shows the effect of varying the area of post-tensioning steel in a panel, $A_p$ on the base-shear-roof-drift response of the walls. Ap is varied while keeping fpi constant. As such, $P_i$ and the initial stress in the concrete $f_{ci}$ both increase with an increase in $A_p$. The effect of $A_p$ on the wall base shear and roof drift response quantities is shown for the walls considered in this parameter investigation in Figures 7.12 and 7.13, and is discussed in the following sections.

*Decompression*
Figure 7.12 shows that as the area of post-tensioning steel, $A_p$ increases, the base shear corresponding to the first occurrence of decompression of a wall panel, $V_{dec}$ also increases. This follows from the fact that as $A_p$ increases, the initial post-tensioning force in the panels, $P_i$ increases, resulting in a larger clamping force between the panel-to-foundation connections, which requires a larger horizontal force on the wall to cause a panel to decompress. Figure 7.13 shows that the roof drift corresponding to the first occurrence of decompression of a wall panel, $\Delta_{dec}/H_w$ is unaffected by the area of post-tensioning steel, $A_p$.

*Linear limit strain of vertical joint connectors*
Figures 7.12 and 7.13 show that the base shear and roof drift corresponding to the linear limit strain of the vertical joint connectors, $V_{llj}$ and $\Delta_{llj}/H_w$, respectively are not significantly affected by the area of post-tensioning steel in a panel.

*Effective linear limit*
Figure 7.12 shows that the base shear corresponding to the effective linear limit, $V_{ell}$ increases with increasing $A_p$. However, as shown in Figure 7.13, the roof drift corresponding to the effective linear limit, $\Delta_{ell}/H_w$ is unaffected by $A_p$. These findings are also shown by the fiber model results plotted in Figure 7.5.

*Linear limit strain of post-tensioning steel*
Figure 7.12 shows that increasing the area of post-tensioning steel, $A_p$ significantly increases the base shear corresponding to the linear limit strain of the post-tensioning steel, $V_{llp}$. The increase in base shear (base moment) capacity with an increase in $A_p$ is shown clearly in the fiber model results in Figure 7.5. However, as shown in Figure 7.13, increasing $A_p$ has only a slight effect on the roof drift corresponding to the linear limit strain of the post-tensioning steel, $\Delta_{llp}/H_w$. This is an interesting result, since it is therefore possible to vary the strength of the wall without significantly influencing the drift at yielding of the post-tensioning steel.

*Summary of parameter investigation*
Increasing the area of post-tensioning steel, $A_p$ increases $V_{dec}$, $V_{ell}$, and $V_{llp}$, but does not significantly affect $V_{llj}$ or any of the roof drift response quantities ($\Delta_{dec}/H_w$, $\Delta_{llj}/H_w$, $\Delta_{ell}/H_w$, and $\Delta_{llp}/H_w$). Figure 7.5 shows that the overall shape of the response curve is very similar for each wall.

### 7.4.6 Effect of the design parameters on the initial lateral stiffness of the walls
The initial lateral stiffness, $k_{wi}$ is an important response quantity for an unbonded post-tensioned precast concrete wall because it controls the lateral displacement of the wall. As discussed in Section 7.2.6, the initial lateral stiffness, $k_{wi}$ of a wall is estimated from the slope of the linear-elastic portion of the base-shear-roof-displacement relationship as $k_{wi}=V_{ell}/\Delta_{ell}$, where $V_{ell}$ and $\Delta_{ell}$ are calculated from closed-form expressions derived in Chapter 3. It was noted that $k_{wi}$ can also be calculated with values obtained from the fiber model as $k_{wi}=V_{dec}/\Delta_{dec}$. Table 7.9 compares the initial lateral stiffness calculated with these two equations for each of the walls considered in the parameter study. Table 7.9 shows that the initial

wall stiffnesses estimated using the closed-form expressions are consistently less than the stiffnesses predicted from the fiber model analyses. This occurs because the stiffnesses of the vertical joint connectors were not considered in the derivation of $\Delta_{ell}$ (Section 3.2.2).

The design parameters that affect the initial wall stiffness are: (1) the length of each panel, $l_x$; (2) thickness of the wall, $t_w$; (3) concrete strength, $f'_c$; and (4) the shear area across each vertical joint, $A_j$. The length and thickness of a wall affect $k_{wi}$ because they affect the moment of inertia of the wall cross-section. The strength of unconfined concrete affects $k_{wi}$ because it affects the modulus of elasticity of concrete. Finally, the area of vertical joints affects $k_{wi}$ because it affects the stiffness in the joints, $k_j$. Of the design parameters investigated, only $A_j$ has an appreciable influence on the initial lateral stiffness of a wall. This is shown in Table 7.9. As the area of vertical joints is increased, the stiffness in the joints increases, which in turn increases the initial lateral stiffness of the wall.

## 7.5 RELATIONSHIP BETWEEN WALL PARAMETERS AND SEISMIC DESIGN CRITERIA

A proposed seismic design approach for buildings with unbonded post-tensioned precast walls is given in Chapter 4. The approach uses seismic design criteria that require the wall capacities to exceed the wall demands for the design objectives to be met. The seismic design criteria presented in Section 4.2 control the following limit states in an unbonded post-tensioned precast concrete wall: (1) softening; (2) base moment capacity; (3) yielding of post-tensioning steel; (4) gap closure at the base; (5) story drift; and (6) crushing of spiral confined concrete. Some of the wall response quantities identified in Section 7.2 are used in the proposed design approach (e.g., $V_{ell}$ and $V_{llp}$). Since a relationship between various wall parameters and these response quantities exists (Section 7.4), it is possible to relate the wall parameters to the seismic design criteria directly. The following sections identify the parameters considered in the design parameter study that affect each criterion of the proposed design approach.

### 7.5.1 Softening

The first criterion of the proposed design approach (Section 4.2.1) controls softening of an unbonded post-tensioned precast wall. This criterion states that the base shear capacity at the effective linear limit, $V_{ell}$ should be larger than the design base shear demand, $V_d$. The criterion is given by Equation 4.1.

The following parameters considered in the design parameter study affect $V_{ell}$: (1) area of vertical joint connectors, $A_j$; (2) initial stress in post-tensioning steel, $f_{pi}$; and (3) area of post-tensioning steel, $A_p$. Table 7.10 identifies the criteria that are violated by each wall in the design parameter study. Table 7.10 shows that Walls 2, 10, 11, and 14 violate the softening criterion (Criterion 1). The lateral load responses of these walls are shown in Figure 7.1. As shown in Figure 7.1, the base shear at the effective linear limit point (•), estimated from Equation 3.3, falls below $V_d$ for these walls.

Table 7.1 shows that Wall 2 and PW1 (which satisfies the criteria) differ only in the area of vertical joint connectors. Thus, this criterion is violated for Wall 2 because insufficient steel is provided in the vertical joints as compared to PW1. Table 7.3 shows that relative to PW1, $f_{pi}$ has been reduced (keeping $A_p$ constant) in Walls 10 and 11. Reducing the initial prestress in the steel while the area of post-tensioning steel remains the same causes a reduction in the clamping force, $P_i$ between the panels and the foundation, thus reducing the capacity to resist overturning effects caused by lateral loads. Lastly, Table 7.4 shows that Wall 14 has less post-tensioning steel than PW1, but has the same initial prestress, $f_{pi}$. Again, this reduces $P_i$, which reduces the lateral load resisting capacity of the wall.

### 7.5.2 Base moment capacity

The second criterion of the proposed design approach (Section 4.2.2) controls the base moment capacity of an unbonded post-tensioned precast wall, which is quantified in terms of the base shear capacity, $V_{llp}$. As stated in Equation 4.2, this criterion states that $\Phi_f V_{llp} > V_d$, where $\Phi_f = 0.75$. In Figure 7.1, the value of $V_d/\Phi_f$ is plotted as a dashed line. This represents the minimum required base shear capacity of the walls.

The following parameters considered in the design parameter study affect $V_{llp}$: (1) area of vertical joint connectors, $A_j$; (2) initial stress in post-tensioning steel, $f_{pi}$; and (3) area of post-tensioning steel, $A_p$. Table 7.10 shows that Walls 2, 3, 6, 10, 11, 14, and 15 violate Criterion 2. Figure 7.1 shows the lateral load response of these walls. Note that for these walls, the base shear at the linear limit strain of the post-tensioning steel (□), estimated from Equation 3.9 is below the minimum required base shear capacity, $V_d/\Phi_f$. Walls 2 and 3 violate this criterion because they have less vertical joint steel than PW1.

Table 7.2 indicates that for Wall 6, $A_p$ is reduced and $f_{pi}$ increased, relative to PW1, but the total prestressing force on a panel, $P_i$ is the same. The capacity of the walls is reduced in these walls because premature yielding in the post-tensioning steel occurs due to the large initial stresses present in the post-tensioning steel prior to the application of lateral loads. Table 7.3 shows that relative to PW1, $f_{pi}$ has been reduced in Walls 10 and 11, but $A_p$ is held constant. As discussed in Section 7.5.1, the reduction in $P_i$ reduces the base shear capacity of these walls. Finally, Table 7.4 shows that Wall 14 has less post-tensioning steel than PW1, but the same prestress, $f_{pi}$. This wall violates Criterion 2 for the same reason discussed in Section 7.5.1.

### 7.5.3 Yielding of post-tensioning steel

The third criterion of the proposed design approach (Section 4.2.3) controls yielding of the post-tensioning steel. According to this criterion, the roof displacement corresponding to yielding of the post-tensioning steel, $\Delta_{llp}$ should be larger than the roof displacement demand for the design level ground motion, $\Delta_d$.

The following parameters considered in the design parameter study affect $\Delta_{llp}$: (1) area of post-tensioning steel, $A_p$; and (2) initial stress in post-tensioning steel, $f_{pi}$. Table 7.10 shows that Walls 6 and 13 violate Criterion 3. Figure 7.1 shows the lateral load response of these

walls. Note that for these walls, the roof displacement corresponding to the linear limit strain of the post-tensioning steel (□), estimated from Equation 3.10, is less than the displacement demand for the design level ground motion, $\Delta_d$.

Table 7.2 shows that Wall 6 has less area of post-tensioning steel, $A_p$ and a larger initial prestress, $f_{pi}$ than PW1. This wall violates Criterion 3 because the large initial stress in the post-tensioning steel causes it to yield prematurely (at low roof displacement levels). Table 7.3 shows that Wall 13 has a larger $f_{pi}$ than PW1, but the same $A_p$ to produce the same $P_i$. This results in the same condition explained above.

### 7.5.4 Gap closure at the base

The fourth criterion of the proposed design approach (Section 4.2.4) controls the minimum level of prestress force on a wall panel, $P_i$ to ensure that the gap which develops at the base of the panels due to lateral loads closes after the removal of the lateral loads. The criterion is given by Equation 4.4. The effect of this criterion on the lateral load behavior cannot be determined under monotonic lateral loads. However, cyclic analyses (presented in Section 7.6) show that when this criterion is satisfied, the gap at the base of the panels after the removal of lateral loads (presented in terms of a residual roof drift) is small.

Equation 4.4 shows that the fourth criterion of the proposed design approach is controlled by the following parameters investigated in the design parameter study: (1) total prestressing force on each panel, $P_i$; and (2) the total area of vertical joint connectors, $A_j$.

### 7.5.5 Story drift

The fifth criterion of the proposed design approach (Section 4.2.5) controls the maximum story drift under the design level ground motion. According to this criterion, the allowable story drift, $\delta_{all}$ should be larger than the estimated maximum story drift demand for the design level ground motion, $\delta_d$. The maximum allowable story drift for the design level earthquake, $\delta_{all}$ used in this research is 2.5%, based on NEHRP (1994). The maximum story drift demand for the design level earthquake, $\delta_d$ is calculated using Equation 4.14. For the prototype wall, $\delta_d$ is equal to 0.3%. Equations 4.16 and 4.17 give the parameters that affect $\delta_d$ for the prototype wall. These parameters were not changed in the design parameter study. Therefore, this criterion is satisfied by all of the walls considered in the design parameter study.

### 7.5.6 Crushing of spiral confined concrete

The sixth criterion of the proposed design approach (Section 4.2.6) controls crushing of the spiral confined concrete. According to this criterion, the roof displacement capacity corresponding to crushing of spiral confined concrete, $\Delta_{csc}$ should be larger than the roof displacement demand for the survival level ground motion, $\Delta_s$. In Figure 7.1, the value of $\Delta_s$ is plotted as a dashed line so that it can be compared with the roof displacement capacity of each wall considered in the design parameter study. As shown in Figure 7.1, the roof displacement of each wall is plotted to a value of 6.72 in., which corresponds to a roof drift of 2%.

Table 7.11 shows the maximum compressive strain that develops at this roof displacement in each wall panel for all the walls considered in the design parameter study. Table 7.11 shows that the maximum compressive strain is developed in the right exterior wall panel of Walls 9 and 18 and is equal to 0.021 in./in. The spiral confined concrete stress-strain relationship used in the analysis is shown in Figure 6.4. At a strain of 0.021 in./in., the concrete strain is well below the strain that causes the spiral confined concrete to crush. Therefore, although the roof displacement value corresponding to crushing of the spiral confined concrete, $\Delta_{csc}$ was not obtained for the walls, it can be seen than this value is greater than the roof displacement demand for the survival level ground motion, $\Delta_s$ for all the walls considered in the design parameter study. Hence, criterion 6 is satisfied for all the walls considered in the design parameter study.

## 7.6 CYCLIC LATERAL LOAD ANALYSES

Three of the walls treated in the monotonic lateral load analyses were also analyzed under the action of static cyclic lateral loads. The three walls treated in the cyclic analyses were the prototype wall PW1, Wall 4, and Wall 13. The walls were loaded in both directions to selected maximum roof displacements per cycle under a triangular lateral load distribution determined from NEHRP (1994).

Table 7.12 summarizes the roof displacement history of each wall. As shown in Table 7.12, PW1 and Wall 4 have the same displacement history. The maximum displacement of the first cycle (0.15 in.) exceeds the roof displacement at which the vertical joint connectors yield in shear, but the displacement remains below the effective linear limit displacement of the walls, $\Delta_{ell}$ (see $\Delta_{llj}$ and $\Delta_{ell}$ for PW1 and Wall 4 in Table 7.5). The second cycle is between $\Delta_{ell}$ and the roof displacement that causes yielding in the post-tensioning steel, $\Delta_{llp}$. The third cycle corresponds to the roof displacement which is slightly below (1%-2%) $\Delta_{llp}$ obtained from the fiber model. The maximum displacement of the fourth and fifth cycles correspond to roof drifts of 1% and 2%, respectively. For Wall 13, the first three cycles fall within the limit states $\Delta_{llj}$, $\Delta_{ell}$, and $\Delta_{llp}$ as described above. Cycles 4-7 in Wall 13 match cycles 2-5 for the other two walls. The following section discusses the findings from the static cyclic lateral load analyses.

### 7.6.1 Cyclic behavior of unbonded post-tensioned precast walls with vertical joint connectors

The cyclic lateral load responses of the three walls are shown in Figures 7.14 through 7.16. These figures show that the walls develop stable hysteresis loops with self-centering behavior. Table 7.12 gives the residual roof displacement and the residual roof drift for the walls after each loading cycle. The residual roof displacement is defined as the roof displacement at the end of each loading cycle when the base shear is zero. Table 7.12 shows that good self-centering behavior (i.e., low residual drift) is observed for the three walls after undergoing a full load cycle to a roof drift of 1%. The roof drift demand for the survival level ground motion, $\Delta_s/H_w$ is 0.65% for these walls. Therefore, these walls maintain their self-centering behavior, even after roof drifts exceed the demands of the survival level ground motion. This

can be attributed to the fact that these walls satisfy Criterion 4 of the seismic design criteria (Section 7.5.4).

The effect of the design parameters on the lateral load cyclic behavior of the walls is investigated. As shown in Table 7.1, Wall 4 has an area of vertical joint connectors, $A_j$ equal to 5.04 $in^2$, which corresponds to a 12% increase from $A_j$ of PW1. All of the other parameters are unchanged. Table 7.12 shows that the residual displacement after each loading cycle is larger for Wall 4 than for PW1. This can be explained using Figure 4.4, which shows the change in direction of the joint shear force in a middle panel when it is displaced laterally under the action of cyclic loads. Figure 4.4 shows that the couple generated by the joint shear forces always counteracts the applied lateral load. Thus, the joint forces contribute to the lateral load resistance of the wall. Upon the removal of lateral loads, the couple generated by the joint forces resists the gravity force, N and the initial prestress force in the post-tensioning steel, $P_i$, which try to close the gap at the base of the panel, and correspondingly reduce the residual roof displacement. Therefore, it can be seen that as the area of vertical joint connectors, $A_j$ is increased, the joint shear force, $P_{ljj}$ increases, which results in a larger gap-opening couple and thus a larger residual roof displacement.

As shown in Table 7.3, the initial stress in the post-tensioning steel for Wall 13 is 120 ksi, which is 25% larger than that of PW1. Since the area of post-tensioning steel, $A_p$ is held constant, the total prestress force on each panel, $P_i$ is larger for Wall 13 than for PW1. Furthermore, the other parameters, including the area of vertical joints, $A_j$ (and thus $P_{ljj}$) are held constant. Therefore, from the discussion above, one would expect that the residual roof displacements would be smaller for Wall 13 than for PW1. However, as shown in Table 7.12, the residual roof displacements of Wall 13 after each loading cycle are larger than the residual roof displacements of PW1 for the corresponding loading cycle. This occurs because the prestressing force, $P_i$ for Wall 13 is large relative to the area of post-tensioning steel, which causes yielding in the post-tensioning steel at very small roof displacements (see Figure 7.1(m)). After yielding the post-tensioning steel (cycle 4 for Wall 13), the prestress force is reduced, which reduces the capacity of the wall panels to close the gap at the base after each cycle. Therefore, a balance between the level of prestress, $f_{pi}$ and the area of post-tensioning, $A_p$ is necessary to ensure that a sufficient prestress force, $P_i$ is generated to limit residual roof displacements without premature yielding in the post-tensioning steel.

The vertical joint connectors contribute significantly to the hysteretic behavior of unbonded post-tensioned precast concrete walls. Recall that the walls considered in this study have four vertical joint connectors across each vertical joint, which are modeled using two simple connection elements across each joint (Figure 6.1). The following discussion treats the two simple connection elements between the center panel and the right exterior panel (the simple connection elements between the left exterior panel and the center panel exhibit similar behavior). The lower connection element is referred to as vertical joint connector 1 (i.e., VJC 1) and the upper connection element is referred to as vertical joint connector 2 (i.e., VJC 2).

Figure 7.17(a) and (b) show the base-shear-roof-displacement behavior during the first two loading cycles of PW1. Figure 7.17(c) and (d) show the corresponding force-deformation behavior of the vertical joint connectors, VJC 1 and VJC 2. As Figure 7.17(c) shows, during the first cycle, VJC 1 yields but VJC 2 does not. As a result the wall response remains nearly linear-elastic with little energy dissipation (Figure 7.17(a)). During the second cycle (Figure 7.17(b)), a notable hysteresis loop is observed in the base-shear-roof-displacement behavior of PW1. This hysteresis loop develops only after both VJC 1 and VJC 2 reach their yield point (Figure 7.17(d)), and the roof drift corresponding to the effective linear limit in the wall base-shear-roof-drift response is exceeded.

Figure 7.17(e) shows the total force across the vertical joint between the center panel and the right exterior panel, $P_j$ versus the wall roof drift, where $P_j$ = VJC 1 + VJC 2. The first two loading cycles are shown in the figure. Point A represents the first occurrence of yielding in the vertical joint during the second loading cycle, (i.e., VJC 1 yields). At point B, yielding of VJC 2 occurs. The maximum roof drift for the cycle occurs at point C. Upon unloading from point C, VJC 1 yields at point D and VJC 2 yields at point E. Figure 7.17(f) shows an enlarged view of the hysteresis loop shown in Figure 7.17(b) (from the first half of the second loading cycle). Points A-E are shown in Figure 7.17(f) to show how the vertical joint connectors influence the hysteretic behavior of PW1.

Using Figure 7.17(f), it is possible to show that the majority of the hysteresis in the wall is a result of the inelastic behavior in the connectors. First, the contribution of the vertical joints to the wall base shear is computed as

$$V_j = \frac{(n-1)\cdot l_x \cdot P_j}{H_w \sum_{i=1,r} \left(r_{H_i} \cdot r_{F_i}\right)} \tag{7.1}$$

where: $V_j$ is the contribution of the vertical joint connectors to the wall base shear; $P_j$ is the total shear force across each vertical joint; n represents the number of panels in the wall; $l_x$ is the length of each panel; $H_w$ is the height of the wall; r is the number of floor levels; $r_{Hi}$ is the ratio of the height of floor level i to the wall height; and $r_{Fi}$ is the fraction of the total base shear applied at floor level i. Equation 7.1 is derived from Equation 3.8 by setting the force in the post-tensioning bars, $T_1$ and $T_2$, and the axial force in each panel, $N_k$ (where k=1 to n) equal to zero.

For the walls considered in the design parameter study, n = 3, $l_x$ = 108 in., $H_w$ = 336 in., r = 2, $r_{Hl}$ = 0.5, $r_{Hr}$ = 1, $r_{Fl}$ = 0.44, and $r_{Fr}$ = 0.56. Thus, $V_j = 0.824P_j$. This expression is applied to the data in Figure 7.17(e) to calculate the contribution of the vertical joint connectors to the wall base shear. Subtracting this contribution from the base shear resistance of PW1 gives the response of PW1 without the contribution of the vertical joint connectors, which is shown in Figure 7.17(f). As shown in Figure 7.17(f), when the vertical joint contribution is neglected, the initial lateral stiffness of the wall and the base shear capacity are reduced. Moreover, the response of the wall is essentially nonlinear-elastic with little energy dissipation. However, when the vertical joint connectors are included, the initial lateral stiffness and the

base shear capacity of the wall are increased. More importantly, a significant increase in inelastic energy dissipation is observed.

The contribution of the vertical joint connectors to the inelastic energy dissipation of PW1 is determined for the first hysteresis loop of the second loading cycle (Figure 7.17(f)). The width of the two hysteresis loops (i.e., when the vertical joint contribution is neglected and when it is included) is measured at a roof drift corresponding to point E. The difference in the two widths represents the joint contribution to the hysteresis curve. This contribution can be expressed as a percent of the total hysteresis. For the prototype wall, it is found that 93% of the area within the hysteresis loops is generated by the force-deformation behavior of the vertical joint connectors. Therefore, it is seen that using unbonded post-tensioning across the horizontal joints of precast concrete walls and allowing inelastic deformations to occur in the vertical joints provides wide, stable hysteresis loops, which provide good inelastic energy dissipation without significant loss in self-centering behavior.

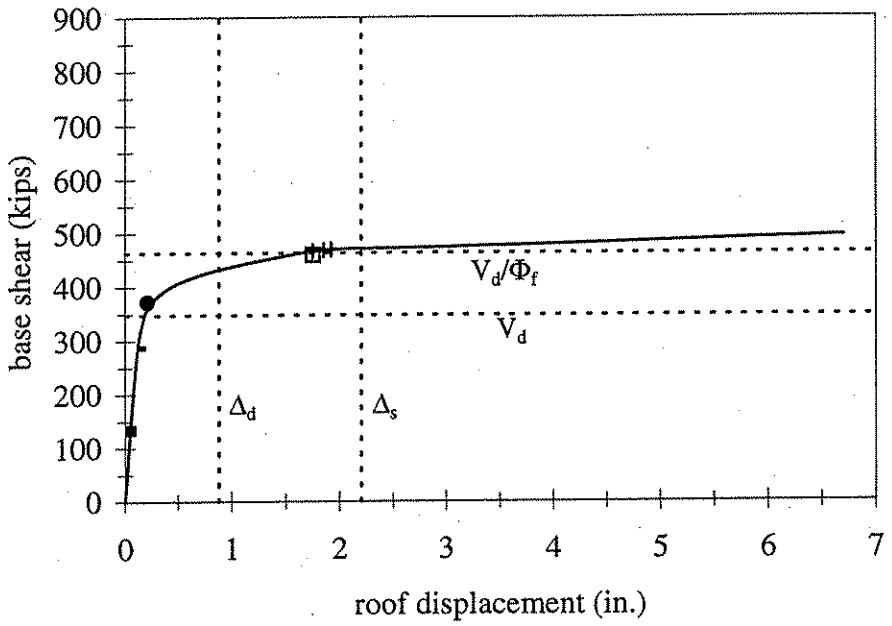


(a) PW1

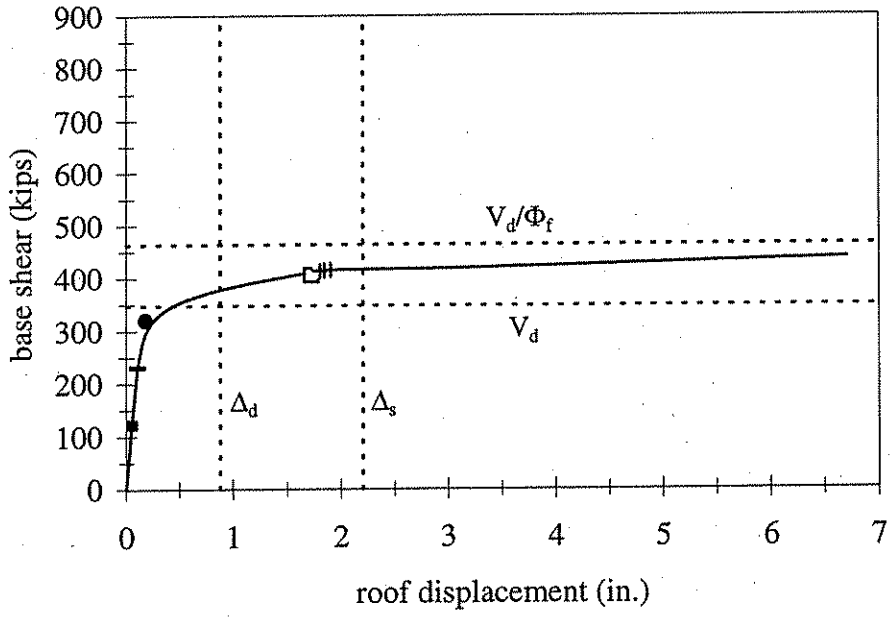


(b) Wall 2

Figure 7.1 Base-shear-roof-displacement response of 18 walls considered in the design parameter study.

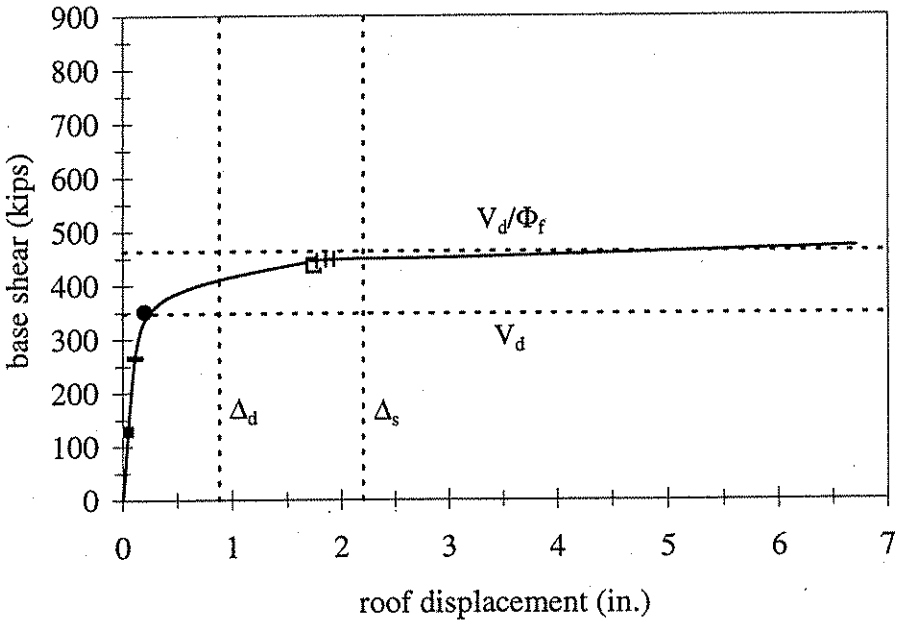


(c) Wall 3

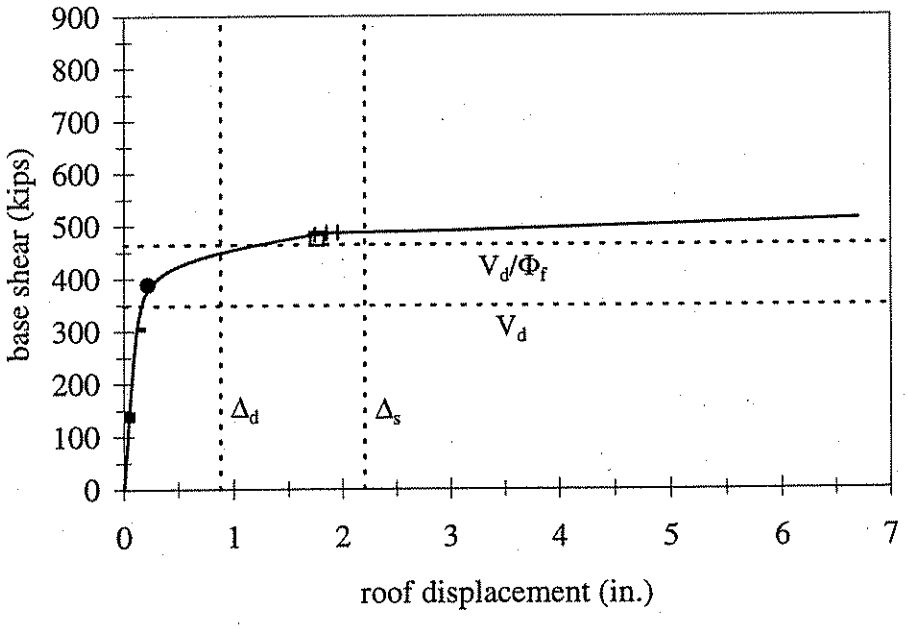


(d) Wall 4

Figure 7.1(continued) Base-shear-roof-displacement response of 18 walls considered in the design parameter study.

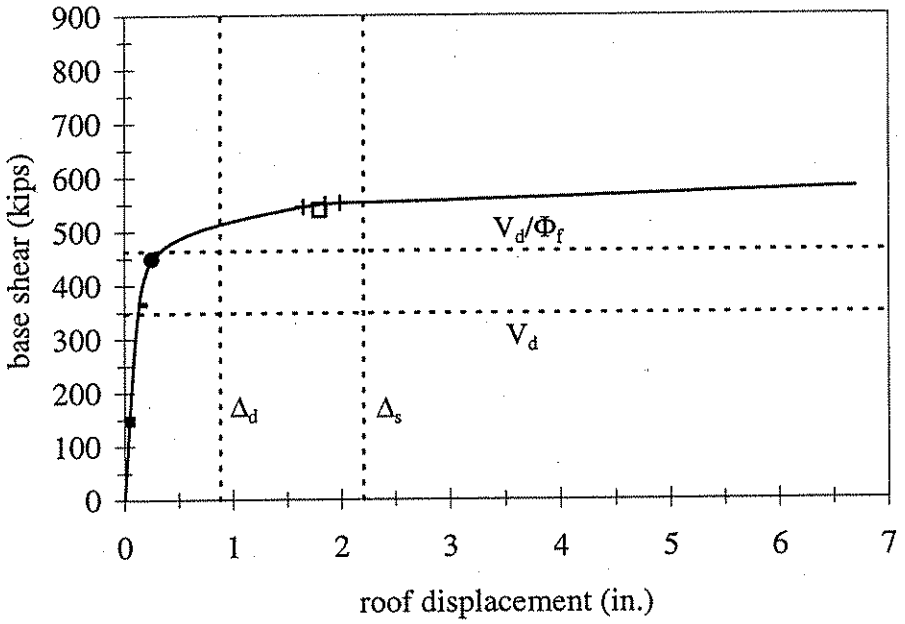


(e) Wall 5

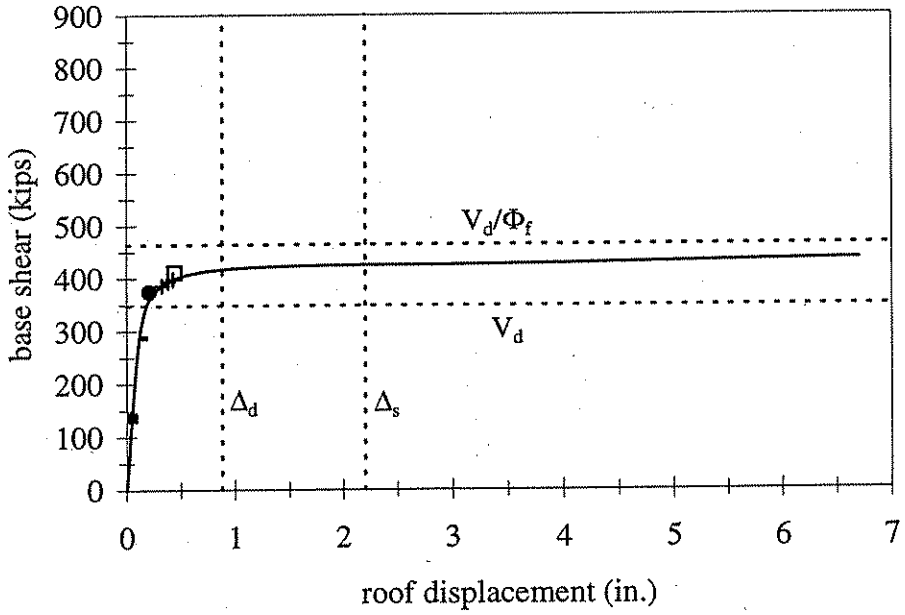


(f) Wall 6

Figure 7.1(continued) Base-shear-roof-displacement response of 18 walls considered in the design parameter study.

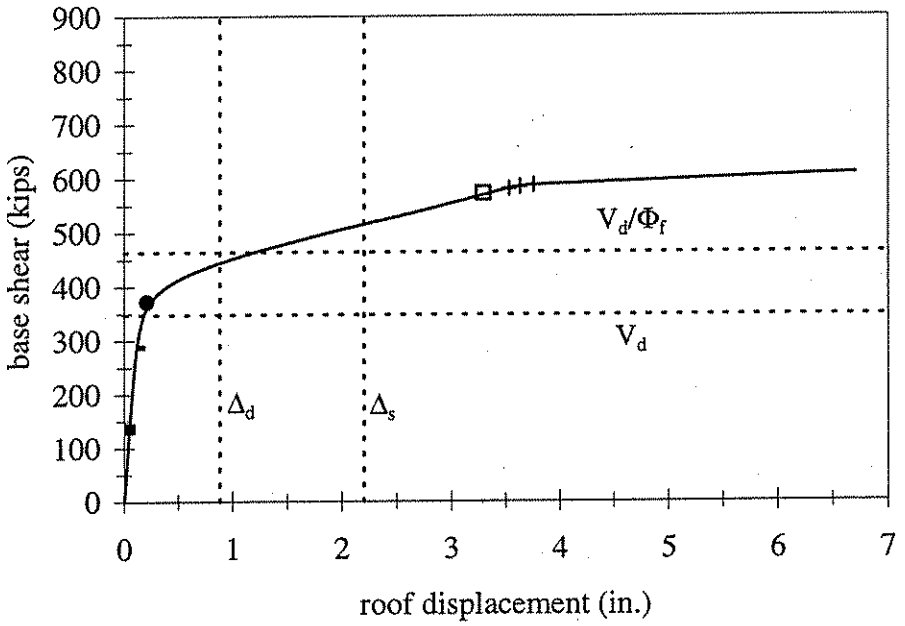


(g) Wall 7

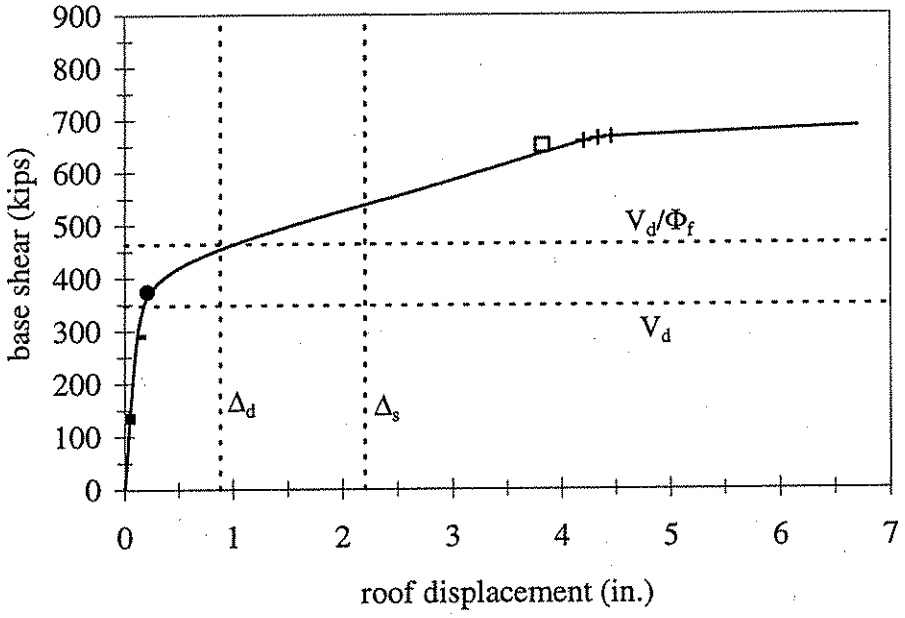


(h) Wall 8

Figure 7.1(continued) Base-shear-roof-displacement response of 18 walls considered in the design parameter study.

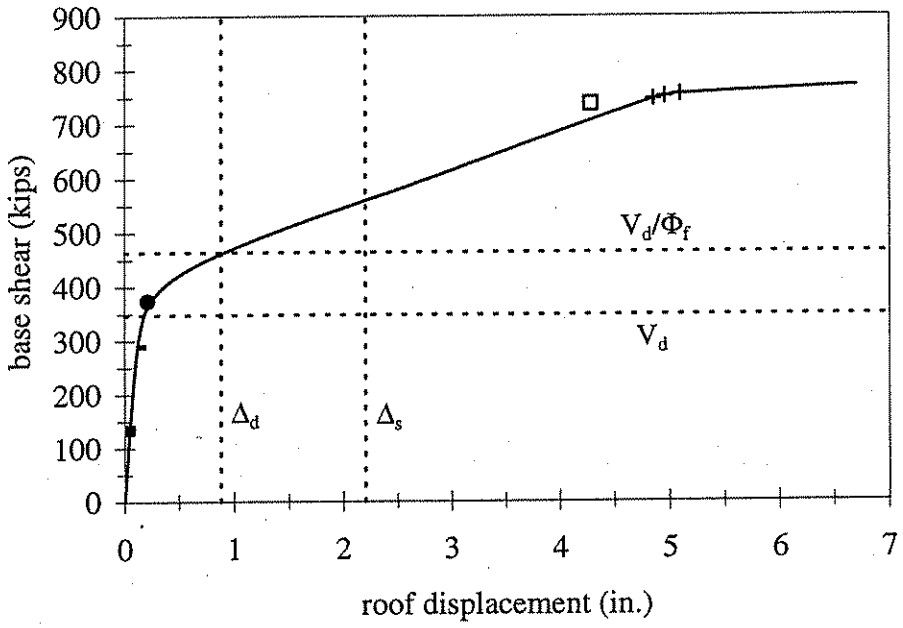


(i) Wall 9

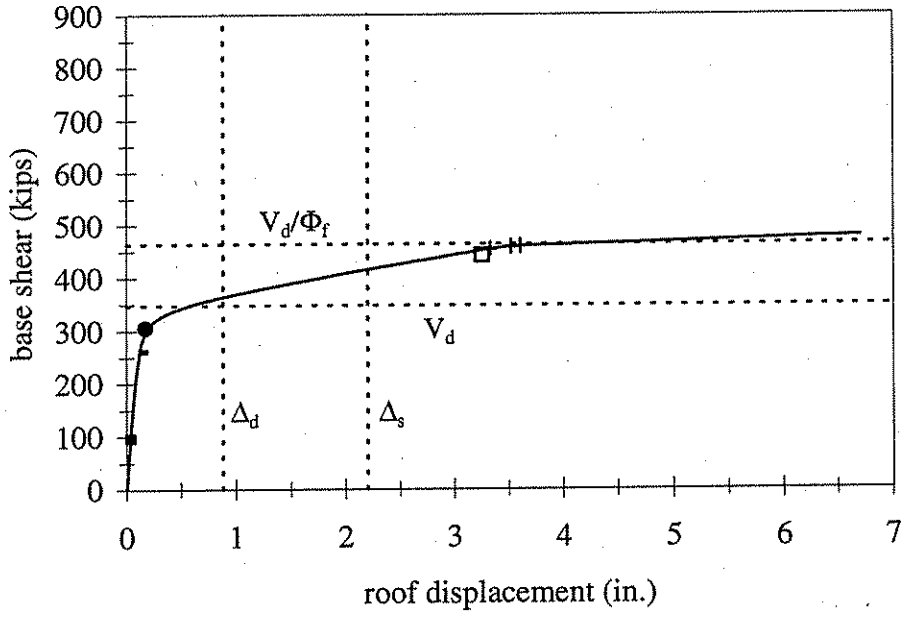


(j) Wall 10

Figure 7.1(continued) Base-shear-roof-displacement response of 18 walls considered in the design parameter study.

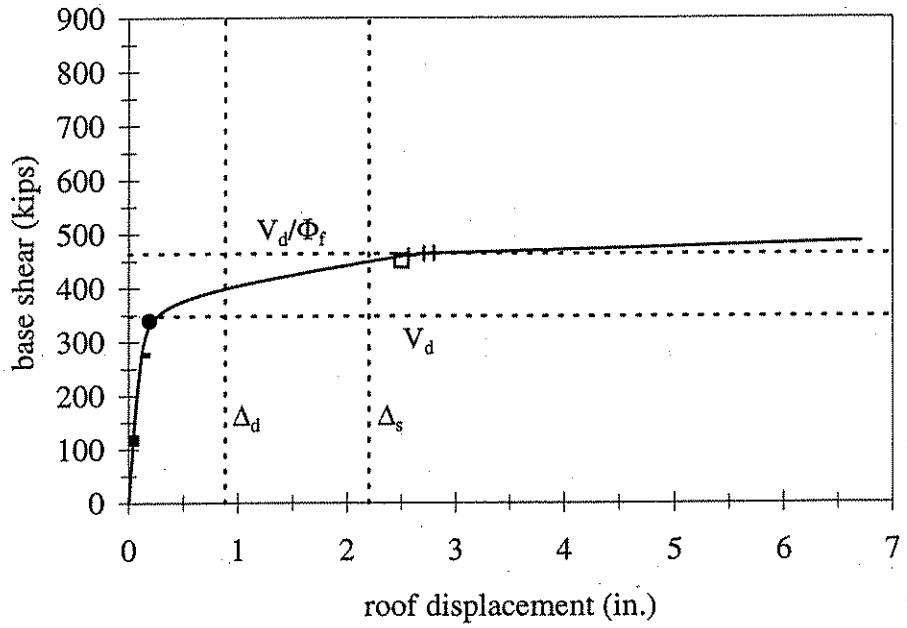


(k) Wall 11

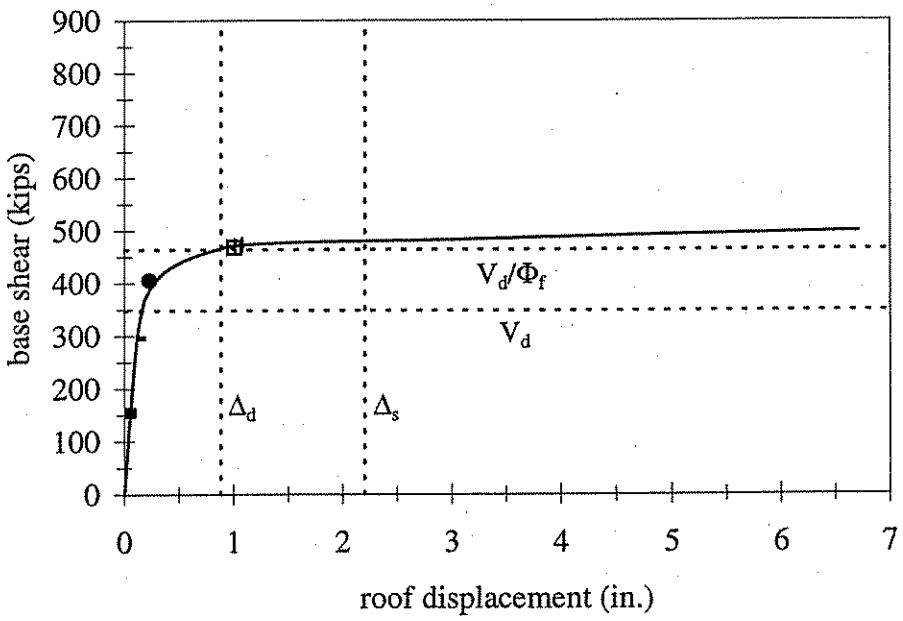


(l) Wall 12

Figure 7.1(continued) Base-shear-roof-displacement response of 18 walls considered in the design parameter study.

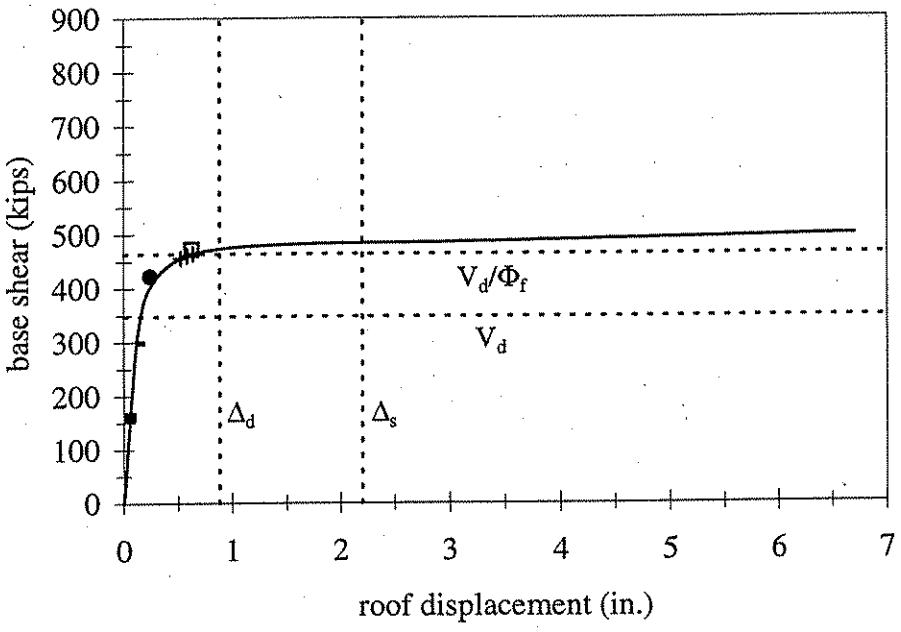


(m) Wall 13

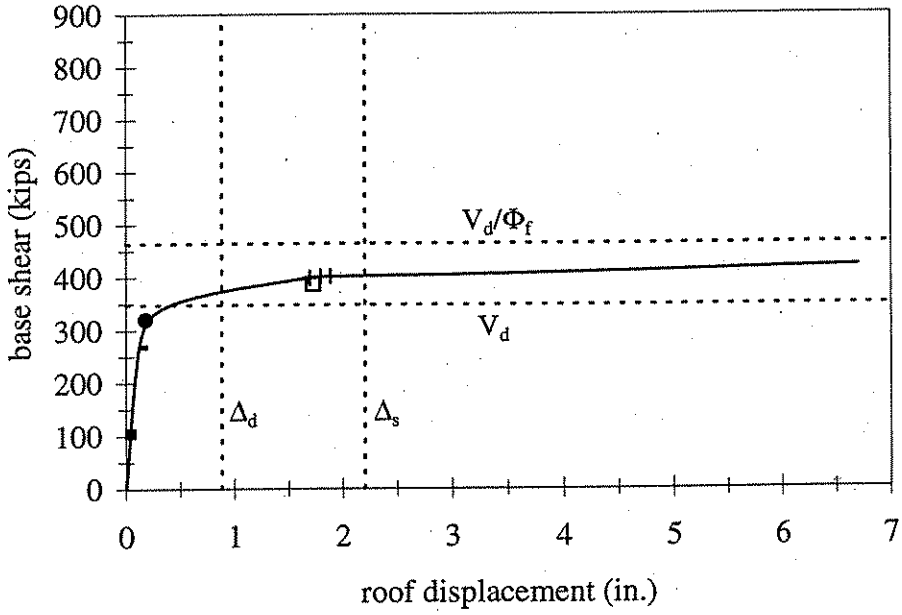


(n) Wall 14

Figure 7.1(continued) Base-shear-roof-displacement response of 18 walls considered in the design parameter study.

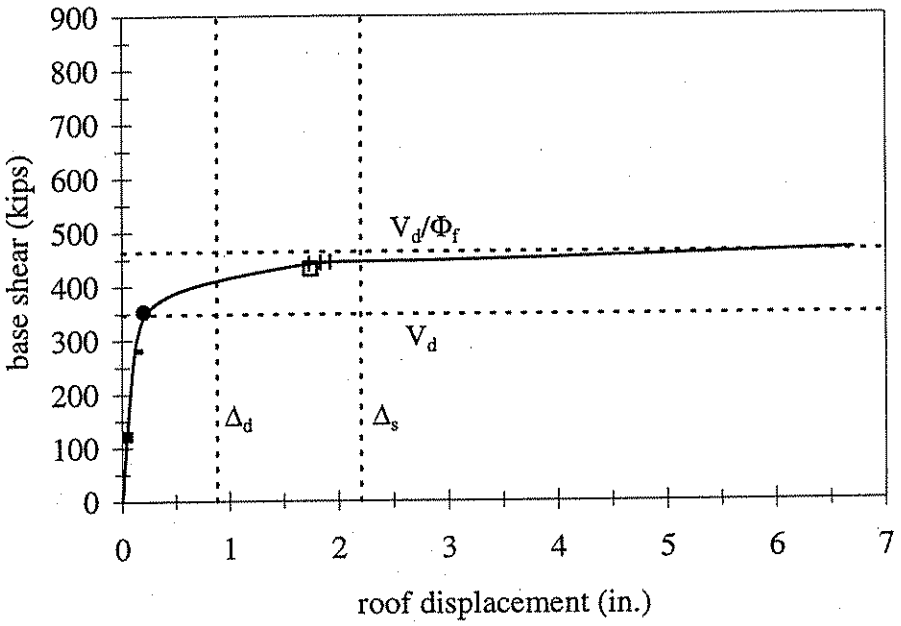


(o) Wall 15

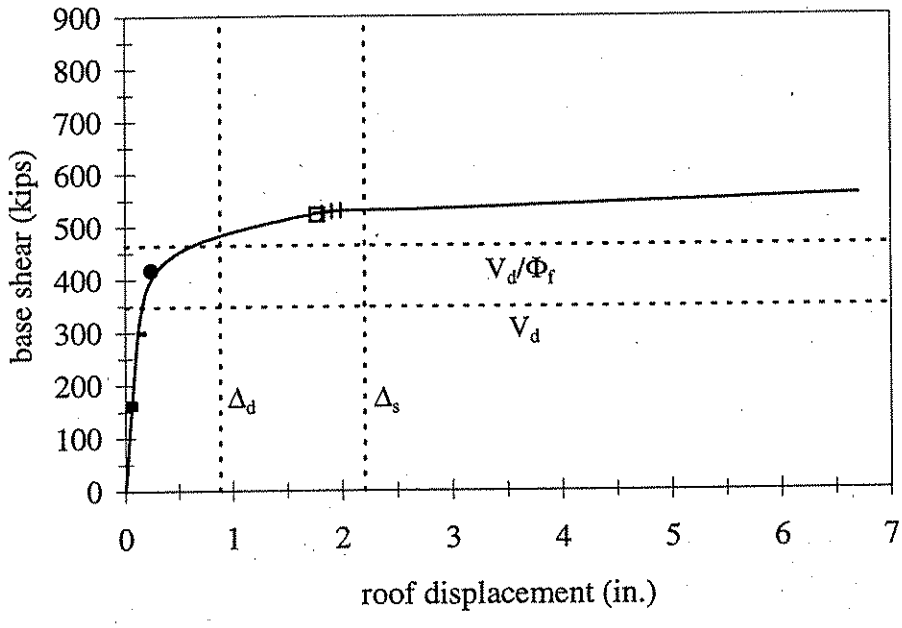


(p) Wall 16

Figure 7.1(continued) Base-shear-roof-displacement response of 18 walls considered in the design parameter study.

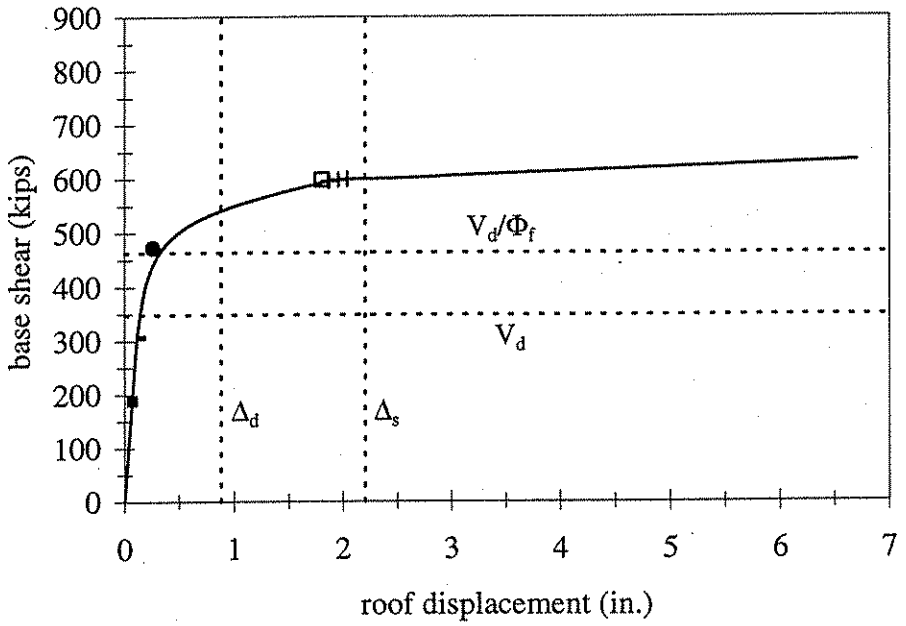


(q) Wall 17

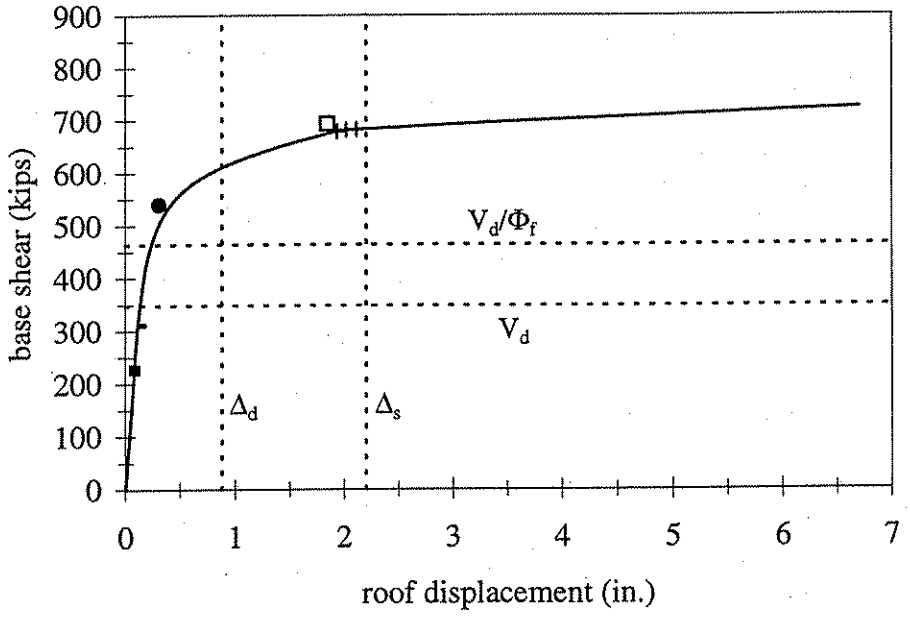


(r) Wall 18

Figure 7.1(continued) Base-shear-roof-displacement response of 18 walls considered in the design parameter study.

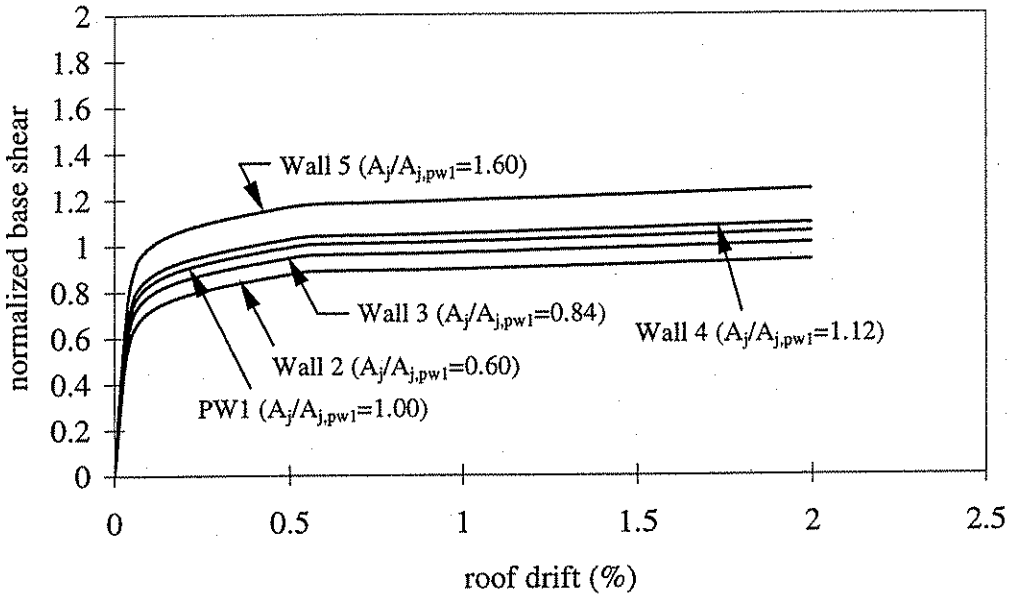


Figure 7.2 Effect of area of vertical joint connectors on the wall base-shear-roof-drift response.

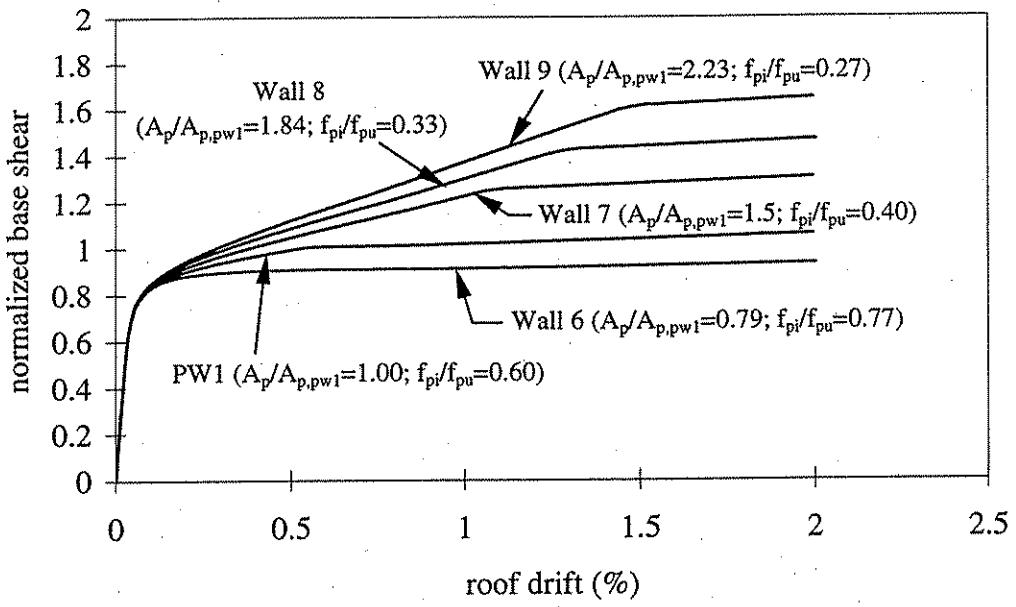


Figure 7.3 Effect of initial stress in post-tensioning steel with variable $A_p$ and constant $P_i$ on the wall base-shear-roof-drift response.

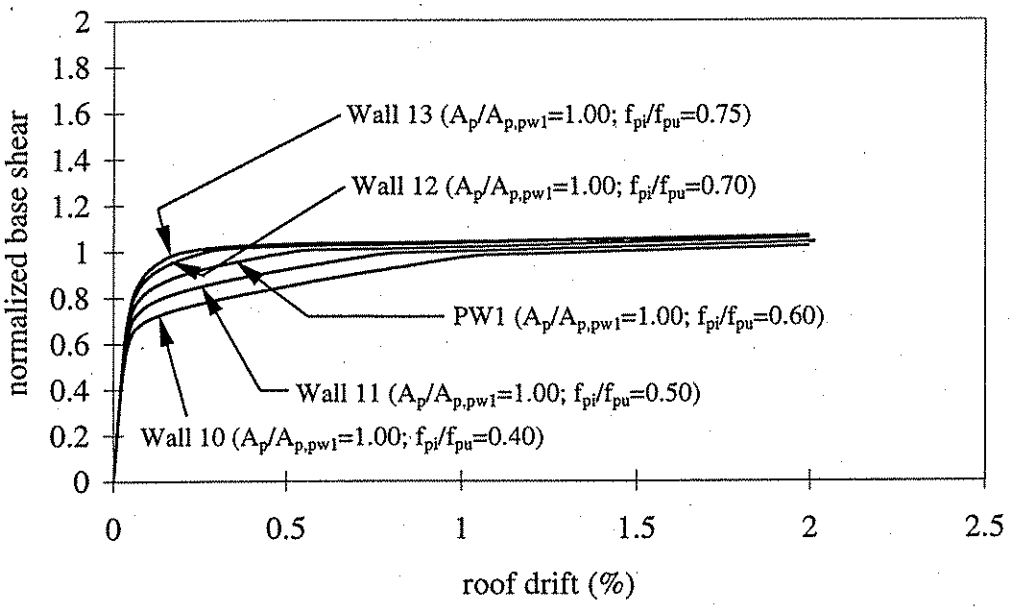


Figure 7.4 Effect of initial stress in post-tensioning steel with constant $A_p$ and variable $P_i$ on the wall base-shear-roof-drift response.

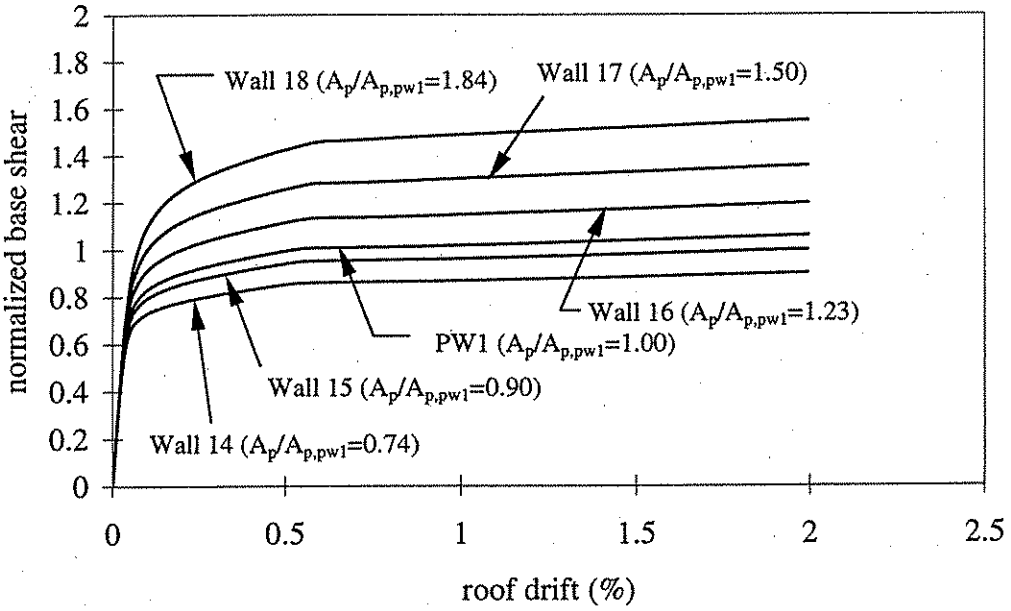


Figure 7.5 Effect of area of post-tensioning steel on the wall base-shear-roof-drift response.

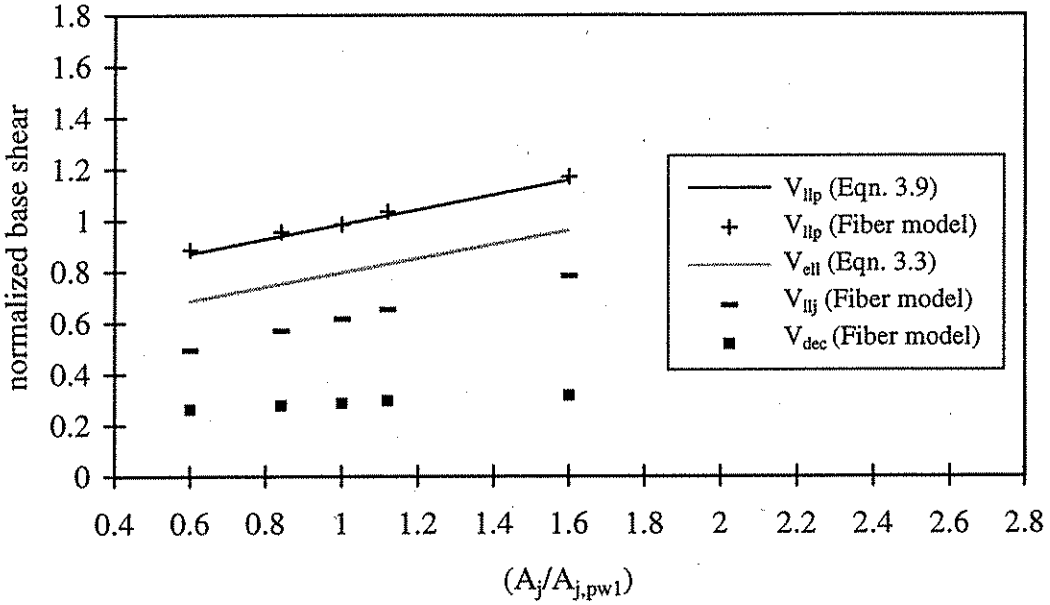


Figure 7.6 Effect of area of vertical joint connectors on the wall base-shear response quantities.

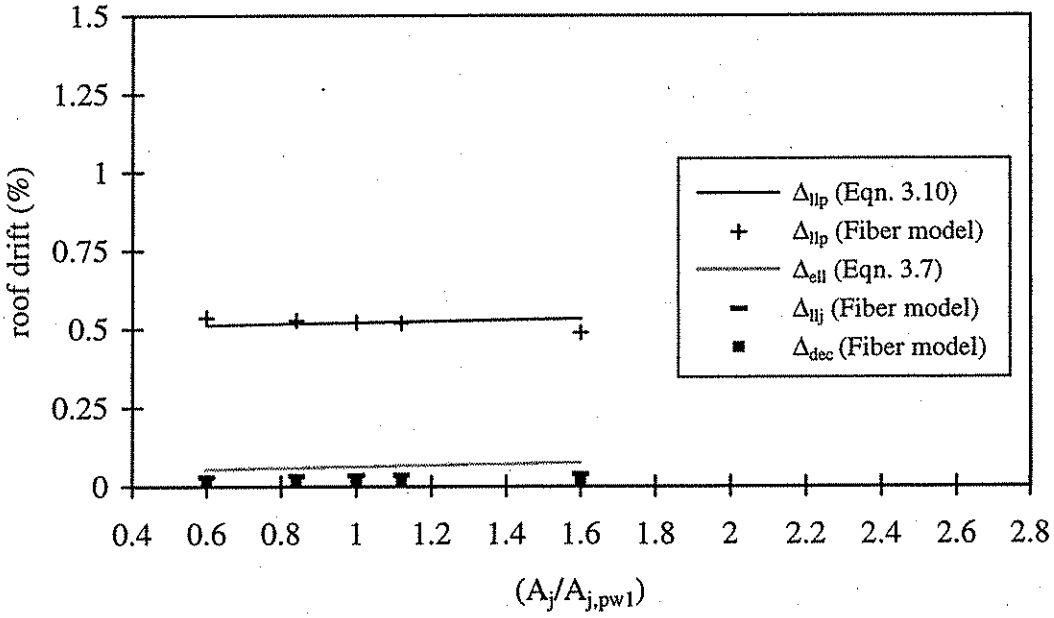


Figure 7.7 Effect of area of vertical joint connectors on the wall roof-drift response quantities.

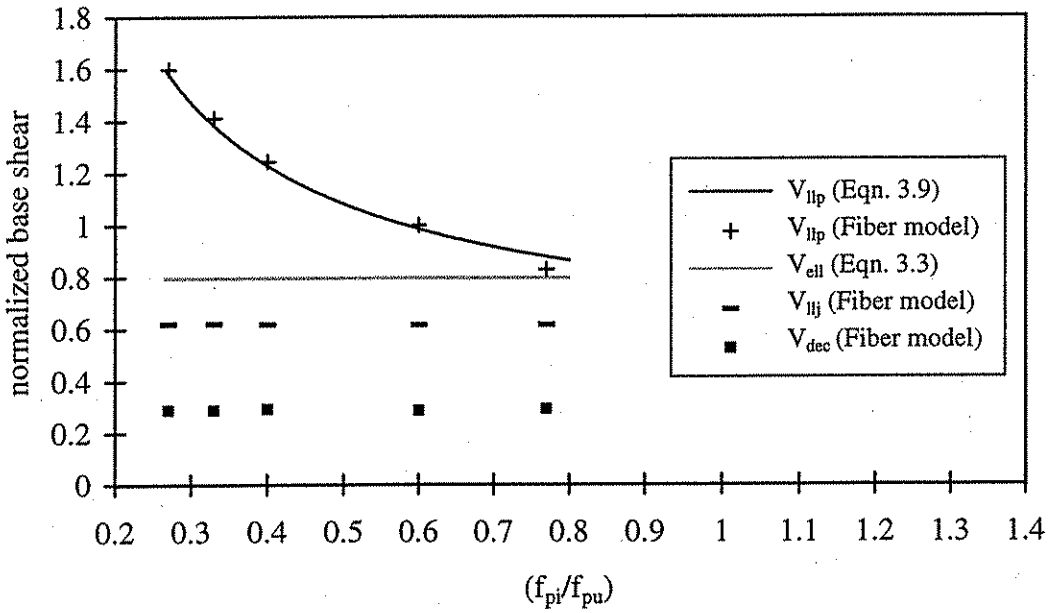


Figure 7.8 Effect of initial stress in post-tensioning steel with variable $A_p$ and constant $P_i$ on the wall base-shear response quantities.

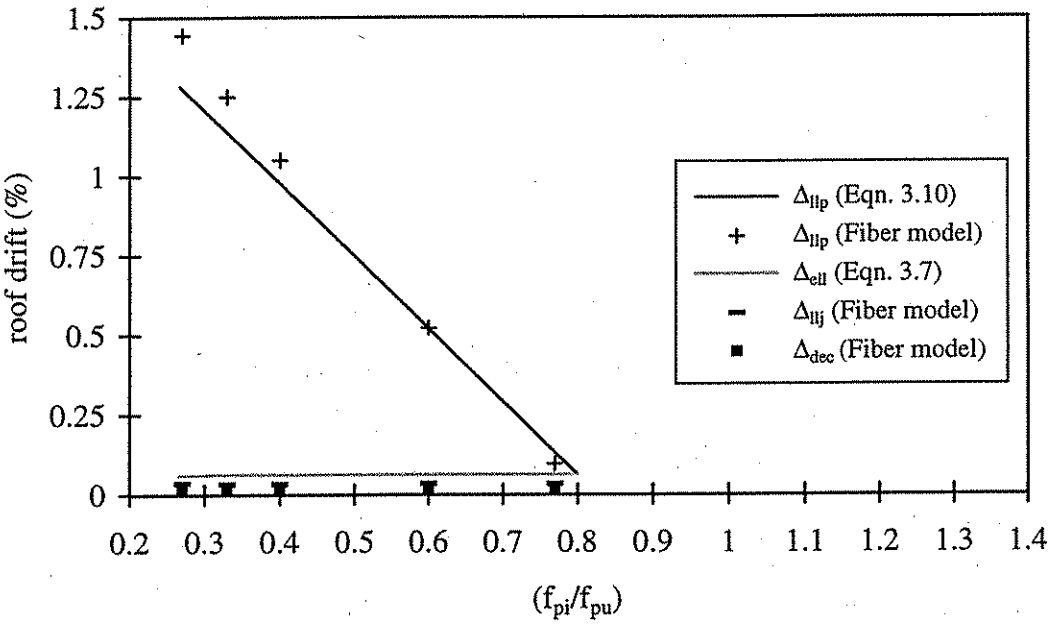


Figure 7.9 Effect of initial stress in post-tensioning steel with variable $A_p$ and constant $P_i$ on the wall roof-drift response quantities.

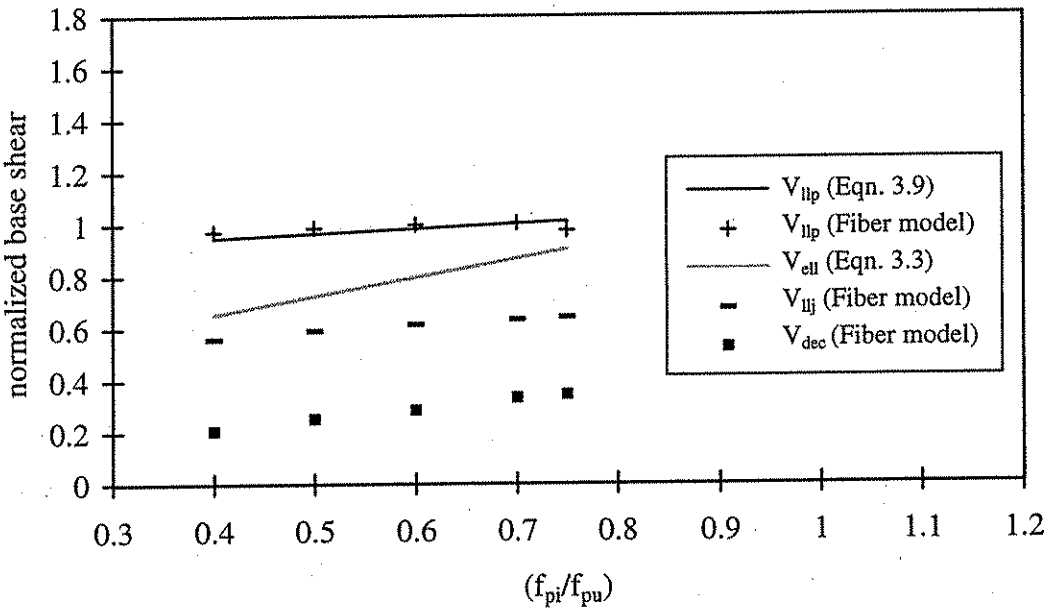


Figure 7.10 Effect of initial stress in post-tensioning steel with constant $A_p$ and variable $P_i$ on the wall base-shear response quantities.

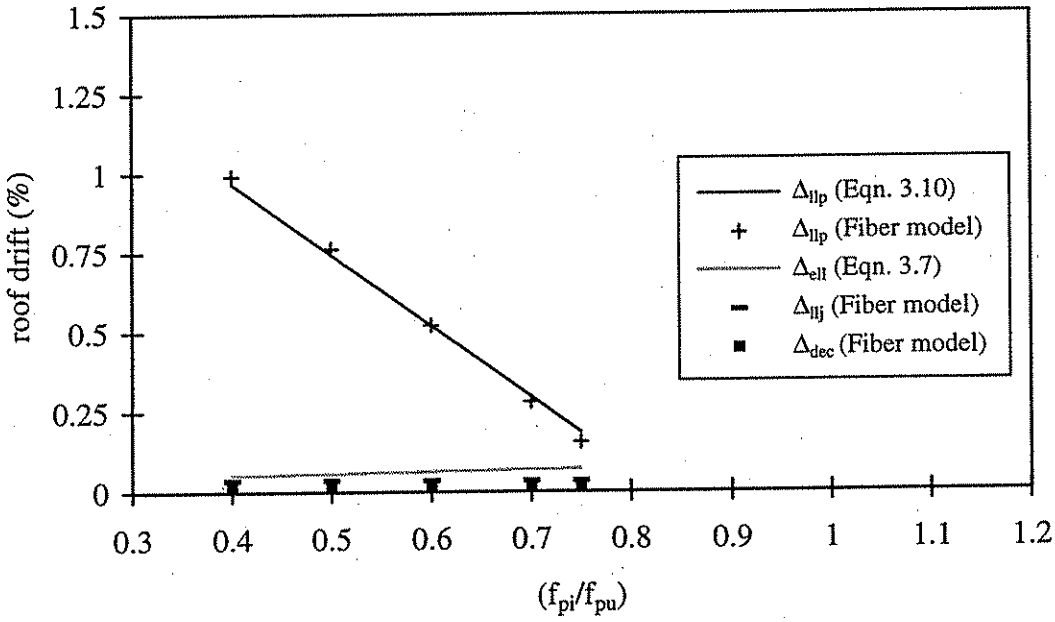


Figure 7.11 Effect of initial stress in post-tensioning steel with constant $A_p$ and variable $P_i$ on the wall roof-drift response quantities.

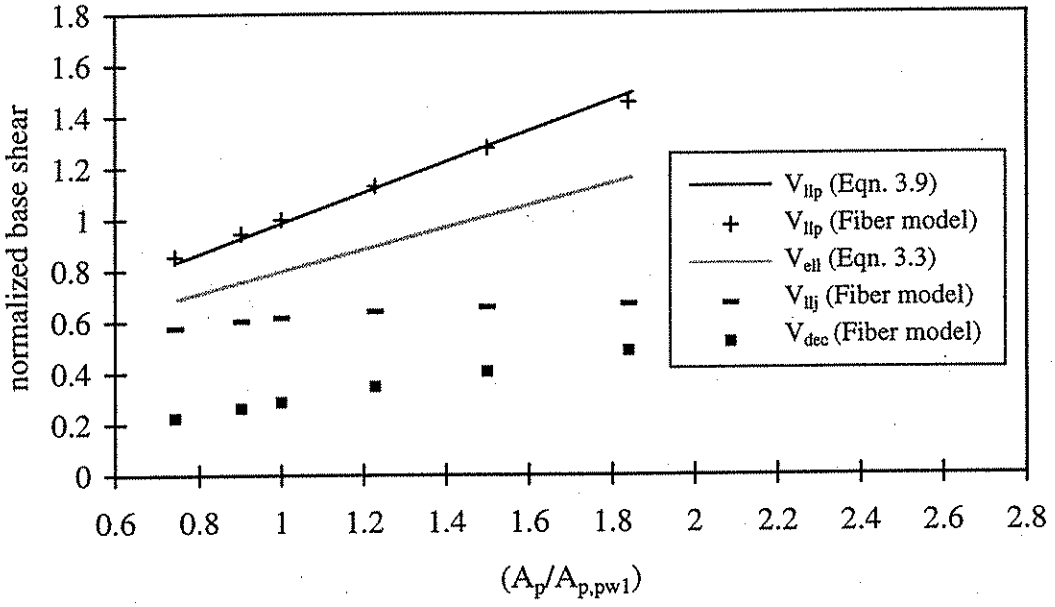


Figure 7.12 Effect of area of post-tensioning steel on the wall base-shear response quantities.

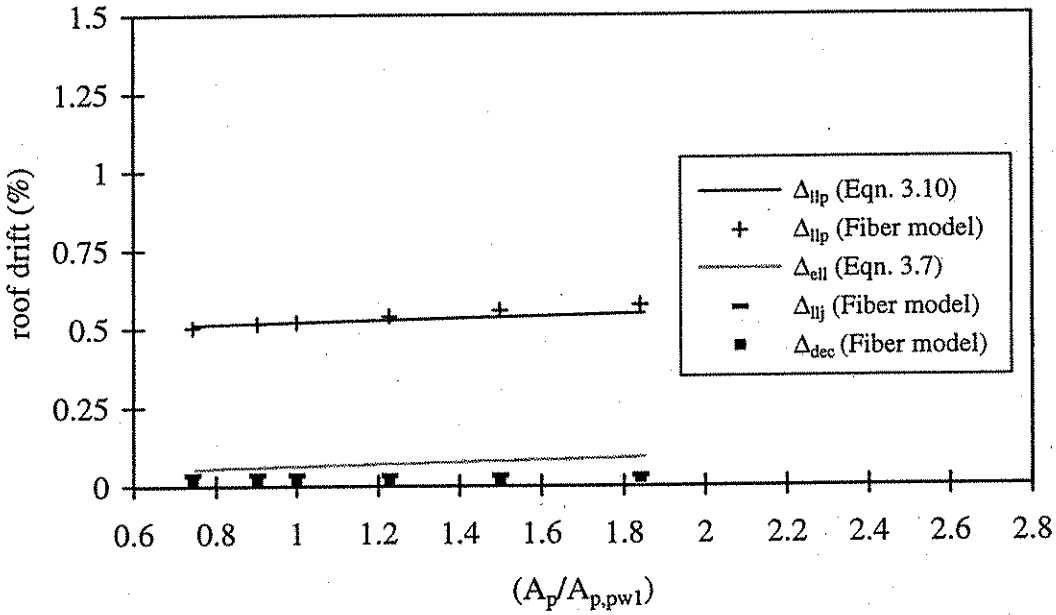


Figure 7.13 Effect of area of post-tensioning steel on the wall roof-drift response quantities.

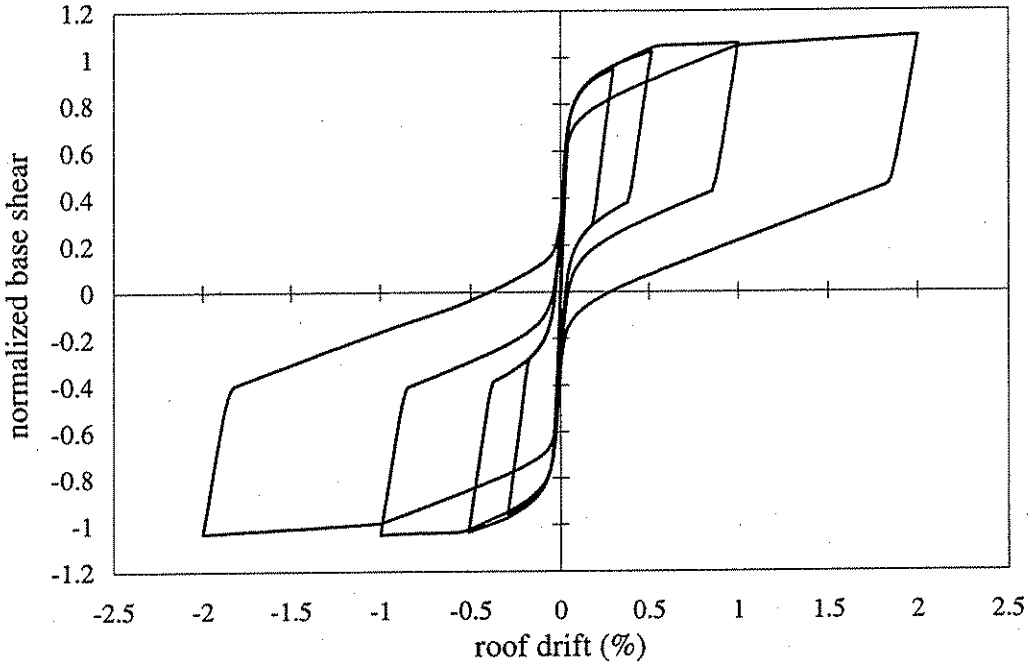


Figure 7.14 Cyclic response of PW1.

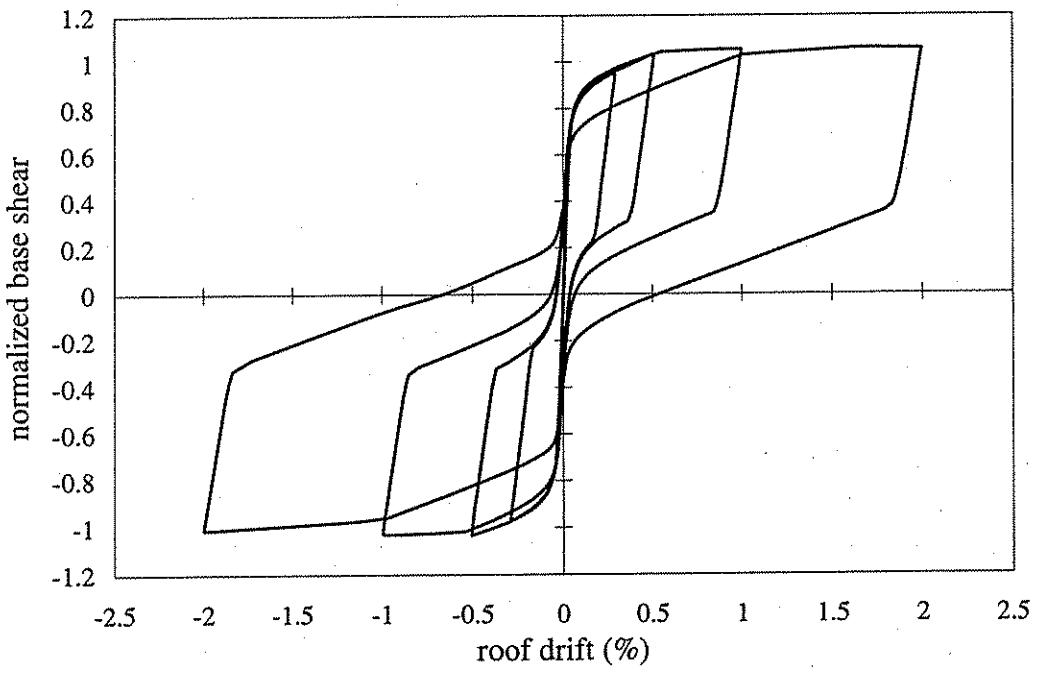


Figure 7.15 Cyclic response of Wall 4.

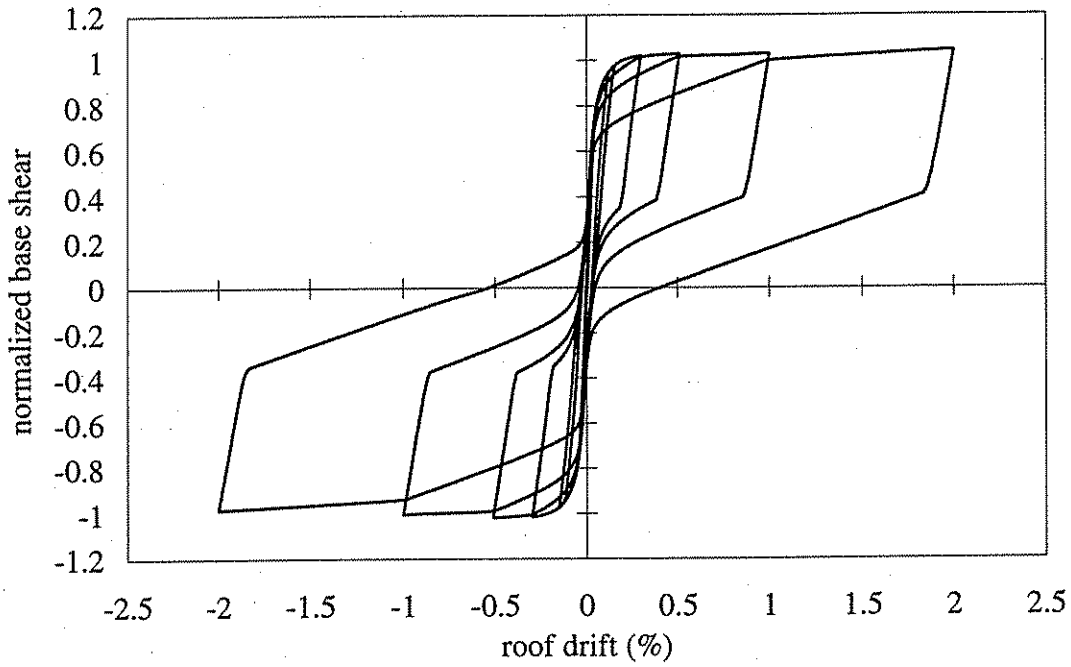


Figure 7.16 Cyclic response of Wall 13.

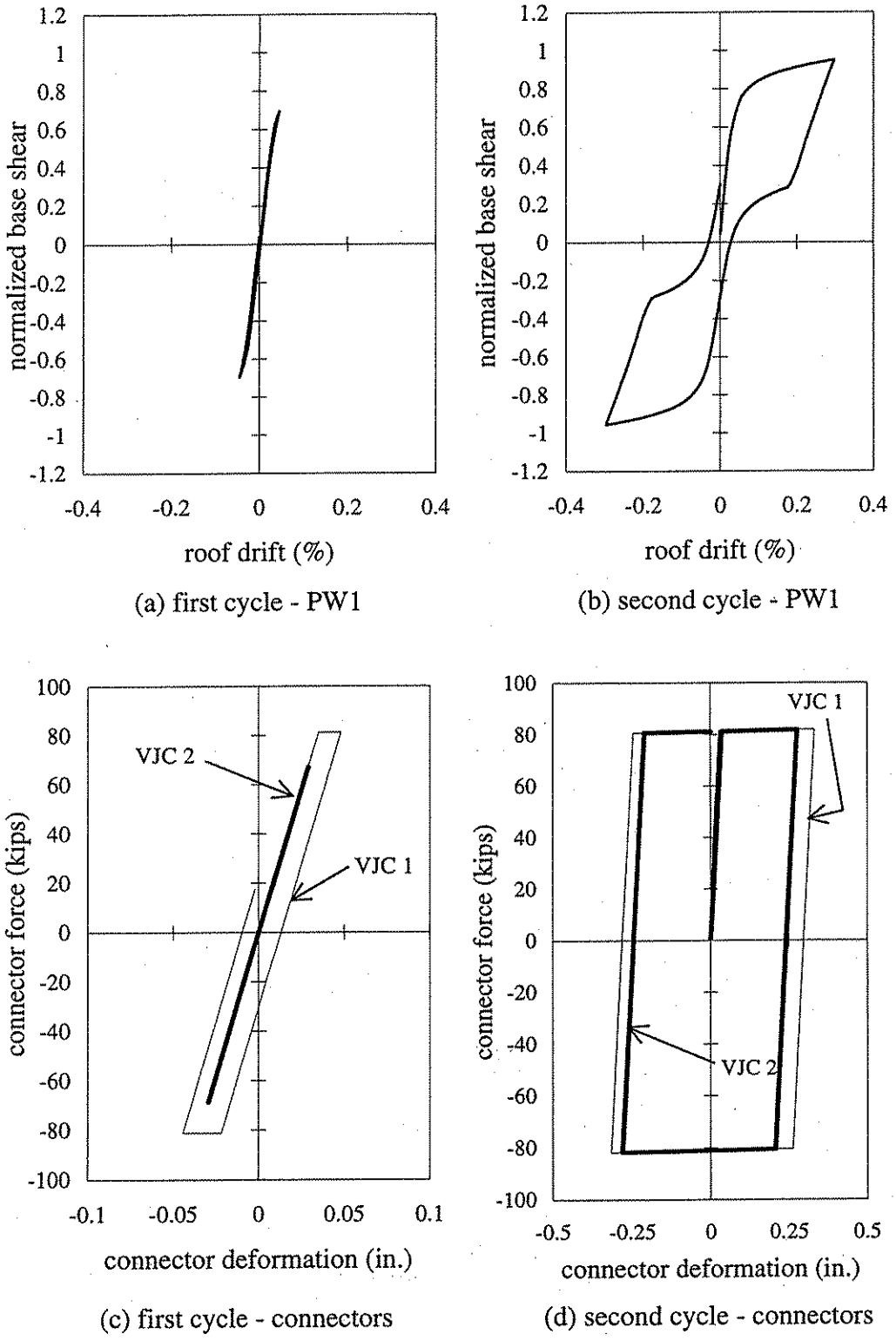


Figure 7.17 Effect of vertical joint connectors on cyclic behavior of PW1.

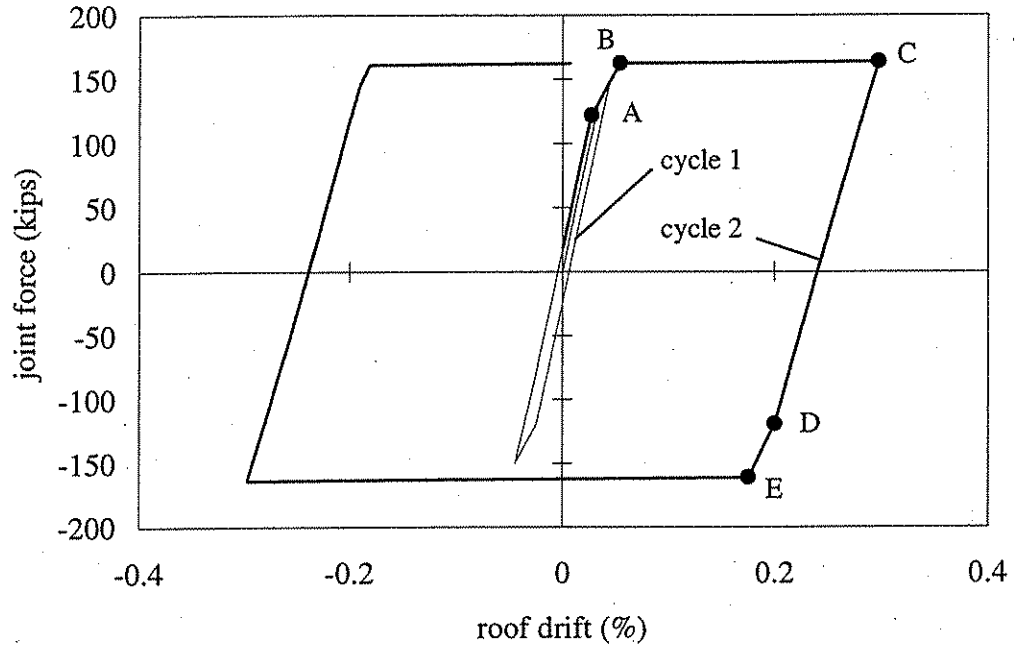


(e) vertical joint force vs. roof drift

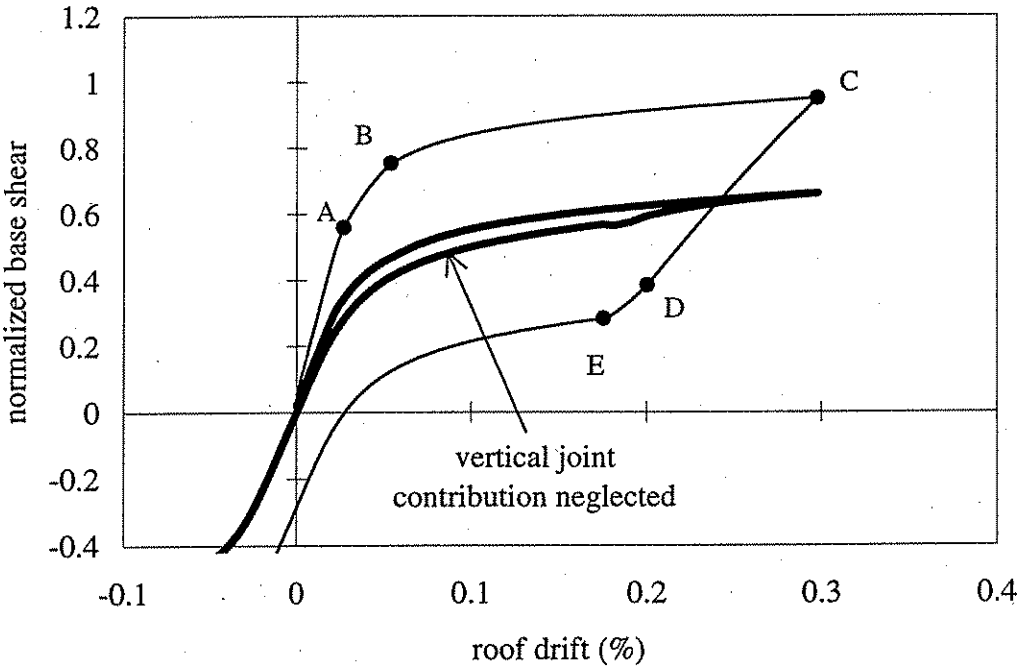


(f) hysteretic behavior - PW1

Figure 7.17(continued) Effect of vertical joint connectors on cyclic behavior of PW1.

Table 7.1 Parameter investigation - Area of vertical joint connectors, $A_j$.

| Wall | $N_b$ (diam.) | $A_p$ ($in^2$) | $f_{pi}$ (ksi) | $P_i$ (kips) | N (kips) | $A_j$ ($in^2$) | $P_{llj}$ (kips) | $f_{ci,P}$ (ksi) | $f_{ci,N}$ (ksi) | $f_{ci}$ (ksi) |
|---|---|---|---|---|---|---|---|---|---|---|
| **2** | 4 (1 1/8") | 4.00 | 96 | 384 | 82.7 | 2.70 | 97 | 0.30 | 0.06 | 0.36 |
| **3** | 4 (1 1/8") | 4.00 | 96 | 384 | 82.7 | 3.78 | 136 | 0.30 | 0.06 | 0.36 |
| **PW1** | 4 (1 1/8") | 4.00 | 96 | 384 | 82.7 | 4.50 | 162 | 0.30 | 0.06 | 0.36 |
| **4** | 4 (1 1/8") | 4.00 | 96 | 384 | 82.7 | 5.04 | 181 | 0.30 | 0.06 | 0.36 |
| **5** | 4 (1 1/8") | 4.00 | 96 | 384 | 82.7 | 7.20 | 259 | 0.30 | 0.06 | 0.36 |

Table 7.2 Parameter investigation - Initial stress in post-tensioning steel, $f_{pi}$, with variable $A_p$ and constant $P_i$.

| Wall | $N_b$ (diam.) | $A_p$ ($in^2$) | $f_{pi}$ (ksi) | $P_i$ (kips) | N (kips) | $A_j$ ($in^2$) | $P_{llj}$ (kips) | $f_{ci,P}$ (ksi) | $f_{ci,N}$ (ksi) | $f_{ci}$ (ksi) |
|---|---|---|---|---|---|---|---|---|---|---|
| **6** | 2 (1") | 3.14 | 123 | 387 | 82.7 | 4.50 | 162 | 0.30 | 0.06 | 0.36 |
| **PW1** | 4 (1 1/8") | 4.00 | 96 | 384 | 82.7 | 4.50 | 162 | 0.30 | 0.06 | 0.36 |
| **7** | 6 (1 1/8") | 6.00 | 64 | 384 | 82.7 | 4.50 | 162 | 0.30 | 0.06 | 0.36 |
| **8** | 6 (1 1/4") | 7.36 | 53 | 389 | 82.7 | 4.50 | 162 | 0.30 | 0.06 | 0.36 |
| **9** | 6 (1 3/8") | 8.91 | 43 | 385 | 82.7 | 4.50 | 162 | 0.30 | 0.06 | 0.36 |

Table 7.3 Parameter investigation - Initial stress in post-tensioning steel, $f_{pi}$, with constant $A_p$ and variable $P_i$.

| Wall | $N_b$ (diam.) | $A_p$ ($in^2$) | $f_{pi}$ (ksi) | $P_i$ (kips) | N (kips) | $A_j$ ($in^2$) | $P_{llj}$ (kips) | $f_{ci,P}$ (ksi) | $f_{ci,N}$ (ksi) | $f_{ci}$ (ksi) |
|---|---|---|---|---|---|---|---|---|---|---|
| **10** | 4 (1 1/8") | 4.00 | 64 | 256 | 82.7 | 4.50 | 162 | 0.20 | 0.06 | 0.26 |
| **11** | 4 (1 1/8") | 4.00 | 80 | 320 | 82.7 | 4.50 | 162 | 0.25 | 0.06 | 0.31 |
| **PW1** | 4 (1 1/8") | 4.00 | 96 | 384 | 82.7 | 4.50 | 162 | 0.30 | 0.06 | 0.36 |
| **12** | 4 (1 1/8") | 4.00 | 112 | 448 | 82.7 | 4.50 | 162 | 0.35 | 0.06 | 0.41 |
| **13** | 4 (1 1/8") | 4.00 | 120 | 480 | 82.7 | 4.50 | 162 | 0.37 | 0.06 | 0.43 |

Table 7.4 Parameter investigation - Area of post-tensioning steel, $A_p$.

| Wall | $N_b$ (diam.) | $A_p$ ($in^2$) | $f_{pi}$ (ksi) | $P_i$ (kips) | N (kips) | $A_j$ ($in^2$) | $P_{llj}$ (kips) | $f_{ci,P}$ (ksi) | $f_{ci,N}$ (ksi) | $f_{ci}$ (ksi) |
|---|---|---|---|---|---|---|---|---|---|---|
| **14** | 2 (1 3/8) | 2.97 | 96 | 285 | 82.7 | 4.50 | 162 | 0.22 | 0.06 | 0.28 |
| **15** | 6 (7/8") | 3.61 | 96 | 347 | 82.7 | 4.50 | 162 | 0.27 | 0.06 | 0.33 |
| **PW1** | 4 (1 1/8") | 4.00 | 96 | 384 | 82.7 | 4.50 | 162 | 0.30 | 0.06 | 0.36 |
| **16** | 4 (1 1/4") | 4.91 | 96 | 471 | 82.7 | 4.50 | 162 | 0.37 | 0.06 | 0.43 |
| **17** | 6 (1 1/8") | 6.00 | 96 | 576 | 82.7 | 4.50 | 162 | 0.45 | 0.06 | 0.51 |
| **18** | 6 (1 1/4") | 7.36 | 96 | 707 | 82.7 | 4.50 | 162 | 0.56 | 0.06 | 0.62 |

Table 7.5 Response quantities - Area of vertical joint connectors, $A_j$.

| Wall | Response Quantity | | | | | | | | | |
|---|---|---|---|---|---|---|---|---|---|---|
| | ■ | | - | | • | | □ | | + | |
| | Fiber model | | Fiber model | | Estimated | | Estimated | | Fiber model | |
| | $V_{dec}$ (kips) | $\Delta_{dec}$ (in.) | $V_{llj}$ (kips) | $\Delta_{llj}$ (in.) | $V_{ell}$ (kips) | $\Delta_{ell}$ (in.) | $V_{llp}$ (kips) | $\Delta_{llp}$ (in.) | $V_{llp}$ (kips) | $\Delta_{llp}$ (in.) |
| **2** | 123 | 0.05 | 231 | 0.10 | 320 | 0.18 | 406 | 1.72 | 414 | 1.80 |
| **3** | 130 | 0.05 | 266 | 0.11 | 351 | 0.20 | 438 | 1.74 | 446 | 1.77 |
| **PW1** | 134 | 0.05 | 288 | 0.12 | 372 | 0.21 | 460 | 1.75 | 467 | 1.75 |
| **4** | 139 | 0.05 | 305 | 0.12 | 388 | 0.22 | 476 | 1.76 | 483 | 1.74 |
| **5** | 148 | 0.05 | 366 | 0.13 | 449 | 0.25 | 540 | 1.79 | 546 | 1.64 |

Table 7.6 Response quantities - Initial stress in post-tensioning steel, $f_{pi}$, with variable $A_p$ and constant $P_i$.

| Wall | Response Quantity | | | | | | | | | |
|---|---|---|---|---|---|---|---|---|---|---|
| | ■ | | - | | • | | □ | | + | |
| | Fiber model | | Fiber model | | Estimated | | Estimated | | Fiber model | |
| | $V_{dec}$ (kips) | $\Delta_{dec}$ (in.) | $V_{llj}$ (kips) | $\Delta_{llj}$ (in.) | $V_{ell}$ (kips) | $\Delta_{ell}$ (in.) | $V_{llp}$ (kips) | $\Delta_{llp}$ (in.) | $V_{llp}$ (kips) | $\Delta_{llp}$ (in.) |
| **6** | 137 | 0.05 | 288 | 0.11 | 374 | 0.21 | 412 | 0.44 | 387 | 0.32 |
| **PW1** | 134 | 0.05 | 288 | 0.12 | 372 | 0.21 | 460 | 1.75 | 467 | 1.75 |
| **7** | 137 | 0.05 | 289 | 0.11 | 372 | 0.21 | 573 | 3.29 | 581 | 3.53 |
| **8** | 135 | 0.05 | 290 | 0.11 | 374 | 0.21 | 651 | 3.82 | 659 | 4.20 |
| **9** | 135 | 0.05 | 290 | 0.12 | 373 | 0.21 | 738 | 4.28 | 747 | 4.85 |

Table 7.7 Response quantities - Initial stress in post-tensioning steel, $f_{pi}$, with constant $A_p$ and variable $P_i$.

| Wall | Response Quantity | | | | | | | | | |
|---|---|---|---|---|---|---|---|---|---|---|
| | ■ | | - | | • | | □ | | + | |
| | Fiber model | | Fiber model | | Estimated | | Estimated | | Fiber model | |
| | $V_{dec}$ (kips) | $\Delta_{dec}$ (in.) | $V_{llj}$ (kips) | $\Delta_{llj}$ (in.) | $V_{ell}$ (kips) | $\Delta_{ell}$ (in.) | $V_{llp}$ (kips) | $\Delta_{llp}$ (in.) | $V_{llp}$ (kips) | $\Delta_{llp}$ (in.) |
| **10** | 97 | 0.04 | 262 | 0.12 | 305 | 0.17 | 443 | 3.25 | 454 | 3.33 |
| **11** | 118 | 0.04 | 277 | 0.12 | 339 | 0.19 | 451 | 2.50 | 461 | 2.56 |
| **PW1** | 134 | 0.05 | 288 | 0.12 | 372 | 0.21 | 460 | 1.75 | 467 | 1.75 |
| **12** | 155 | 0.06 | 296 | 0.11 | 405 | 0.23 | 468 | 1.00 | 469 | 0.94 |
| **13** | 161 | 0.06 | 300 | 0.11 | 422 | 0.24 | 473 | 0.62 | 456 | 0.52 |

Table 7.8 Response quantities - Area of post-tensioning steel, $A_p$.

| Wall | Response Quantity | | | | | | | | | |
|---|---|---|---|---|---|---|---|---|---|---|
| | ■ | | - | | • | | □ | | + | |
| | Fiber model | | Fiber model | | Estimated | | Estimated | | Fiber model | |
| | $V_{dec}$ (kips) | $\Delta_{dec}$ (in.) | $V_{llj}$ (kips) | $\Delta_{llj}$ (in.) | $V_{ell}$ (kips) | $\Delta_{ell}$ (in.) | $V_{llp}$ (kips) | $\Delta_{llp}$ (in.) | $V_{llp}$ (kips) | $\Delta_{llp}$ (in.) |
| **14** | 105 | 0.04 | 269 | 0.12 | 320 | 0.18 | 388 | 1.72 | 399 | 1.69 |
| **15** | 123 | 0.04 | 282 | 0.12 | 353 | 0.20 | 433 | 1.74 | 441 | 1.73 |
| **PW1** | 134 | 0.05 | 288 | 0.12 | 372 | 0.21 | 460 | 1.75 | 467 | 1.75 |
| **16** | 162 | 0.06 | 299 | 0.11 | 417 | 0.24 | 523 | 1.77 | 527 | 1.81 |
| **17** | 189 | 0.07 | 307 | 0.11 | 472 | 0.26 | 599 | 1.80 | 596 | 1.87 |
| **18** | 227 | 0.08 | 312 | 0.11 | 539 | 0.31 | 694 | 1.84 | 679 | 1.93 |

Table 7.9 Initial lateral stiffness of the walls.

| Wall | $k_{wi} = V_{ell}/\Delta_{ell}$ (closed-form solutions) (kips/in.) | $k_{wi} = V_{dec}/\Delta_{dec}$ (fiber model) (kips/in.) |
|---|---|---|
| **PW1** | 1772 | 2792 |
| **2** | 1778 | 2460 |
| **3** | 1755 | 2600 |
| **4** | 1764 | 2780 |
| **5** | 1796 | 2960 |
| **6** | 1781 | 2796 |
| **7** | 1772 | 2796 |
| **8** | 1781 | 2813 |
| **9** | 1776 | 2813 |
| **10** | 1794 | 2771 |
| **11** | 1784 | 2810 |
| **12** | 1761 | 2818 |
| **13** | 1758 | 2776 |
| **14** | 1778 | 2838 |
| **15** | 1765 | 2796 |
| **16** | 1738 | 2793 |
| **17** | 1815 | 2779 |
| **18** | 1739 | 2803 |

Table 7.10 Seismic design criteria violated by the walls.

| Design parameter varied | Wall | Design Criteria Violated | | | | | |
|---|---|---|---|---|---|---|---|
| | | 1 | 2 | 3 | 4 | 5 | 6 |
| Prototype Wall | PW1 | | | | | | |
| $A_p$ | 2 | ✓ | ✓ | | | | |
| | 3 | | ✓ | | | | |
| | 4 | | | | | | |
| | 5 | | | | ✓ | | |
| $f_{pi}$ for variable $A_p$ and constant $P_i$ | 6 | | ✓ | ✓ | | | |
| | 7 | | | | | | |
| | 8 | | | | | | |
| | 9 | | | | | | |
| $f_{pi}$ for constant $A_p$ and variable $P_i$ | 10 | ✓ | ✓ | | ✓ | | |
| | 11 | ✓ | ✓ | | ✓ | | |
| | 12 | | | | | | |
| | 13 | | | ✓ | | | |
| $A_p$ for constant $f_{pi}$ and variable $P_i$ | 14 | ✓ | ✓ | | ✓ | | |
| | 15 | | ✓ | | | | |
| | 16 | | | | | | |
| | 17 | | | | | | |
| | 18 | | | | | | |

Table 7.11 Maximum compressive strain in the wall panels at 2% roof drift.

| Wall | Left Panel Strain (in./in.) | Middle Panel Strain (in./in.) | Right Panel Strain (in./in.) |
|---|---|---|---|
| **PW1** | 0.011 | 0.014 | 0.015 |
| **2** | 0.012 | 0.014 | 0.015 |
| **3** | 0.011 | 0.014 | 0.015 |
| **4** | 0.011 | 0.014 | 0.016 |
| **5** | 0.009 | 0.014 | 0.017 |
| **6** | 0.009 | 0.012 | 0.014 |
| **7** | 0.013 | 0.015 | 0.018 |
| **8** | 0.015 | 0.018 | 0.019 |
| **9** | 0.016 | 0.018 | **0.021** |
| **10** | 0.010 | 0.012 | 0.015 |
| **11** | 0.011 | 0.013 | 0.015 |
| **12** | 0.011 | 0.014 | 0.016 |
| **13** | 0.011 | 0.014 | 0.016 |
| **14** | 0.009 | 0.011 | 0.014 |
| **15** | 0.011 | 0.012 | 0.015 |
| **16** | 0.012 | 0.015 | 0.017 |
| **17** | 0.015 | 0.017 | 0.019 |
| **18** | 0.017 | 0.019 | **0.021** |
| **Max. $\varepsilon_c$ =** | 0.017 | 0.019 | **0.021** |

Table 7.12 Roof displacement history of the walls under cyclic loading.

| Wall | Cycle | Maximum displacement per cycle (in.) | Maximum drift per cycle (%) | Residual displacement after cycle (in.) | Residual drift after cycle (%) |
|---|---|---|---|---|---|
| **PW1** | 1 | 0.15 | 0.04 | 0.02 | 0.00 |
| | 2 | 1.00 | 0.30 | 0.10 | 0.03 |
| | 3 | 1.72 | 0.51 | 0.10 | 0.03 |
| | 4 | 3.36 | 1.00 | 0.14 | 0.04 |
| | 5 | 6.72 | 2.00 | 1.33 | 0.40 |
| **4** | 1 | 0.15 | 0.04 | 0.02 | 0.00 |
| | 2 | 1.00 | 0.30 | 0.12 | 0.04 |
| | 3 | 1.72 | 0.51 | 0.13 | 0.04 |
| | 4 | 3.36 | 1.00 | 0.23 | 0.07 |
| | 5 | 6.72 | 2.00 | 2.25 | 0.67 |
| **13** | 1 | 0.15 | 0.04 | 0.02 | 0.00 |
| | 2 | 0.40 | 0.12 | 0.09 | 0.03 |
| | 3 | 0.51 | 0.15 | 0.09 | 0.03 |
| | 4 | 1.00 | 0.30 | 0.09 | 0.03 |
| | 5 | 1.72 | 0.51 | 0.11 | 0.03 |
| | 6 | 3.36 | 1.00 | 0.16 | 0.05 |
| | 7 | 6.72 | 2.00 | 1.81 | 0.54 |

# Chapter 8

# SUMMARY, CONCLUSIONS, AND FUTURE WORK

This research investigates the seismic behavior and design of unbonded post-tensioned precast concrete walls with vertical joints and ductile connectors. The research addresses the analytical modeling and behavior of the walls under lateral load, the development of a design approach for the walls, the design of a prototype wall for a particular prototype structure, and a lateral load analysis of the prototype wall and other similar walls under monotonic and cyclic lateral loads. The research presented in this report is summarized in Section 8.1. Section 8.2 presents the conclusions of this study. Finally, Section 8.3 identifies future research needs.

## 8.1 SUMMARY

Chapter 2 presents background information. This includes a summary of previous research on the seismic design and behavior of unbonded post-tensioned precast concrete walls with horizontal joints. Chapter 2 also provides an overview of the type of wall that is the focus of this research, namely a precast concrete wall composed of precast concrete panels that are attached to each other along vertical joints with ductile connectors, and to the foundation along horizontal joints with unbonded post-tensioning steel. Finally, Chapter 2 reviews previous research on the seismic behavior of various vertical joint connector details, and one connector detail is selected for use in the vertical joints of the walls considered in this study.

Chapter 3 discusses the expected lateral load behavior of unbonded post-tensioned precast concrete walls with vertical joints and ductile connectors. Under the action of lateral loads, the expected behavior includes: (1) decompression at the base of the wall; (2) yielding of vertical joint connectors; (3) significant reduction in lateral stiffness (i.e., softening) due to gap opening in flexure along the panel-to-foundation connection; (4) yielding of post-tensioning steel; (5) peak base shear; (6) loss of prestress due to inelastic straining of post-tensioning steel; and (7) crushing of spiral confined concrete. The lateral load behavior of an unbonded post-tensioned precast concrete wall with vertical joints and ductile connectors is idealized using a proposed tri-linear idealization of the base-shear versus roof-displacement response. The tri-linear idealization is defined by three key points on the base-shear-roof-displacement response of the wall. Each key point has a wall base shear and roof displacement capacity associated with it. The base shear and roof displacement capacity of a wall corresponding to the effective linear limit are denoted by $V_{ell}$ and $\Delta_{ell}$, respectively. The base shear and roof displacement corresponding to the linear limit strain of the post-tensioning steel are denoted by $V_{llp}$ and $\Delta_{llp}$, respectively. Lastly, the base shear and roof displacement corresponding to crushing of the spiral confined concrete are denoted as $V_{csc}$ and $\Delta_{csc}$, respectively. Closed-form expressions are derived to estimate the first two key points that define the lateral load behavior of these walls using the proposed tri-linear idealization.

Chapter 4 proposes a seismic design approach for buildings with unbonded post-tensioned precast concrete walls with vertical joints and ductile connectors as the primary lateral load

resisting system. The proposed design approach is a performance-based design approach which allows the designer to specify and predict the performance (degree of damage) of a building for a specified level of ground motion intensity. Two seismic demand levels (design level and survival level) are considered. The proposed design approach includes seismic design criteria to achieve the required performance. The criteria control the following: (1) softening; (2) base moment capacity (quantified in terms of the base shear capacity of the wall); (3) yielding of post-tensioning steel; (4) the requirement for the gap that develops at the base of the panels due to lateral loads to close after the removal of the lateral loads; (5) story drift; and (6) crushing of spiral confined concrete. Chapter 4 also discusses the estimation of design capacities and demands to check the design criteria.

Chapter 5 describes the design of a prototype wall using the seismic design approach proposed in Chapter 4. The chapter summarizes general properties of the prototype structure for which the prototype wall was designed. The wall capacities and demands considered in the seismic design of the wall are identified.

Chapter 6 describes the analytical model that was developed to model the behavior of unbonded post-tensioned precast walls with vertical joints and ductile connectors. The model that was developed was implemented in the DRAIN-2DX analysis program. The fiber beam-column element in the program is used to represent the gap opening of the wall panels under flexure and the nonlinear inelastic behavior of the concrete at the base of the wall panels. A truss element in the program is used to model the inelastic behavior of unbonded post-tensioning steel in the wall panels. Finally, a simple connection element in the program is used to represent the inelastic behavior of the ductile connectors in the vertical joints of the wall. Chapter 6 discusses the analysis and modeling assumptions and describes how each component of the wall is modeled in the DRAIN-2DX program.

Chapter 7 presents the results of a series of monotonic and cyclic static lateral load analyses of unbonded post-tensioned precast concrete walls with vertical joints and ductile connectors. A series of monotonic lateral load analyses were performed to evaluate the effect of four structural design parameters on the lateral load response of 18 walls, including the prototype wall described in Chapter 5. The structural design parameters treated are: (1) the total shear area of connectors across each vertical joint; (2) the initial stress in the post-tensioning steel with variable post-tensioning steel area to produce a constant prestress force in the post-tensioning steel; (3) the initial stress in the post-tensioning steel with constant post-tensioning steel area to produce a variable prestress force in the post-tensioning steel; and (4) the total area of post-tensioning steel with constant stress in the post-tensioning steel and variable prestress force in the post-tensioning steel. The lateral load response of the walls is represented by the following base shear and roof displacement response quantities: (1) base shear and roof displacement corresponding to initial gap opening (i.e., decompression) at the base of the wall ($V_{dec}$ and $\Delta_{dec}$, respectively); (2) base shear and roof displacement at which the vertical joint connectors reach their linear limit strain ($V_{llj}$ and $\Delta_{llj}$, respectively); (3) base shear and roof displacement at which the effective linear limit of the base-shear-roof-displacement relationship is reached ($V_{ell}$ and $\Delta_{ell}$, respectively); (4) base shear and roof dis-

placement corresponding to the linear limit strain of the post-tensioning steel ($V_{llp}$ and $\Delta_{llp}$, respectively); and (5) base shear corresponding to the peak base shear, $V_{max}$ (assumed equal to $V_{llp}$). For the walls considered in the design parameter study, the accuracy of the tri-linear idealization (estimated from the closed-form expressions derived in Chapter 3) is verified with the behavior of the walls predicted by the fiber model. Chapter 7 also discusses the analysis of three walls (including the prototype wall) under the action of cyclic static lateral loads. These analyses are performed using the fiber model to determine the effect of the following two parameters on the cyclic lateral load response of the walls: (1) total shear area across each vertical joint; and (2) initial stress in the post-tensioning steel with constant post-tensioning steel area. In particular, the effect of these parameters on the self-centering behavior of the walls is investigated. The self-centering behavior of the walls is quantified in terms of the residual roof displacements at the end of each loading cycle when the base shear is zero. Lastly, the cyclic static lateral load analysis of the prototype wall is used to determine the contribution of the ductile vertical joints to the inelastic energy dissipation of the wall.

## 8.2 CONCLUSIONS

The conclusions that are drawn from this research are summarized below.

### 8.2.1 Tri-linear idealization idealization of the base-shear-roof-displacement behavior

1. The wall base-shear-roof-displacement behavior can be represented by the tri-linear idealization estimated from closed-form approximations for two key points on the base-shear-roof-displacement response of the wall.

2. In general, excellent agreement is obtained between the estimated values that define the key points of the tri-linear idealization of the lateral load behavior of the walls considered in the study, and predicted behavior obtained using fiber model analyses.

### 8.2.2 Fiber wall model

1. A fiber model of an unbonded post-tensioned precast concrete wall with vertical joints and ductile connectors can be easily implemented in the DRAIN-2DX program to predict the lateral load response of the wall. In this model, the fiber beam-column element can be used to model gap opening of the wall panels as well as the nonlinear inelastic behavior of the concrete near the base of the wall panels. Truss elements can be used to model the post-tensioning steel in a wall, and the simple connection element can be used to model the inelastic behavior in the vertical joint connectors. To prevent the wall panels from overlapping or from separating at the vertical joints in the fiber model, a rigid link should be placed at each floor level between the nodes of adjacent elements modeling the concrete panels.

### 8.2.3 Monotonic lateral load analyses

The following conclusions can be drawn based on the monotonic lateral load analyses:

*Effect of shear area of vertical joint connectors*

1. Increasing the area of vertical joint connectors, $A_j$ increases the wall base shear response quantities ($V_{dec}$, $V_{llj}$, $V_{ell}$, and $V_{llp}$), but has no effect on the wall roof displacement response quantities ($\Delta_{dec}$, $\Delta_{llj}$, $\Delta_{ell}$, and $\Delta_{llp}$).

2. Increasing $A_j$ increases the initial lateral stiffness of a wall by increasing the effective linear limit point on the base-shear-roof-displacement response.

3. Increasing $A_j$ increases the base shear capacity of a wall.

*Effect of initial stress in post-tensioning steel with variable $A_p$ and constant $P_i$*

1. Changing the initial stress in the post-tensioning steel, $f_{pi}$ while varying $A_p$ to provide constant $P_i$ has no effect on the following base shear and roof displacement response quantities: $V_{dec}$, $\Delta_{dec}$, $V_{llj}$, $\Delta_{llj}$, $V_{ell}$, and $\Delta_{ell}$.

2. As $f_{pi}$ is increased and $A_p$ is decreased, the base shear and roof displacement corresponding to the linear limit strain of the post-tensioning steel, $V_{llp}$ and $\Delta_{llp}$ are significantly reduced.

3. A wall that has more post-tensioning steel and lower prestressing levels displays a greater range of roof displacement over which gap-opening along the panel-to-foundation connections occurs before yielding of the post-tensioning steel.

4. Increasing the post-tensioning steel and reducing the prestressing levels increases the lateral load base shear capacity of a wall.

*Effect of initial stress in post-tensioning steel with constant $A_p$ and variable $P_i$*

1. Increasing the initial stress in the post-tensioning steel, $f_{pi}$ with constant $A_p$ and variable $P_i$ increases $V_{dec}$, $V_{llj}$, and $V_{ell}$, decreases $\Delta_{llp}$, and does not significantly affect $\Delta_{dec}$, $\Delta_{llj}$, $\Delta_{ell}$, or $V_{llp}$.

*Effect of area of post-tensioning steel*

1. Increasing the area of post-tensioning steel, $A_p$ increases $V_{dec}$, $V_{ell}$, and $V_{llp}$, but does not significantly affect $V_{llj}$ or any of the roof displacement response quantities ($\Delta_{dec}$, $\Delta_{llj}$, $\Delta_{ell}$, and $\Delta_{llp}$).

*Effect of design parameters on the wall initial lateral stiffness*

1 The design parameters that affect the initial wall stiffness, $k_{wi}$ of an unbonded post-tensioned precast concrete wall with vertical joints and ductile connectors are: (1) the length of each panel, $l_x$; (2) thickness of the wall, $t_w$; (3) concrete strength, $f'_c$; and (4) the shear area across each vertical joint, $A_j$. The only parameter varied in the study is $A_j$.

2 As $A_j$ is increased, the stiffness of the wall increases.

3 The stiffness of a wall estimated using the closed-form expressions (i.e., $k_{wi} = V_{ell}/\Delta_{ell}$) is consistently less than the stiffness predicted from a fiber model analysis ($k_{wi} = V_{dec}/\Delta_{dec}$). This occurs because the stiffness contribution of the vertical joint connectors is neglected in the derivation of the closed-form expressions.

### 8.2.4 Cyclic lateral load analyses

1. Unbonded post-tensioned precast concrete wall with vertical joints and ductile connectors can develop stable hysteresis loops with good self-centering behavior.

2. The vertical joint connectors contribute significantly to the hysteretic behavior of unbonded post-tensioned precast walls. For the prototype wall considered in the study, 93% of the area within the hysteresis loops is generated by the force-deformation behavior of the vertical joint connectors.

3. Using unbonded post-tensioning across the horizontal joints of a precast concrete wall and allowing inelastic deformations to occur in the vertical joints provides wide, stable hysteresis loops, which provide good inelastic energy dissipation without significant loss in self-centering behavior.

## 8.3 FUTURE WORK

The following areas of future work need to be investigated:

1. This research investigates the effect of a limited set of design parameters on the lateral load response of unbonded post-tensioned precast concrete walls with vertical joints and ductile connectors. A larger set of parameters (e.g., number, length and height of wall panels, location of applied gravity loads, different prestress levels in groups of post-tensioning steel, etc.) needs to be investigated to determine the effectiveness of the closed-form expressions in estimating the lateral load response of these walls.

2. A closed-form expression needs to be developed for estimating the roof drift capacity of a wall when spiral confined concrete crushes. With such an expression, the wall capacities that define the tri-linear idealization of the lateral load response of a wall can be estimated without the use of a fiber model.

3. The cyclic lateral load analyses presented consist of only three walls. Therefore a complete design parameter study under the action of cyclic lateral loads is needed to understand the effect of more parameters on the hysteretic behavior of the prototype wall treated in this research. In particular, a wall which violates the gap closing criterion needs to be analyzed under cyclic lateral loads to determine if the residual roof drift for that wall is significantly larger than the residual roof drift of the prototype wall. This way, the validity of the design criterion in limiting the residual roof of a wall and introducing self-centering behavior can be assessed.

4. Nonlinear dynamic time-history analyses are needed to investigate the seismic response of these walls to design level and survival level ground motions. These analyses are necessary to determine if the goals of the proposed design approach are met for each of the ground motions considered. The nonlinear dynamic time-history analyses should include ground motion records for different U.S. seismic regions with varying site soil characteristics.

5. Large-scale tests of unbonded post-tensioned precast concrete walls with vertical joints and ductile connectors need to be performed under monotonic lateral loads in order to define the various base-shear and roof-displacement response quantities corresponding to: (1) the first occurrence of decompression of a wall panel; (2) yielding of the vertical joint connectors; (3) the effective linear limit point; (4) yielding of the post-tensioning steel; and (5) crushing of the spiral confined concrete. Monotonic lateral load test results can be used to compare the lateral load response of a wall to the lateral load response estimated using the proposed tri-linear idealization (with closed-form expressions) and a fiber model of the wall. These comparisons can establish the effectiveness of the closed-form expressions and of the fiber model in representing the lateral load behavior of a wall.

6. The cyclic lateral load behavior of large-scale unbonded post-tensioned precast concrete walls with vertical joints and ductile connectors needs to be investigated to confirm the results presented in this study, namely that unbonded post-tensioned precast concrete walls with vertical joints and ductile connectors display good hysteretic behavior and inelastic energy dissipation without loss in self-centering behavior, and that the vertical joint contributes significantly to the energy dissipation capacity of these walls.

## REFERENCES


ACI Committee 318, "Building Code Requirements for Reinforced Concrete," American Concrete Institute, Detroit, MI, 1989, 1992, 1995.

American Institute of Steel Construction, "News Briefs..." Modern Steel Construction, April 1997, 18 pp.

Building Seismic Safety Council, "NEHRP Recommended Provisions for the Development of Seismic Regulations for New Buildings," BSSC, Washington, D.C., 1994.

Cheok, G., Stone, W., and Lew, H., "Model Precast Concrete Beam-to-Column Connections Subject to Cyclic Loading," *PCI Journal*, Precast/Prestressed Concrete Institute, Vol. 38, No. 4, July-August 1993, pp. 80-92.

El-Sheikh, Magdy, R. Sause, S. Pessiki, L.-W. Lu, Y. Kurama, "Seismic Analysis, Behavior, and Design of Unbonded Post-Tensioned Precast Concrete Frames," Earthquake Engineering Research Report, No. EQ-97-02, Department of Civil and Environmental Engineering, Lehigh University, Bethlehem, PA, November 1997.

Fintel, M., "Performance of Buildings with Shear Walls in Earthquakes of the Last Thirty Years," *PCI Journal*, Precast/Prestressed Concrete Institute, Vol. 40, No. 3, May-June 1995, pp. 62-80.

Freeman, S., "Racking Tests of High-Rise Building Partitions," *Journal of Structural Engineering*, American Society of Civil Engineers, Vol. 103, No. ST8, August 1977, pp. 1673-1685.

Ghosh, S., "Observations on the Performance of Structures in the Kobe Earthquake of January 17, 1995," *PCI Journal*, Precast/Prestressed Concrete Institute, Vol. 40, No. 2, March-April 1995, pp. 14-22.

Iverson, J. and Hawkins, N., "Performance of Precast/Prestressed Concrete Building Structures During Northridge Earthquake," *PCI Journal*, Precast/Prestressed Concrete Institute, Vol. 39, No. 2, March-April 1994, pp. 38-55.

Kurama, Yahya Cuneyt, "Seismic Analysis, Behavior, and Design of Unbonded Post-Tensioned Precast Concrete Walls," Ph.D. Dissertation, Department of Civil and Environmental Engineering, Lehigh University, Bethlehem, PA, May 1997.

Kurama, Y., S. Pessiki, R. Sause, L.-W. Lu, M. El-Sheikh, "Analytical Modeling and Lateral Load Behavior of Unbonded Post-Tensioned Precast Concrete Walls," Earthquake

Engineering Research Report, No. EQ-96-02, Department of Civil and Environmental Engineering, Lehigh University, Bethlehem, PA, November 1996.

MacRae, G., and Priestley, M., "Precast Post-Tensioned Ungrouted Concrete Beam-Column Subassemblage Tests," Report No. PRESSS – 94/01, Department of Applied Mechanics and Engineering Sciences, Structural Systems, University of California, San Diego, CA, March 1994.

Mander, J., Priestley, M., and Park, R., "Theoretical Stress-Strain Model for Confined Concrete," Journal of Structural Engineering, American Society of Civil Engineers, Vol. 114, No. 8, August 1988a, pp. 1804-1826.

Mander, J., Priestley, M., and Park, R., "Observed Stress-Strain Behavior of Confined Concrete," Journal of Structural Engineering, American Society of Civil Engineers, Vol. 114, No. 8, August 1988b, pp. 1827-1849.

Paulay, T. and Priestley, M., "Seismic Design of Reinforced Concrete and Masonry Buildings," John Wiley & Sons, Inc., 1992, 744 pp.

Prakash, V. and Powell, G., "DRAIN-2DX Base Program Description and User Guide; Version 1.10,"Report No. UCB/SEMM-93/17, Structural Engineering Mechanics and Materials, Department of Civil Engineering, University of California, Berkeley, CA, November 1993.

Precast Concrete Institute, "PCI Design Handbook – Precast and Prestressed Concrete," PCI, Chicago, Illinois, 1992.

Priestley, M., "Overview of PRESSS Research Program," *PCI Journal*, Precast/Prestressed Concrete Institute, Vol. 36, No. 4, July-August 1991, pp. 50-57.

Priestley, M. and Tao, J., "Seismic Response of Precast Prestressed Concrete Frames with Partially Debonded Tendons," *PCI Journal*, Precast/Prestressed Concrete Institute, Vol. 38, No. 1, January-February 1993, pp. 58-69.

Shultz, A. E., and Magaña, R. A., "Seismic Behavior of Connections in Precast Concrete Walls," Mete A. Sozen Symposium, SP-162, 1996.

Stanton, John F., "Guidelines For Design of Seismic Connections in Precast Concrete Structures," Department of Civil Engineering, University of Washington, Seattle, WA, 98195, Presented at the 1994 Spring Convention, American Concrete Institute, San Francisco, CA, March 20-25, 1994.